

CATALYTIC CRACKING OF FUSEL OIL TO LIGHT OLEFINS OVER ZEOLITE CATALYSTS



A Dissertation Submitted in Partial Fulfillment of the Requirements
for the Degree of Doctor of Philosophy in Petrochemistry and Polymer Science

Field of Study of Petrochemistry and Polymer Science

FACULTY OF SCIENCE

Chulalongkorn University

Academic Year 2020

Copyright of Chulalongkorn University

การแตกตัวเชิงแรงปฏิกิริยาของฟูเซลอยล์เป็นโอเลฟินส์เบาบนตัวเร่งปฏิกิริยาซีโอไลต์



วิทยานิพนธ์นี้เป็นส่วนหนึ่งของการศึกษาตามหลักสูตรปริญญาวิทยาศาสตรดุษฎีบัณฑิต
สาขาวิชาปิโตรเคมีและวิทยาศาสตร์พอลิเมอร์ สาขาวิชาปิโตรเคมีและวิทยาศาสตร์พอลิเมอร์

คณะวิทยาศาสตร์ จุฬาลงกรณ์มหาวิทยาลัย

ปีการศึกษา 2563

ลิขสิทธิ์ของจุฬาลงกรณ์มหาวิทยาลัย

Thesis Title CATALYTIC CRACKING OF FUSEL OIL TO LIGHT OLEFINS
 OVER ZEOLITE CATALYSTS
By Miss Rachatawan Yaisamlee
Field of Study Petrochemistry and Polymer Science
Thesis Advisor Associate Professor PRASERT REUBROYCHAROEN, Ph.D.

Accepted by the FACULTY OF SCIENCE, Chulalongkorn University in Partial
Fulfillment of the Requirement for the Doctor of Philosophy

..... Dean of the FACULTY OF SCIENCE
(Professor POLKIT SANGVANICH, Ph.D.)

DISSERTATION COMMITTEE

..... Chairman
(Assistant Professor WARINTHORN CHAVASIRI, Ph.D.)

..... Thesis Advisor
(Associate Professor PRASERT REUBROYCHAROEN, Ph.D.)

..... Examiner
(Assistant Professor Duangamol Tungasmita, Ph.D.)

..... Examiner
(Professor Chawalit Ngamcharussrivichai, Ph.D.)

..... External Examiner
(Associate Professor Chanatip Samart, Ph.D.)

รชตวัน ไยสำลี : การแตกตัวเชิงเร่งปฏิกิริยาของฟิวเซลอยล์เป็นโอเลฟินส์เบาบนตัวเร่งปฏิกิริยาซีโอไลต์. (CATALYTIC CRACKING OF FUSEL OIL TO LIGHT OLEFINS OVER ZEOLITE CATALYSTS) อ.ที่
 ปริญญาหลัก : รศ. ดร.ประเสริฐ เรียบร้อยเจริญ

ฟิวเซลอยล์เป็นผลพลอยได้จากการผลิตไบโอเอทานอล ซึ่งถือเป็นวัตถุดิบทดแทนและเป็นมิตรต่อสิ่งแวดล้อม เนื่องจากการใช้งานอย่างจำกัดของฟิวเซลอยล์ ทำให้ตลาดไม่สามารถรองรับความต้องการของฟิวเซลอยล์ทั้งหมดได้ส่งผลให้มีราคาค่อนข้างต่ำ ด้วยเหตุนี้ฟิวเซลอยล์จึงเป็นแหล่งหมุนเวียนใหม่ที่ที่น่าสนใจในการนำมาเพิ่มมูลค่าผ่านกระบวนการเปลี่ยนพลังงานชีวภาพที่มีประสิทธิภาพสูง ในงานวิจัยนี้ได้ศึกษาการแตกตัวเชิงเร่งปฏิกิริยาของฟิวเซลอยล์เป็นโอเลฟินส์เบา (เอทิลีน โพรพิลีนและบิวทิลีน) ด้วยเครื่องปฏิกรณ์แบบเบดคงที่โดยใช้ซีโอไลต์เป็นตัวเร่งปฏิกิริยา นอกจากนี้ยังมีศึกษาคุณสมบัติทางเคมีกายภาพของฟิวเซลอยล์ พร้อมทั้งศึกษาผลของลักษณะโทโพโลยีของซีโอไลต์ที่รู้จักดีทั้งสามชนิดได้ชนิดได้แก่ ZSM-5 HY และ H-beta ต่อปฏิกิริยานี้ ผลการวิจัยพบว่าตัวเร่งปฏิกิริยา HZSM-5 ให้ปริมาณโอเลฟินส์เบาที่สุดภายใต้สภาวะเดียวกันเนื่องจากมีโครงสร้างรูพรุนที่เหมาะสม ด้วยเหตุนี้ซีโอไลต์ HZSM-5 จึงได้รับเลือกสำหรับการศึกษาผลของปัจจัยในการทำปฏิกิริยาเช่นอุณหภูมิและอัตราการไหลของสารป้อนต่อไป จากผลการทดลองพบว่าอุณหภูมิและอัตราการไหลของสารป้อนเป็นปัจจัยสำคัญในการควบคุมการเกิดปฏิกิริยาข้างเคียง เช่น ปฏิกิริยาการถ่ายโอนไฮโดรเจน อะโรมาไทเซชัน ไอโซเมอไรเซชัน เป็นต้น ซึ่งเป็นปฏิกิริยาที่ก่อให้เกิดสารประกอบไฮโดรคาร์บอนที่ไม่ต้องการ โดยภาวะเหมาะสมที่ให้โอเลฟินส์เบาสูงสุดคือที่อุณหภูมิ 550 องศาเซลเซียส อัตราการไหลของสารป้อนเท่ากับ 0.04 มิลลิลิตรต่อนาทีและที่น้ำหนักตัวเร่งปฏิกิริยา 0.2 กรัม นอกจากนี้ยังศึกษาผลของการให้น้ำร่วมและสารตั้งต้น ผลการวิจัยแสดงให้เห็นถึงบทบาทสำคัญของอัตราส่วนของน้ำและบทบาทของสารตั้งต้นต่อปฏิกิริยาการแตกตัวเชิงเร่งปฏิกิริยาของฟิวเซลอยล์ ความเสถียรของตัวเร่งปฏิกิริยา HZSM-5 ในการแตกตัวเชิงเร่งปฏิกิริยาของฟิวเซลอยล์ได้รับการตรวจสอบในการทำปฏิกิริยา 20 ชั่วโมง พบว่าตัวเร่งปฏิกิริยา HZSM-5 ให้ปริมาณโอเลฟินส์เบาลดลงเล็กน้อย ดังนั้น HZSM-5 จึงเป็นตัวเร่งปฏิกิริยาที่เหมาะสมในการพัฒนาความเสถียรและประสิทธิภาพการเร่งปฏิกิริยาในการผลิตโอเลฟินส์เบาโดยการแตกตัวเชิงเร่งปฏิกิริยาของฟิวเซลอยล์ในอนาคต

จุฬาลงกรณ์มหาวิทยาลัย
 CHULALONGKORN UNIVERSITY

สาขาวิชา	ปิโตรเคมีและวิทยาศาสตร์พอลิเมอร์	ลายมือชื่อนิสิต
ปีการศึกษา	2563	ลายมือชื่อ อ.ที่ปรึกษาหลัก

6072870123 : MAJOR PETROCHEMISTRY AND POLYMER SCIENCE

KEYWORD: Catalytic cracking, Fusel oil, HZSM-5 zeolite, Light olefins

Rachatawan Yaisamlee : CATALYTIC CRACKING OF FUSEL OIL TO LIGHT OLEFINS OVER ZEOLITE CATALYSTS. Advisor: Assoc. Prof. PRASERT REUBROYCHAROEN, Ph.D.

Fusel oil is a by-product of bioethanol production. It is considered a renewable feedstock as well as an environmentally friendly material. However, due to the limitation of its application, the market is not able to absorb the demand for fuel oil, which results in a relatively low price. As a consequence, fusel oil is an interesting new renewable source to convert into value-added products via a high-efficiency bioenergy conversion process. In the present work, the catalytic cracking of fusel oil to light olefins (ethylene, propylene, and butylene) was investigated in a fixed bed reactor using zeolites as catalysts. The physicochemical properties of fusel oil were also examined. The three well-known zeolites; ZSM-5, HY, and H-beta were selected to study the effect of the topology of zeolite on this reaction. Under the same condition, the results found that HZSM-5 gave the highest carbon in light olefins yield because of its suitable pore structure. As a result, HZSM-5 zeolite was chosen for further study to achieve the highest catalytic performance. The effect of operating parameters such as reaction temperature and fusel oil feed flowrate on gas carbon yields was studied. The operating reactions play a vital role in gas product and distribution in order to control the side reactions (i.e., H-transfer, aromatization, isomerization) which produce undesired hydrocarbons. With the consideration of light olefins, the optimum condition was at 550°C with 0.04 mL/min fusel oil feed flow rate with 0.2 g catalyst. Moreover, the effect of co-feeding water and reactants were also studied. The results exhibited the significant role of the ratio of co-fed water and the role of reactants in catalytic cracking reaction over HZSM-5 catalyst. The stability of HZSM-5 on catalytic cracking of fusel oil was also examined. There was a slight drop in light olefins yield over 20 h of time on stream on HZSM-5. Thus, HZSM-5 showed good merit to develop stability and catalytic performance in the novel way to produce light olefins via catalytic cracking of fusel oil in future work.

Field of Study:	Petrochemistry and Polymer Science	Student's Signature
Academic Year:	2020	Advisor's Signature

ACKNOWLEDGEMENTS

I would like to express my heartfelt gratitude to everyone who has contributed to this dissertation. This work could not be accomplished without their support and help.

I am grateful to my advisor, Assoc. Prof. Dr. Prasert Reubroycharoen, for giving me advice and encouragement, as well as for providing me with this invaluable opportunity. His support encourages me to focus and move forward.

Besides, I would like to thank the chairman and committees for devoting their precious time to reviewing and providing guidance on this work. Also, I deeply appreciated all of the researchers who have devoted their efforts and published their research for my better understanding and knowledge.

I would like to acknowledge the financial support from my Science Achievement Scholarship of Thailand (SAST) for living allowance through the Ph.D. program. A special thank goes to the academic advisor and laboratory staff of the Department of Chemical Technology, Faculty of Science, Chulalongkorn University for their kind assistance and collaboration.

Last but not least, I would like to express my special thank to my friend and family for their love, friendship, empathy, and motivate me to complete this milestone throughout the graduate study.

จุฬาลงกรณ์มหาวิทยาลัย
CHULALONGKORN UNIVERSITY

Rachatawan Yaisamlee

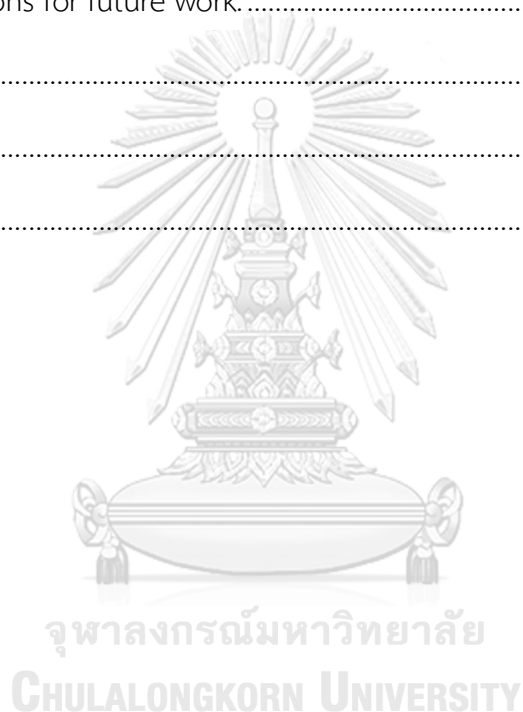
TABLE OF CONTENTS

	Page
ABSTRACT (THAI).....	iii
ABSTRACT (ENGLISH).....	iv
ACKNOWLEDGEMENTS	v
TABLE OF CONTENTS	vi
LIST OF TABLES.....	x
LIST OF FIGURES.....	xi
LIST OF SCHEMES.....	xiv
LIST OF ABBREVIATIONS	xv
CHAPTER 1 INTRODUCTION	1
1.1 Statement of problem.....	1
1.2 Objectives.....	4
1.3 Scopes of work.....	5
1.4 Expected results.....	7
CHAPTER 2 THEORY AND LITERATURE REVIEWS.....	8
2.2 Light olefins	9
2.3 Cracking reaction	11
2.3.1 Thermal cracking [39].....	11
2.3.2 Catalytic cracking	12
2.4 Dehydration of alcohol.....	15
2.5 Catalyst deactivation	16
2.6 Zeolite	19

2.6.1 Zeolite structure	19
2.6.2 Acidity of zeolite	23
2.6.3 Shape selectivity	24
2.6.4 ZSM-5	28
2.6.5 Zeolite beta	29
2.6.6 Zeolite Y	30
2.7 Heterogeneous catalytic reactor [66].....	31
2.7.1 Insignificant motion catalyst.....	31
2.7.1.1 Fixed bed reactor	31
2.7.1.2 Trickle bed reactor.....	33
2.7.1.3 Moving bed reactor.....	34
2.7.1.4 Rotating packed bed reactor.....	35
2.7.2 Significant motion catalyst.....	36
2.7.2.1 Fluidized bed reactor (FBR).....	36
2.7.2.2 Slurry reactor.....	37
2.8 literature reviews.....	38
2.8.1 Catalytic conversion of oxygenated compounds over zeolites.....	38
2.8.2 Role of feedstocks.....	41
2.8.3 Role of zeolite topology	43
2.8.4 Effect of co-feeding water.....	44
2.8.5 Role of operating parameters	47
2.8.5.1 Effect of reaction Temperature	47
2.8.5.2 Effect of space velocity.....	48
2.8.6 Stability of zeolite on catalytic cracking	48

CHAPTER 3 METHODOLOGY	51
3.1 Chemicals.....	51
3.2 Instruments.....	52
3.3 Physicochemical properties of fusel oil	53
3.3.1 The higher heating value (HHV)	53
3.3.2 Density.....	53
3.3.3 water content.....	53
3.3.4 Chemical composition of fusel oil	53
3.4 The textual properties and acidity of zeolites.....	55
3.5 Catalytic cracking performance	55
3.5.1 Effect of zeolite topology	57
3.5.2 Effect of reaction temperature	57
3.5.3 Effect of feed flowrate.....	57
3.5.4 Effect of feedstock.....	57
3.5.5 Effect of co-feeding water.....	58
3.5.6 The stability of zeolite on catalytic cracking of fusel oil.....	58
3.6 Product analysis.....	58
3.7 Catalyst deactivation analysis.....	61
CHAPTER 4 RESULTS AND DISCUSSION.....	63
4.1 Physicochemical of fusel oil.....	63
4.2 Effect of zeolite topology.....	65
4.3 Parametric study.....	69
4.3.1 Effect of reaction temperature	69
4.3.2 Effect of feed flowrate.....	71

4.4 Effect of feedstocks	73
4.5 Effect of co-feeding water	75
4.6 Liquid fraction derived from catalytic cracking of fusel oil	77
4.7 Catalyst stability and deactivation.....	80
4.8 Purpose mechanisms	87
CHAPTER 5 CONCLUSIONS.....	94
Recommendations for future work.....	95
APPENDIX.....	97
REFERENCES	107
VITA.....	117



LIST OF TABLES

	Page
Table 2.1 Comparison between thermal cracking and catalytic cracking [44]	14
Table 2.2 Summarization of catalyst deactivation [44].....	17
Table 2.3 Molecular size of reactants and pore size diameter of zeolites.....	25
Table 2.4 Molar selectivity (%) for n-hexane cracking over HZSM-5, HBEA, and HMOR	43
Table 3.1 The list of chemicals and sources.....	51
Table 3.2 Temperature program for fusel oil components analysis	54
Table 3.3 Temperature program for gas product analysis.....	59
Table 4.1 Physicochemical of fusel oil.....	63
Table 4.2 Chemical Composition of fusel oil.....	64
Table 4.3 The textural properties and acidity of three zeolite	67
Table 4.4 The topology of three zeolites [90], [91].....	68
Table 4.5 Chemical composition of liquid fraction derived from catalytic cracking of fusel oil.....	79
Table 4.6 The coke content and the elemental analysis at different TOS for the used HZSM-5 sample.....	83
Table 4.7 Textural properties and total acidity of three types of zeolite and the used HZSM-5 at different TOS	84
Table 4.8 The acidity of fresh and spent HZSM-5 at different TOS	86

LIST OF FIGURES

	Page
Figure 1.1 The biofuel production worldwide.....	1
Figure 2.1 The propylene gap between demand and supply [36]......	10
Figure 2.2 The proposed mechanism catalytic cracking over zeolite catalyst [43].....	13
Figure 2.3 The mechanism dehydration of ethanol to ethylene and diethyl ether over zeolite catalyst [46]	16
Figure 2.4 Primary building unit (PBU) of zeolite structure [51].....	19
Figure 2.5 Secondary building units founding in the zeolite structures [50].....	20
Figure 2.6 The development of zeolite structures from primary building units to secondary building units and zeolite structures [52]	21
Figure 2.7 The ring size of zeolite refers to the number of tetrahedrons and the example [53].....	22
Figure 2.8 The formation of BAS and LAS in zeolite [57].....	24
Figure 2.9 Three types of shape selectivity in the zeolite [60].....	27
Figure 2.10 Framework structure of ZSM-5 [63].....	28
Figure 2.11 Framework structure of zeolite beta [64]	29
Figure 2.12 Framework structure of zeolite Y [65]	30
Figure 2.13 Fixed bed reactor [68].....	32
Figure 2.14 Trickle bed reactor [70].....	33
Figure 2.15 Moving bed reactor [71].....	34
Figure 2.16 Rotating packed bed reactor [73]	35
Figure 2.17 Fluidized bed reactor (FBR).....	36
Figure 2.18 Slurry reactors [75].....	37

Figure 2.19 Overall reaction pathway for conversion of bio-oil over zeolite catalyst (TE: Thermal effect, TCE: Themo-catalytic effect).....	38
Figure 2.20 overall reaction pathway for co-pyrolysis of biomass and fusel oil over a zeolite catalyst.....	40
Figure 2.21 The effect of co-feeding water on the conversion of ethanol to propylene on the function of reaction temperature.....	46
Figure 2.22 Reaction route of catalytic cracking of naphtha on ZSM-5 catalyst.....	49
Figure 2.23 Possible route of coke formation on the outer surface.....	50
Figure 3.1 Schematic diagram of the fixed bed reactor process for catalytic cracking of fusel oil.....	56
Figure 4.1 Fusel oil.....	63
Figure 4.2 The GC chromatogram of fusel oil.....	64
Figure 4.3 Catalytic activity of three zeolites in the catalytic cracking of fusel oil, in terms of the (a) carbon yield and (b) carbon selectivity of the gas mixture products. Reaction condition: 550°C, feed flow rate of 0.04 mL/min, time on stream of 4 h. ...	65
Figure 4.4 Effect of the reaction temperature on the (a) carbon yield and (b) carbon selectivity of the gaseous products in the catalytic cracking of fusel oil. Reaction condition: catalyst HZSM-5, feed flowrate of 0.04 mL/min, for 4 h.....	69
Figure 4.5 Effect of the feed flow rate on the (a) carbon yield and (b) carbon selectivity of the gaseous products in the catalytic cracking of fusel oil. Reaction condition: catalyst HZSM-5, 550°C, for 4 h.	71
Figure 4.6 Effect of the reactant on the (a) carbon yield and (b) carbon selectivity on the gaseous products in the catalytic cracking of fusel oil. Reaction condition: catalyst HZSM-5, 550°C, feed flowrate of 0.04 mL/min, for 4 h.....	73
Figure 4.7 Effect of co-feeding water on the (a) carbon yield and (b) carbon selectivity of the gaseous products in the catalytic cracking of fusel oil. Reaction condition: catalyst HZSM-5, 550°C, feed flowrate of 0.04 mL/min, for 4 h.....	75

Figure 4.8 Stability of HZSM-5 in the catalytic cracking of fusel oil. Reaction condition: catalyst HZSM-5, 550°C, feed flowrate of 0.04 mL/min, for 4 h.....	80
Figure 4.9 The TGA thermogram of fresh and spent HZSM-5 at different TOS.....	82
Figure 4.10 The TGA thermogram of fresh and spent HZSM-5 at different TOS	82
Figure 4.11 the NH ₃ -TPD profiles of the fresh and spent HZSM-5 at different TOS....	85
Figure 4.12 Dealumination hydrothermal of zeolite	86
Figure 4.13 overall reaction pathway for observed products on catalytic cracking of fusel oil over HZSM-5 catalyst.....	87

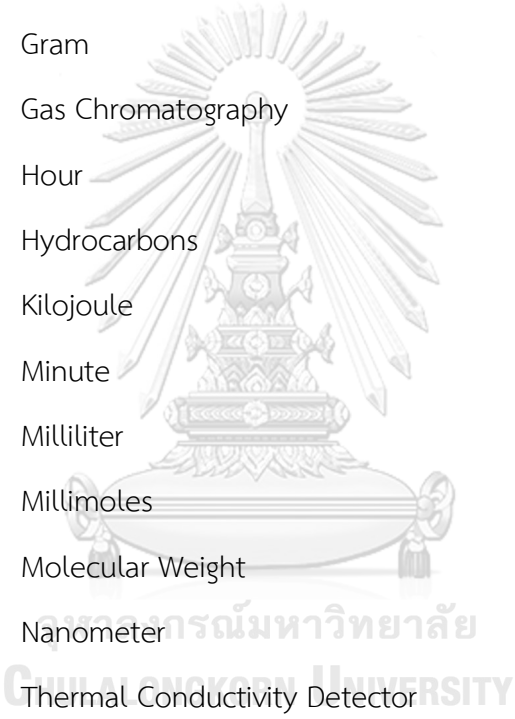


LIST OF SCHEMES

	Page
Scheme 1 The dehydration of various alcohols in fusel oil to alkenes	88
Scheme 2 Mechanism of dehydration of isoamyl alcohol to pentenes.	89
Scheme 3 The intermolecular dehydration of isoamyl alcohol.....	89
Scheme 4 Cracking reaction of alkenes to smaller molecules.....	90
Scheme 5 Mechanism for catalytic cracking over a zeolite catalyst	90
Scheme 6 The dehydrogenation cracking of isoamyl alcohol to Isovaleraldehyde	91
Scheme 7 Mechanism of dehydrogenation cracking over a zeolite catalyst.....	91
Scheme 8 The acetalization of Isovaleraldehyde with isoamyl alcohols.	92
Scheme 9 Mechanism of acetalization of aldehyde to acetal [108].....	92
Scheme 10 The hydrocarbon pool mechanism over HZSM-5 catalyst [109].....	93

LIST OF ABBREVIATIONS

°C	Degree Celsius
%	Percentage
%wt	Weight Percentage
Å	Angstrom
FID	Flam Ionization Detector
g	Gram
GC	Gas Chromatography
h	Hour
HCs	Hydrocarbons
kJ	Kilojoule
min	Minute
mL	Milliliter
mmol	Millimoles
MW	Molecular Weight
nm	Nanometer
TCD	Thermal Conductivity Detector
TOS	Time stream
WHSV	Weight Hourly Space Velocity
ΔH	Enthalpy



CHAPTER 1

INTRODUCTION

1.1 Statement of problem

With an increasing energy demand, the depletion of non-renewable fossil fuels has become a major concern for the global energy system over the past decade [1] [2], [3]. In order to overcome this crisis, the use of renewable biofuels as an alternative fuel source is a promising way for a long-term partial solution [4, 5]. Bioethanol is one alternative energy (fuel) source, and its production level is growing annually, as can be seen in Fig.1.1 [6]. Nevertheless, bioethanol production gives fusel oil as a by-product between 1.0-11.0 L per 1000 L of ethanol produced, which is a large amount at an industrial scale [7].

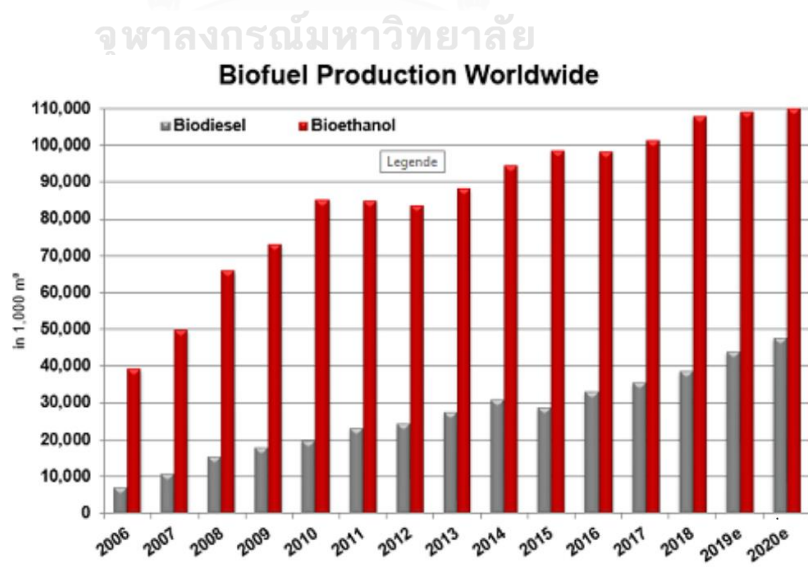


Figure 0.1 The biofuel production worldwide

Generally, fusel oil (also known as fusel alcohol) is a mixture of various alcohols (ethanol, propanol, isobutanol, n-butanol, and isoamyl alcohol), mainly isoamyl alcohol, with a water content of 2.5–20.0% by weight (wt.%) [8]. It can be used as a solvent, foam coating, flavoring agents, or fuel additive in gasoline to improve engine combustion [7],[9],[10]. However, the utilization of fusel oil is limited, which results in its relatively low cost. In addition, since fusel oil is non-toxic to aquatic wildlife, it is considered an eco-friendly material[8]. For all the above reasons, fusel oil is an attractive renewable source to convert into value-added products via a high-efficiency process.

Catalytic cracking is one of the well-known thermochemical conversion processes that has been commonly used in petroleum refineries [11]. This process has several advantages, such as higher cracking conversion level, less coke formation, and more environmentally friendly way, as compared with thermal cracking [12], [13]. Moreover, catalytic cracking of bio-oil also gives a high selectivity of light olefins, such as ethylene and propylene, which are key raw materials in the petrochemical industry [14]. Undoubtedly, numerous researchers have focused on transforming low-cost feedstock to light olefins over the catalytic cracking process [15]. In catalytic cracking of oxygenated compounds, the oxygens are removed rapidly as a stream (H_2O), carbon dioxide (CO_2), and carbon monoxide (CO) via deoxygenation reactions [16]. The hydrocarbons (HCs) are cracked C-C bonds into olefins and then transformed to various aromatics via the side reactions under acidic catalyst conditions. The light olefins yield

is mainly controlled by the catalyst, feedstocks, and operating conditions [15], [17]. Zhang et al.[18] studied the effect of operating parameters on the conversion of biomass to light olefins. For ex-situ pyrolysis, the reaction temperature and gas flow rate have essential roles in controlling secondary reactions of volatiles, affecting the light olefins yield and distribution. According to Gong et al.[19], the maximum selectivity of light olefins (59.0%) was obtained at the reaction temperature of 600°C and weight hourly space velocity (WHSV) of 0.4 h⁻¹ in catalytic cracking of bio-oil over modified HZSM-5 catalyst.

Zeolite catalysts are important factors that dictate the product yield and distribution in the cracking process. Due to their surface chemistry and unique framework, zeolites can enhance catalytic conversion and control the selectivity of products [20], [21]. Among them, HZSM-5 was found to be an excellent catalyst in the cracking process because of its acidity, moderate internal pore space, and steric hindrance [21], [22], [23]. The Brønsted acid sites are catalytically active sites for cracking, deoxygenation, and aromatization reactions. According to Luo et al. [24], HZSM-5 showed a better catalytic activity, higher alkenes selectivity, and outstanding thermal stability than H-MOR, H-BEA, and USY zeolites in hexane cracking. The pore-size restrictions in HZSM-5 lead to suppressing the oligomerization of olefins to larger aromatic molecules. Chen et al. [25] studied the catalytic cracking of bio-oil over HZSM-5 catalysts using different model compounds, such as acetic acid, guaiacol, n-heptane, acetol, and ethyl acetate. They found that the percentage of carbon yield

was different, depending on the feedstock. Ethylene was found to be the highest carbon selectivity, followed by propylene and butylene. Zhang et al. [26] employed HZSM-5 to enhance aromatic production (BTX) in the co-fast pyrolysis of corn stover and fusel oil in a fluidized bed reactor. They reported that the dehydration of fusel oil to various ranges of alkenes favors aromatic HCs formation under acidic conditions.

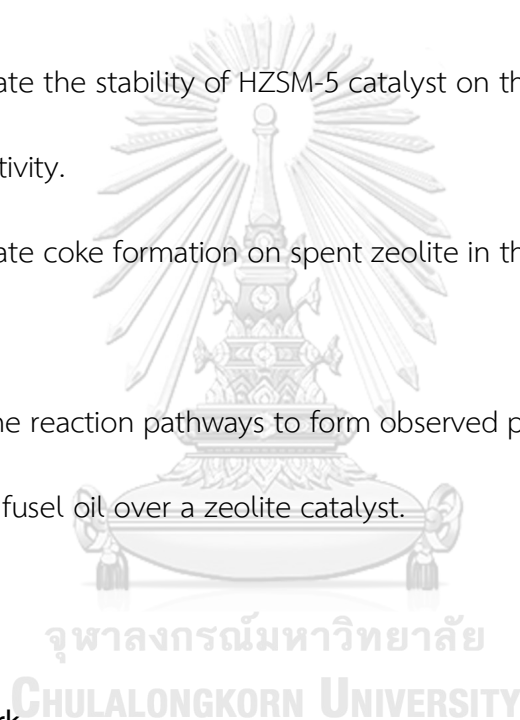
To the best of our knowledge, there has not been previous research investigating the catalytic cracking of fusel oil to light olefins as target products. In this work, the gaseous products of catalytic cracking of fusel oil were studied in a fixed bed reactor. The physicochemical aspects of the fusel oil were examined. The effect of zeolite topology was investigated. The effect of the operating parameters, such as the reaction temperature and fusel oil feed flow rate, was investigated over HZSM-5 to increase the yield of ethylene and propylene. Moreover, the impact of co-feeding water and reactants in fusel oil was also determined in experiments.



1.2 Objectives

1. To study catalytic cracking of fusel oil to light olefins over zeolites catalysts in a fixed bed reactor
2. To study the effect of zeolite topology on the catalytic cracking of fusel oil activity.

3. To study the influence of operating parameters (i.e., reaction temperature and fusel oil feed flow rate) on the catalytic cracking of fusel oil activity.
4. To study the influence of various alcohols feedstocks in fusel oil on catalytic cracking over a zeolite catalyst.
5. To study the influence of co-feeding water on the catalytic cracking of fusel oil activity.
6. To investigate the stability of HZSM-5 catalyst on the catalytic cracking of fusel oil activity.
7. To investigate coke formation on spent zeolite in the catalytic cracking of fusel oil.
8. To study the reaction pathways to form observed product in catalytic cracking of fusel oil over a zeolite catalyst.



1.3 Scopes of work

1. Design and set up fix bed reactor for catalytic cracking of fusel oil
2. Investigate physicochemical of fusel oil
 - higher heating value (HHV)
 - Density
 - water content
 - Chemical composition

3. Investigate the topology of zeolites on catalytic cracking of fusel oil by using three well-known zeolites as follows;
 - HZSM-5
 - HY
 - H-beta
4. Investigate the effect of operating parameters on the gas product from catalytic cracking of fusel oil
 - Reaction temperature (350, 450, 550, and 650°C)
 - Feed flow rate of fusel oil (0.02, 0.04, 0.08, and 1.6 ml/min)
5. Investigate the influence of reactant on catalytic cracking of fusel oil by various the feedstock as follows;
 - Ethanol, propanol, n-butanol, isobutanol, isoamyl alcohol
6. Compare the catalytic performance between model fusel oil and fusel oil under the same condition.
7. Investigate the effect of co-feeding water on catalytic cracking of fusel oil.
The various water ratio in feeding shows as follows;
 - Water content (0, 6.3, 12.6 and 25.2%wt)
8. Investigate the liquid composition of catalytic cracking of fusel oil under optimal conditions by gas chromatography-mass spectrometry (GC-MS).

9. Study the stability of HZSM-5 on catalytic cracking of fusel oil over 20 h of time on stream under optimal conditions.
10. Investigate the characterization of the spent catalyst under optimized conditions by TGA, elemental analysis, N_2 adsorption-desorption, and NH_3 -TPD.
11. Study reaction pathways of catalytic cracking of fusel oil to light olefins over a zeolite catalyst.

1.4 Expected results

The high light olefins yield (ethylene, propylene, and butylene) is expected to obtain in the catalytic cracking of fusel over zeolites catalyst in a fixed bed reactor under optimal conditions. The zeolite catalyst has excellent stability in this reaction over a long time on stream.

CHAPTER 2

THEORY AND LITERATURE REVIEWS

2.1 Fusel oil

Fusel oil (also known as fusel alcohol) is a mixture of various alcohols (ethanol, propanol, isobutanol, n-butanol, and isoamyl alcohol), mainly isoamyl alcohol, with a water content of 2.5–20.0% by weight (wt.%). Fusel oil is a by-product of bioethanol production [27]. Generally, the bioethanol distillation process gives fusel oil approximately 1-11L per 1000L of ethanol produced [10]. During hydrous ethanol fuel (HEF) distillation, fusel oil is extracted in a manner similar to but rougher than that used for beverages. This removal usually entails a side withdrawal that is cooled prior to phase separation and from which the aqueous phase, which contains ethanol and water, is returned to the distillation column [9]. The yield of fusel oil depends on the type of feedstock, and the condition of fermentation and distillation. Based on its application, fusel oil can be used as a solvent, foam coating, flavoring agent, or fuel additive in gasoline to improve engine combustion [28] [29]. In addition, since fusel oil is non-toxic to aquatic wildlife, it is considered an eco-friendly material [10]. However, the use of fusel oil in industrial is quite limit and there is a limitation in separation to the pure component. Therefore, fusel oil is relatively low cost.

2.2 Light olefins

Light olefins (ethylene, propylene butylene) are the key raw material in the petrochemical industry [19]. Their demands are continuously growing annually due to the increase in human consumption [30] [31]. Worldwide production of ethylene and propylene exceeds 140 and 90 million tons per year, respectively, with global demand expected to reach 130 million tons by 2023 [32] [33].

Ethylene is produced from steam cracking [34]. In general, ethylene is a relatively low cost. Nevertheless, it can be converted to a high-value product by reacting with the high tonnage compound such as chlorine, hydrogen chloride, oxygen. For example, the high-value product from ethylene is ethanol, ethylene glycol, epoxide, PVC, and ethylbenzene [30].

Propylene is the second largest building block in the petrochemical industry. There is a continuous increase in the demand for propylene worldwide [35]. Additionally, its demands are higher than ethylene. There is a huge propylene gap between demand and supply, as shown in Fig.2.1 [36]. Normally, propylene is the by-product of the oil refining process. Recently, the major propylene has been obtained from steam cracking (SC) of hydrocarbons feedstock derived from naphtha and natural gas liquid [37]. Propylene is used in various applications such as packaging, reusable container, and textile plastic part.

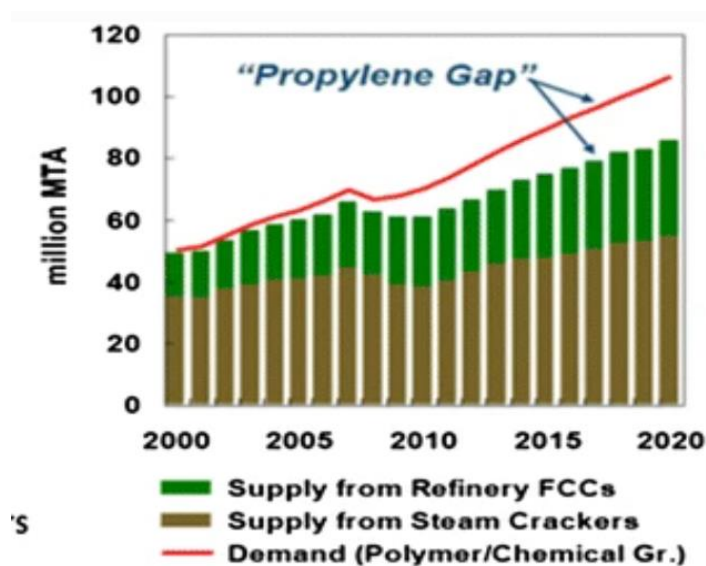


Figure 0.1 The propylene gap between demand and supply [36].

Butylene is produced from the fluid catalytic cracking (FCC) process and streams cracking on a large scale [38]. Due to the limited application, its demand is relatively low with a cheap price. Butylene can be used as a monomer in polybutylene it is not frequently used. Isobutene is mostly used as a raw material in the manufacture of alkylates to produce fuel additives such as methyl tert-butyl ether (MTBT) in order to enhance the octane number [30]

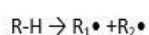
Traditionally, the major of light olefins is obtained from petroleum resources which are now renewable source. Furthermore, the production process consumes high energy and processes a larger amount of CO₂. Therefore, it is urgent to find a novel renewable source to produce light olefins.

2.3 Cracking reaction

2.3.1 Thermal cracking [39]

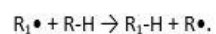
Thermal cracking is the reaction that breaking large hydrocarbons into smaller ones via heat in the absence of the catalyst. The large molecules are cracked by receiving higher energy than bonding energy. Thus, this reaction requires a high temperature (850-900°C) and high pressure (up to 70 atmospheres), which is intensive energy consumption [40]. This process produces a large amount of greenhouse and coke deposition. Besides, it is difficult to control product selectivity because this process is carried out without a catalyst. However, the catalyst regenerator is not required. Additionally, the isomerize reactions are not favored in this process. The mechanism of thermal cracking occurs via free radicals. There are three steps of free radical chain reactions, as follows;

(1) Initiation

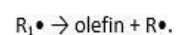


Homolysis -homolytic bond cleavage

(2) Propagation

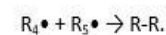


Hydrogen abstraction – favored at high pressures



β Scission – Favored at low pressures

(3) Termination

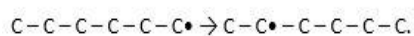


Radical combinations

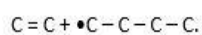


Disproportionation

Isomerization reactions



Not favored



β Scission, faster than isomerization

where R-H is the paraffin chain, n is the number of carbon atoms in alkanes, and o represents the radical unpaired electron.

2.3.2 Catalytic cracking

Catalytic cracking is the most important and widely used in the refinery process. It converts heavy hydrocarbon molecules into a varied range of smaller products, including liquid hydrocarbon fuel by breaking the C-C bond. This process can operate at much lower temperatures (often at 500–600°C) with the consequent energy savings catalysts with high activity, thermal stability, and shape selectivity are needed in this process [30]. In commercial, zeolite, having a unique framework, is widely used as solid catalysts to supply proton and to improve selectivity. The mechanism of catalytic cracking on zeolite proceeds via a carbocation intermediate (with complications caused by oligomerization reactions) [41].

2.3.2.1 Proposed mechanism catalytic cracking over Zeolites [42]

Fig.2.2 shows the reaction network and mechanism in zeolite-assisted cracking of hydrocarbon molecules. There are many reaction steps of hydrocarbon cracking. Firstly, proton transfer from zeolite Brønsted site to alkane to form carbonium ion. Then, proton transfer from zeolite to the alkene to form carbenium ion. The direction of this reaction mostly obeys the stability rule of carbenium ions: primary < secondary < tertiary [41]. Next hydride transfers from alkane to zeolite to form carbenium ion. Finally, Beta scission of a carbenium ion form a new carbenium ion and an alkene.

Besides the primary cracking reaction to form smaller hydrocarbons, there is a secondary reaction due to hydrogen transfer mechanisms like isomerization or cyclization which lead to coke formation. With equal carbon number, the rate of cracking decrease in the following order: i-olefins > n-olefins > i-paraffins = naphathenes > n-parafins > aromatics.

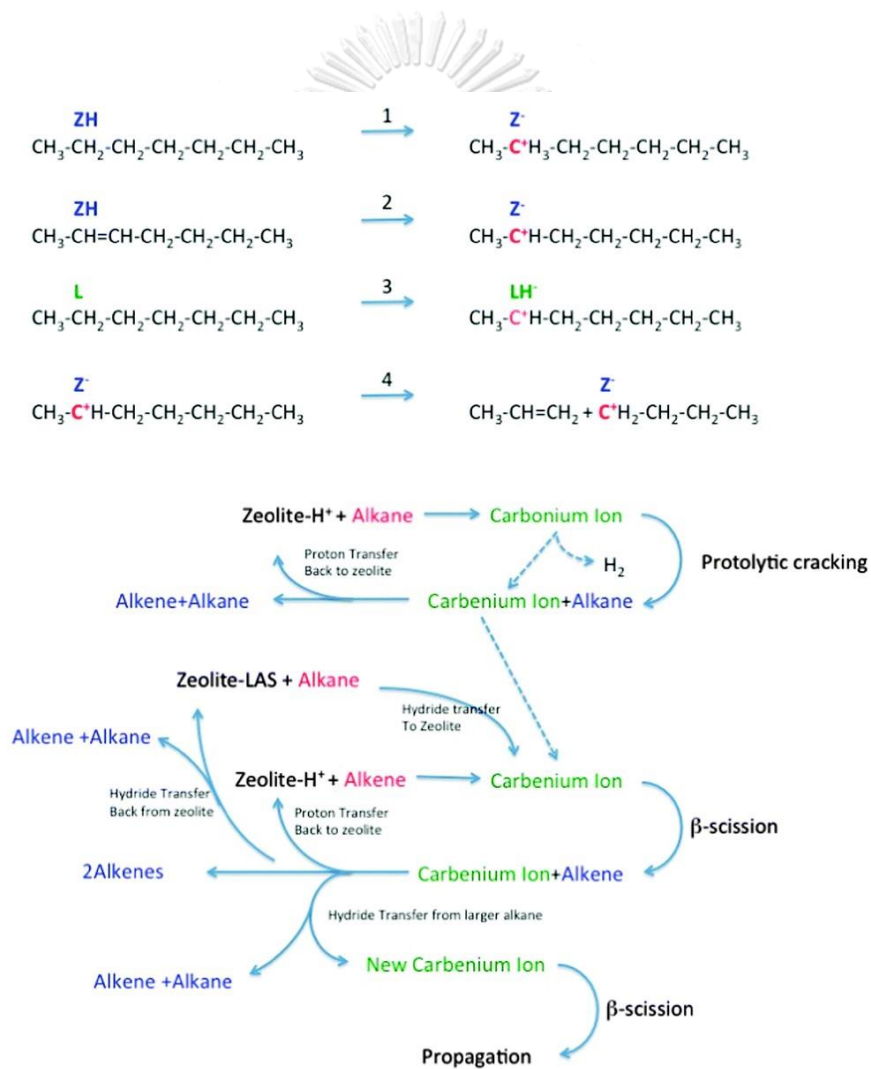


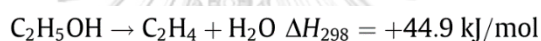
Figure 0.2 The proposed mechanism catalytic cracking over zeolite catalyst [43]

Table 0.1 Comparison between thermal cracking and catalytic cracking [44]

Particulars	Thermal cracking	Catalytic cracking
Definition	Breaking of larger hydrocarbons into smaller ones by the application of heat	Breaking of larger hydrocarbons into smaller ones by the application of heat in the presence of a catalyst
Temperature	400-1000°C	440-540°C
Regenerator	Not required	Required for catalyst recovery
Waste generation	A large amount of coke is generated	Coke formation is low
Pressure	10-15 kg/cm ²	<5 kg/cm ²
Mechanism	Free radical mechanism	Carbonium ion mechanism
Pre-treatment of feed	General treatments are sufficient, eliminating non-volatile gases and removal of S and N	Highly specific and immense to safeguard the life of the catalyst, along with S removal
products	Generally, ring structures and unsaturated	Generally, focused on producing gasoline of high octane value

2.4 Dehydration of alcohol

The dehydration reaction is a conversion of the oxygenated reactant (i.e. alcohol, carboxylic, amide) along with losing water. Commonly, this reaction is controlled by temperature under acidic conditions. There, this reaction is the one-factor reaction in upgrading the low-cost oxygenated feedstocks. For example, the dehydration of bioethanol to light olefins, the transformation of bioethanol to propylene, and the pyrolysis of bio-oil occur via the dehydration pathways. The dehydration of ethanol to ethylene is shown as a followed equation:



This reaction is endothermic but is largely favored thermodynamically already at moderate temperatures (e.g., 473– 573 K) [45].

Fig.2.3 shows the dehydration of ethanol to ethylene mechanism over zeolites catalyst. In the intramolecular dehydration process, the hydroxy groups are protonated by acidic zeolite to form carbonates intermediate. Then, the water is eliminated by producing ethylene. However, the diethyl ether can be formed via intermolecular dehydration pathways. Nevertheless, temperature plays a vital factor to control the reaction pathways to achieve the desired products [46].

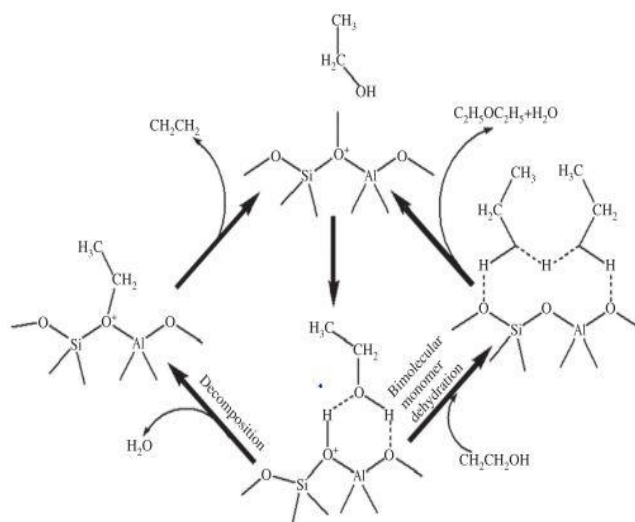


Figure 0.3 The mechanism dehydration of ethanol to ethylene and diethyl ether over zeolite catalyst [46]

2.5 Catalyst deactivation

Catalyst deactivation results in a change of physical and chemical properties of the catalyst [44]. These changes include losing active sites, decreasing surface area or pore volume, and changing phase. Intrinsic mechanisms of catalyst deactivation can be classified into six distinct types: (i) poisoning, (ii) fouling, (iii) thermal degradation, (iv) vapor compound formation accompanied by transport, (v) vapor-solid and/or solid-solid reactions, and (vi) attrition/crushing. Table 2.2 summarises the types and definitions of catalyst deactivation.

Table 0.2 Summarization of catalyst deactivation [44]

Mechanism	Type	Brief definition/description
Poisoning	Chemical	Strong chemisorption of species on catalytic sites which block sites for catalytic reaction
Fouling	Mechanical	Physical deposition of species from fluid phase onto the catalytic surface and in catalyst pores
Thermal degradation and sintering	Thermal Thermal/chemical	Thermally induced loss of catalytic surface area, support area, and active phase-support reactions
Vapor formation	Chemical	Reaction of gas with catalyst phase to produce volatile compound
Vapor–solid and solid–solid reactions	Chemical	Reaction of vapor, support, or promoter with catalytic phase to produce inactive phase
Attrition/crushing	Mechanical	Loss of catalytic material due to abrasion; loss of internal surface area due to mechanical-induced crushing of the

Coke formation in catalytic cracking.

In the catalytic cracking process, carbonaceous deposits, which strongly adsorb on Brønsted and Lewis acid sites and block pore entrances, were found to be the main factor that reduces catalyst activity. It is worth noting that the acidity of the catalyst plays a crucial role in the reaction. In the catalytic field, it is very important to overcome the barrier of catalyst deactivation and to prolong the life of the catalyst. Furthermore, Gusisnet and Magnoux [47] summarized that accelerating coke rate in the zeolite, which is used in the hydrocarbon transformation process, can be attributed to four main factors, as follows;

(1) Nature of reactant

The rate of coke formation depends on the reaction pathways. The olefin tends to coke rapidly due to its easy to produce hydrocarbon pool or coke

precursor. While the conversion of alkane to coke precursor needs more reaction pathways.

(2) Pore structure

There is coke resistance for the smaller pore of zeolite. Besides, the long channel of zeolite can increase the coking rate due to the long contact time to form coke.

(3) Acidity

High acidity and the strong acid site can promote side reactions such as aromatization and isomerization, leading to produce undesired products and coke deposition.

(4) Operating parameters.

The operating parameters such as reaction temperature, space velocity are important factors to control side reactions for coke deposition.

2.6 Zeolite

2.6.1 Zeolite structure

Zeolites, microporous material, are hydrated crystalline aluminosilicate compounds [48]. Typically, the crystal structure of zeolite is classified into two types; primary building units (PBUs) and secondary building units (SBUs) [49]. For the PBUs (Fig.2.4), four oxygen anions are bonded with either silica $[\text{SiO}_4]^{4-}$ or aluminum cation $[\text{AlO}_4]^{5-}$ at the center to form three dimensions as a tetrahedral structure [50].

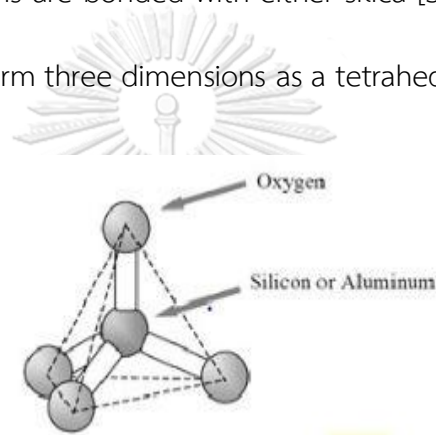


Figure 0.4 Primary building unit (PBU) of zeolite structure [51]

The secondary building units (SBUs) are the combination of PBUs via sharing oxygen atoms to form a specific arrangement of simple geometric forms [51]. This combination also makes the channels and chambers in particular dimensions [50]. Consequently, there are multiple types of SBUs, leading to a unique framework in each zeolite. Nowadays, there are 23 different types of SBUs found in the zeolite structures [50]. Although the classification of zeolite bases on SBUs is commonly used,

it is still not perfect. Fig.2.5 shows the code and secondary building units founding in the zeolite structures.

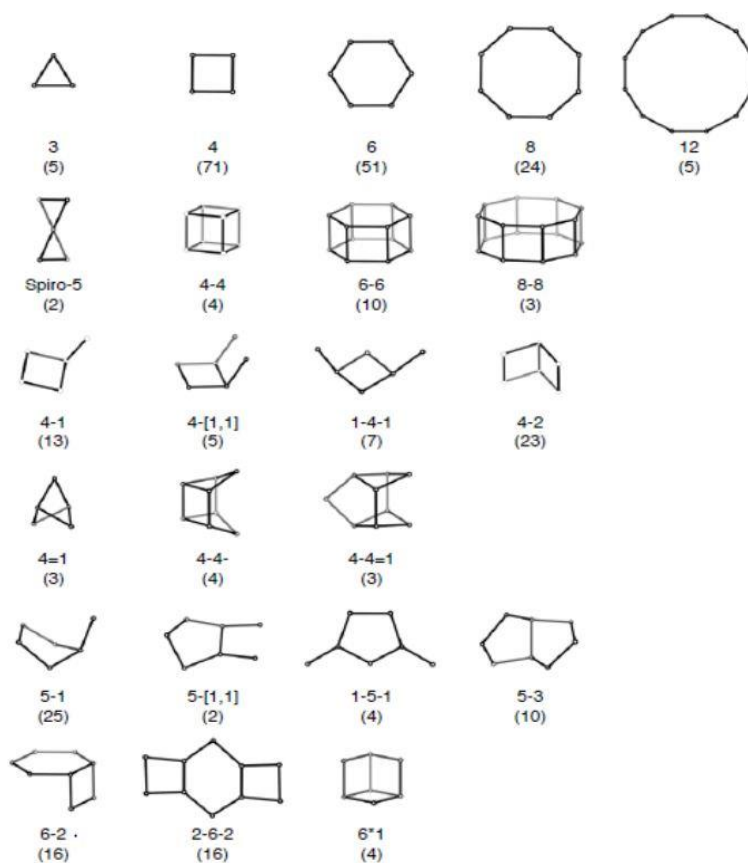


Figure 0.5 Secondary building units founding in the zeolite structures [50]

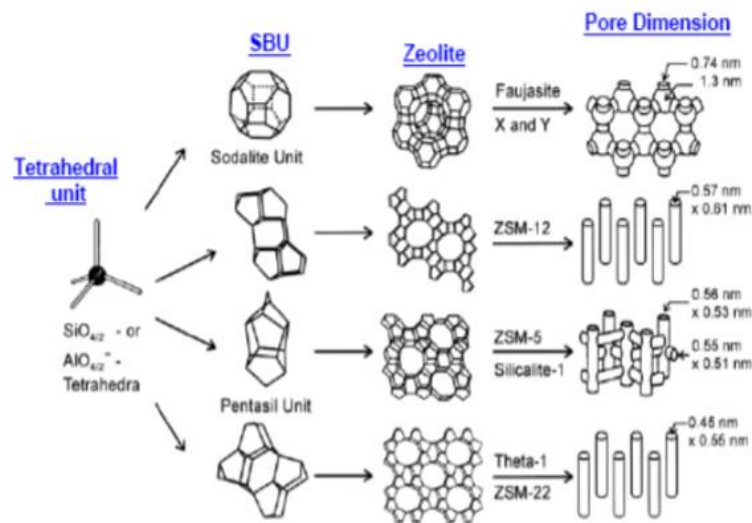


Figure 0.6 The development of zeolite structures from primary building units to secondary building units and zeolite structures [52]

The development of zeolite structures from primary building units to secondary building units and zeolite structures is illustrated in Fig.2.6. Zeolites can be classified into four groups based on the different pore sizes. The ring size of zeolite refers to the number of tetrahedrons, as shown in Fig.2.7. The large pore zeolite consists of 12-membered rings, which diameter is more than 12 Å. For example, zeolite beta, zeolite x, zeolite Y, and mordenite are classified as large-pore zeolites. The medium pore zeolites, for instance, ZSM-5, TS-1, and ZSM-11 contain ten membered rings with a dimension between 5 Å and 6 Å. For the small pore size zeolites, their structures construct 8-membered rings with a diameter less than 6 Å. Zeolite A and chabazite are in this type. In the extra-large groups, the membered ring can be higher than 12, such as VPI-5 [53].

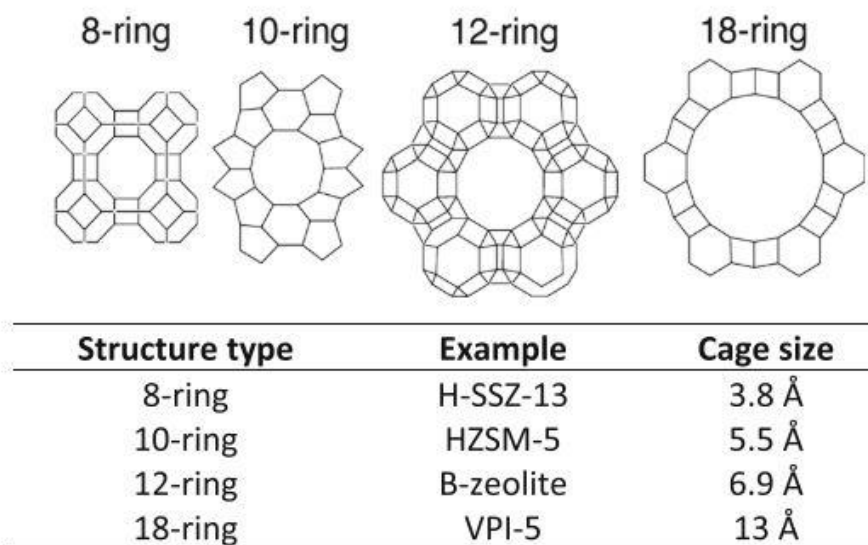
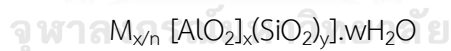


Figure 0.7 The ring size of zeolite refers to the number of tetrahedrons and the example [53].

The empirical formula of aluminosilicate zeolite is expressed based on their crystallographic unit cell, as follows [54] ;



CHULALONGKORN UNIVERSITY

Where M represents the extra framework cations. M is usually an alkali or alkaline earth metal cation, but it can be other metals, nonmetals, or organic cations. x and y are the number of $[SiO_4]^{4-}$ and $[AlO_4]^{5-}$ in the unit cell of zeolites, respectively. w is the water molecules in the zeolite structure [54].

2.6.2 Acidity of zeolite

The acidity of zeolites is one of the essential factors in catalytic activity [55]. Typically, the synthesized zeolite has the cation, such as Ca^{2+} , Na^+ , to balance to charge in the zeolite structure. These cations can be exchanged via an ion-exchange process to proton form and behaved as acidic, as shown in Fig.2.8. The acidity of zeolites is considered into three properties as follows [56];

- (1) Type of acid site: There are three types of acid site. Brønsted acid site (BAS) is the proton donor, while the Lewis acid site (LAS) is the electron acceptor. Also, the silanol group ($=\text{Si-O-H}$), occurring from the crystalline zeolites defect, behaves as acidic.
- (2) Amount of acid site: This property depends on the amount of aluminum atom in the zeolite structure. Besides, the Si/Al ratio can be considered to LAS or BAS in the zeolite structure.
- (3) Strength of the acid site: It is related to the ability of a proton donor or electron acceptor. The strength of the acid site is in the followed order; $\text{BAS} > \text{LAS} > \text{silanol groups}$.

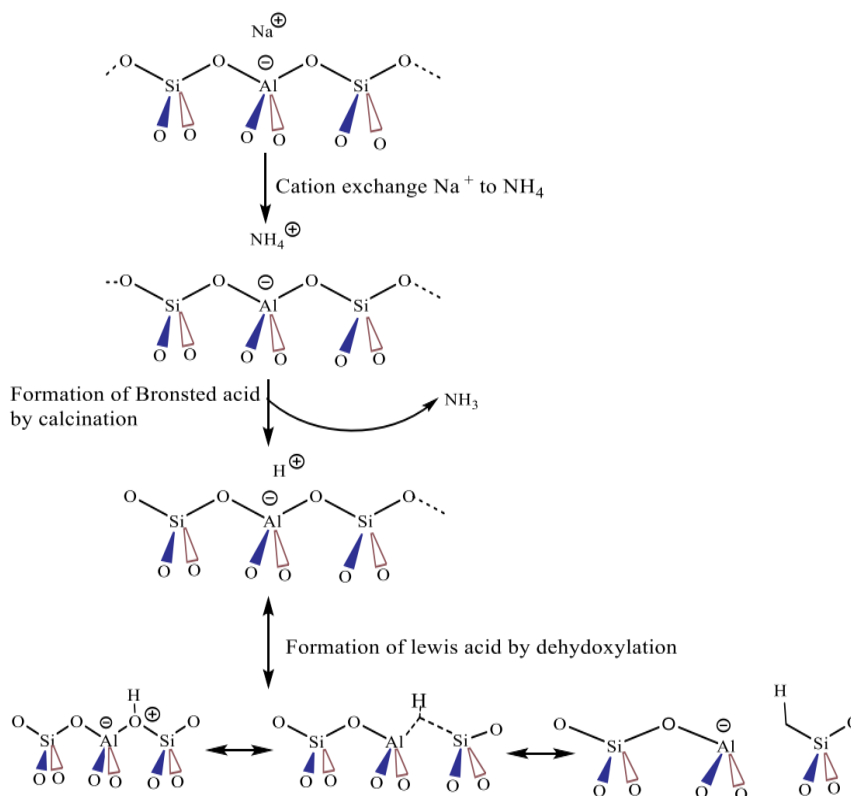


Figure 0.8 The formation of BAS and LAS in zeolite [57]

2.6.3 Shape selectivity

Each zeolite has a unique framework, benefiting the catalytic reaction that requires high selectivity to the product [58], [59]. There are three types of shape selectivity in the zeolite, as shown in Fig.2.9.

(1) Reactant shape selectivity

The reactants with a smaller size than the pore size of the zeolite can diffuse and react in the pore of zeolite. In contrast, the larger molecules of the reactant cannot diffuse into the pore due to the steric hindrance.

Therefore, the kinetic diameter of the reactant and the pore size of zeolites are vital considered factors to predict the reactant shape selectivity, as displayed in Table 2.3. However, the diffusion of the reactant also depends on the reaction temperature.

Table 0.3 Molecular size of reactants and pore size diameter of zeolites

Reactant	Diameter (Å)	zeolite	Pore size diameter (Å)
He	2.5	KA	3.0
NH ₃	2.6	LiA	4.0
H ₂ O	2.8	NaA	4.1
N ₂ and SO ₂	3.6	CaA	5.0
Propane	4.3	Erionite	3.8 x5.2
n-hexane	4.9	ZSM-5	5.4x5.6, 5.2x5.5
i-butane	5.0	ZSM-12	5.7x6.9
Benzene	5.3	CaX	6.9
p-xylene	5.7	Morenite	6.7-7.0
CCl ₄	5.9	NaX	7.4
Cyclohexane	6.2	AIPO-5	8.0
o-xylene and m-xylene	6.3	VPI-5	12.0

(2) Product shape selectivity

Fig.2.9. demonstrated the product shape selectivity of methylation of toluene on ZSM-5. According to the thermodynamic theory, p-xylene is the lowest isomer product. However, p-xylene showed the highest selectivity over ZSM-5 catalyst due to the less steric hindrance, leading to the faster diffusion out of the pore. In the meantime, the other xylene converts to p-xylene via isomerization inside of zeolite. Product shape selectivity also depends on the crystal size of zeolites. The larger crystal size refers to the more extended diffusion pathway, leading to the higher product shape selectivity.

(3) Transition state shape selectivity

The pore size of zeolite is one factor of transition-state shape selectivity. For example, the disproportion of m-xylene gives various trimethyl benzene (Fig.2.9). For FAU as a catalyst, 1,3,5-trimethyl benzene is the major product; while, MOR gives 1,2,4 trimethyl benzene as a significant product. This is because FAU has a big pore-size enough for the transition-state of 1,3,5-trimethylbenzene formation.

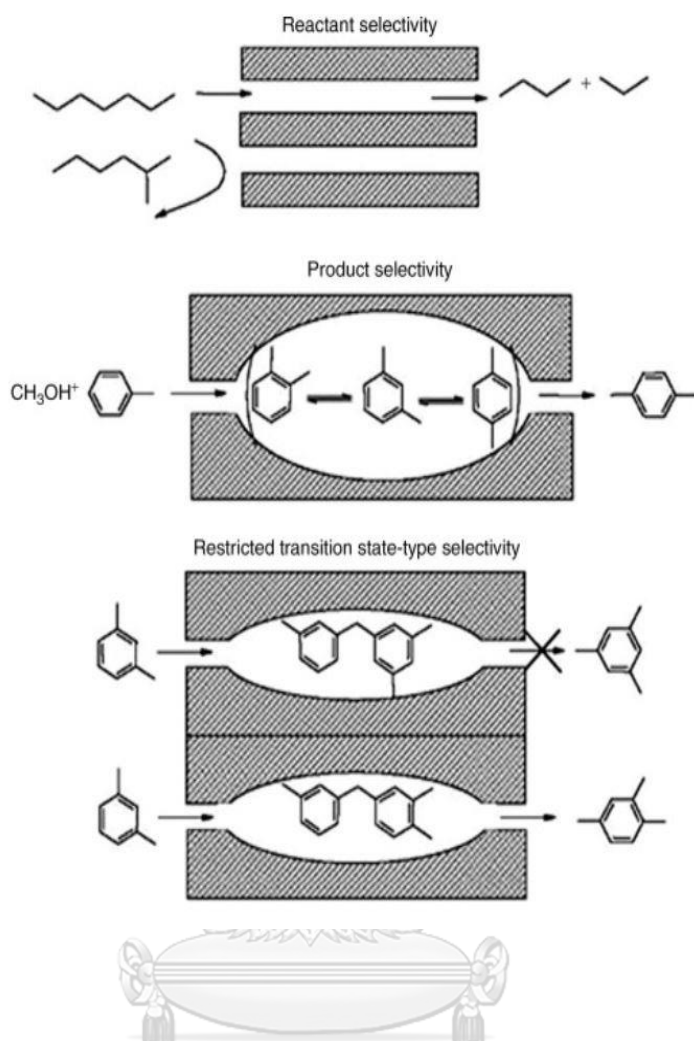


Figure 0.9 Three types of shape selectivity in the zeolite [60]

2.6.4 ZSM-5

ZSM-5 (Zeolite Socony Mobil-5) is microporous material with MFI framework types. The composition of ZSM-5 is $\text{Na}_n[\text{Si}_{96-n}\text{Al}_n\text{O}_{192}] \cdot 16\text{H}_2\text{O}$, where n is between 0 and 27. ZSM-5 was first prepared by Landolt and Argauer in 1965. Then, it was developed and patented by Mobil Oil company in 1972 [61]. Fig.2.10. illustrates the framework of ZSM-5. ZSM-5 has a 10-membered (10 MR) ring structure with a three-dimensions (3D) channel [62]. The straight channel (5.3Å X 0.56Å) is interconnected by the sinusoidal channels (5.1Å X 5.6Å). The less deactivating characteristic of ZSM-5 is the most important factor for application in various catalytic reactions.

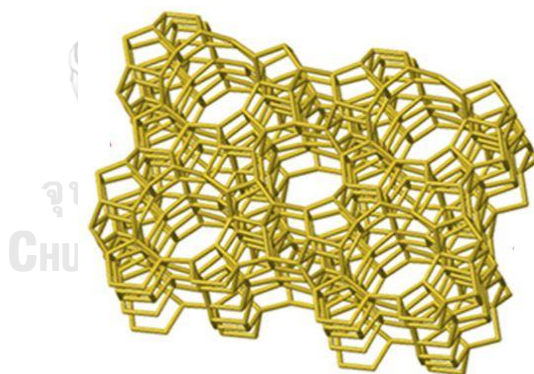


Figure 0.10 Framework structure of ZSM-5 [63]

2.6.5 Zeolite beta

Zeolite beta (IZA code: BEA) was first synthesized and patented by the Mobil Oil corporation in 1967. The chemical formula is $[x\text{Na} \cdot (1-x)\text{TEA}] \text{AlO}_2 \cdot y\text{SiO}_2 \cdot w\text{H}_2\text{O}$; where $x < 1.0$, $5 < y < 100$, and TEA are tetraethylammonium cation. The framework structure of zeolite beta is shown in Fig.2.11. Zeolite beta is classified in a large pore system with 12-membered (12 MR) rings with a diameter of 6.7Å. The three-dimension channel system of BEA consists of two intergrowth structures: polymorph A and polymorph B.

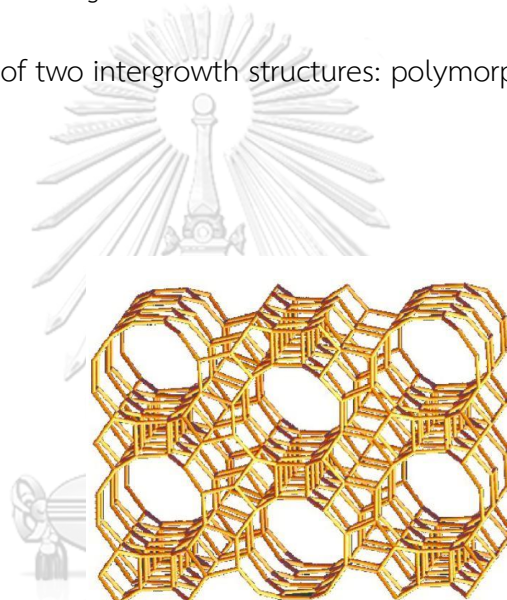


Figure 0.11 Framework structure of zeolite beta [64]

2.6.6 Zeolite Y

Zeolite Y, a faujasite molecular sieve, is an aluminosilicate with FAU framework type. It was synthesized by Breck in 1967. The framework structure of zeolite Y is revealed in Fig.2.12. Zeolite Y has a three-dimensional pore structure with an extensive pore system of 7.4Å diameter. The structural units of zeolite Y are the sodalite cages, consisting of 24 tetrahedra cuboctahedral units.

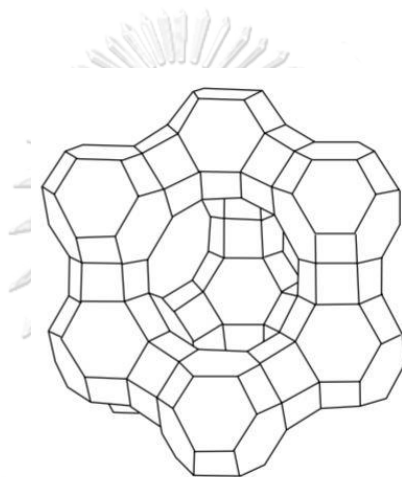


Figure 0.12 Framework structure of zeolite Y [65]

2.7 Heterogeneous catalytic reactor [66]

Nowadays, there are various types of heterogeneous catalytic reactors in the chemical engineer industry. Therefore, to achieve the highest efficiency, multiple factors such as the state of reactants (gas/liquid), kinetic, thermodynamic, and the characteristic of catalyst are all considered crucial points to design a catalytic reactor. Generally, the type of reactor is classified by the relative motion of the catalyst particles, which is the reactors with the significant and insignificant motion of catalyst particles

2.7.1 Insignificant motion catalyst

2.7.1.1 Fixed bed reactor

A fixed bed reactor has been extensively used in the laboratory because it is easy to operate and control the parameters. Additionally, the catalyst can be used in small amounts (approximately 1 g). This reactor can be used in both gas and liquid reactants. There are two main types of this reactor, including (1) single pass and (2) recycle. For The single-pass fixed bed reactor, the reactants are fed through the reactor via the reactor's inlet and an outlet for a single time, as shown in Fig.2.13. Therefore, this type of reactor is suitable for the high catalytic conversion reaction. Meanwhile, the recycle fix bed reactor is ideal for the low conversion reaction. During its process, the unreacted reactants are separated and fed into the reactor for a repeating reaction [67].

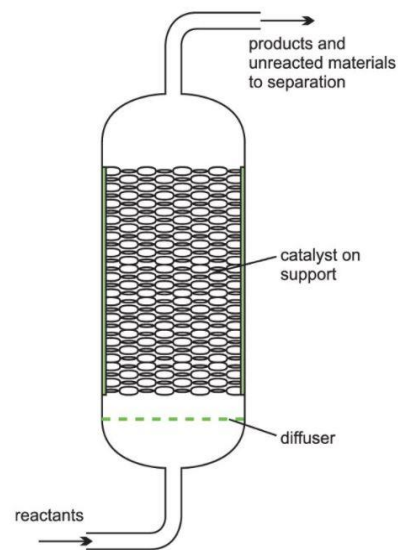


Figure 0.13 Fixed bed reactor [68]

The advantages of this reaction are it is easy to scale up from laboratory scale to pilot plant. Moreover, the catalytic separation section is unnecessary in this reactor. However, the catalyst has to be formed before packing because catalyst powder can cause a pressure reduction in the reactor.

2.7.1.2 Trickle bed reactor

Trickle bed reactor is considered as the simplest reactor type for the catalytic reaction where both reactants are gas or liquid. Fig.2.14 shows the diagram of the trickle bed reactor. For the counter-current system, the liquid is fed on the top of the column through the packed catalyst inside the reactor; meanwhile, the reactant as gas is fed into the bed at the bottom of the column. In the case of co-current systems (downflow or up-flow), the reactants are mixed and fed into the packed catalyst. The unreacted reactant is provided to the reactor again after separated from the mixture products. However, the trickle bed reactor has an expensive operating cost in the pilot plant [69].

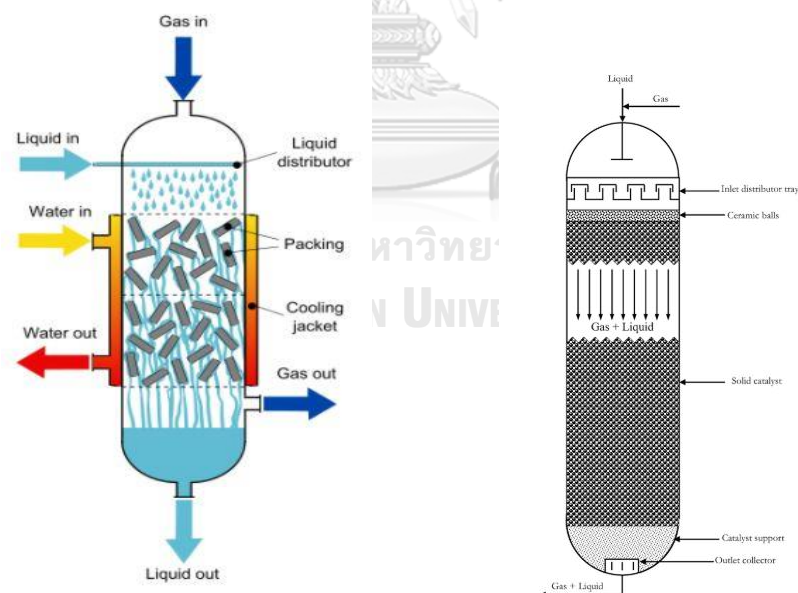


Figure 0.14 Trickle bed reactor [70]

2.7.1.3 Moving bed reactor

A moving bed reactor (MBR) is not extensively used due to some limitations, such as it required superior control and hard to operate. Fig.2.15 displays the Moving bed reactor diagram. Normally, MBR consist of the catalytic reactor part and the regeneration part. The reactants are put through in the catalytic reactor. During this process, the catalysts in granule form move along in the catalyst layer and react with the reactant. The unreacted reactants are further separated in the regeneration unit and reused again in the reactor unit.

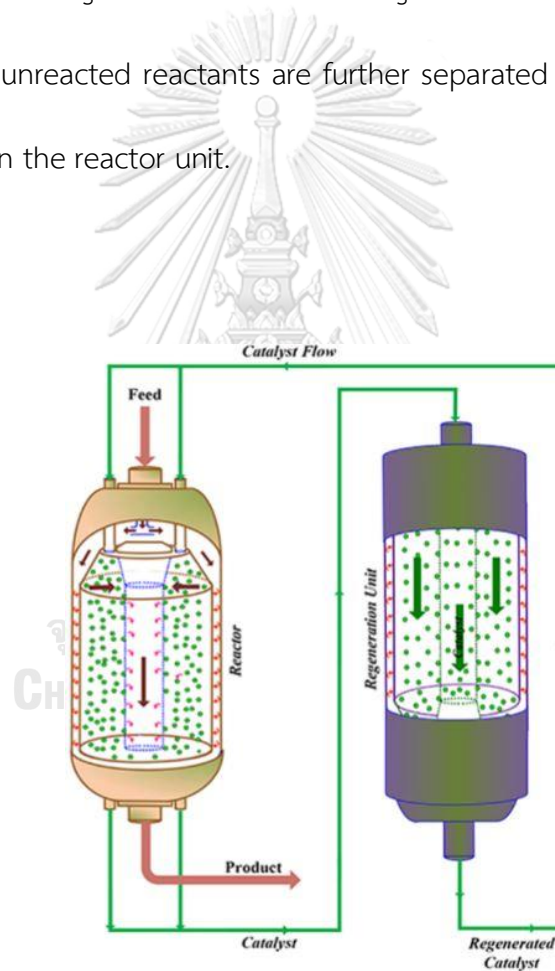


Figure 0.15 Moving bed reactor [71]

2.7.1.4 Rotating packed bed reactor

A rotating packed bed reactor (RPB) has been developed in order to enhance the mass transfer in different phases. Commonly, the RPB reactor is suitable for the heterogeneous system with the solid-liquid reaction. In the reactor, the catalysts are packed in a rotating cylinder connected with the motor, as can be seen in Fig. 2.16. The reactants (liquid/gas) are fed through the reactor while the rotating cylinder is spinning, enhancing the dispersion between different phases. However, there is limited use for this reactor in the industrials [72].

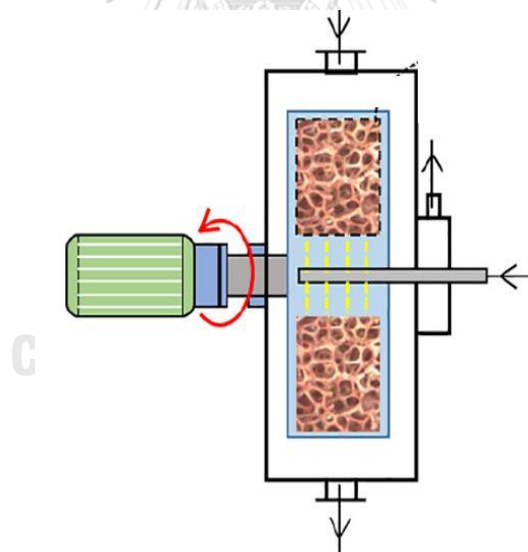


Figure 0.16 Rotating packed bed reactor [73]

2.7.2 Significant motion catalyst

2.7.2.1 Fluidized bed reactor (FBR)

A fluidized bed reactor has been used in many industrials (Fig. 2.17). This reactor has a high potential for mass transfer and heat transfer. According to the principle, the carrier fluid (gas or liquid) is fed upward through the solid materials with high speed at the bottom to depart on the top of the reactor. The bubble occurs during this process. The solid materials can be the catalyst, reactant, or inert. Therefore, this reactor can be used for both catalytic and non-catalytic reactions. This reactor is suitable for high conversion and exothermic reactions [66].

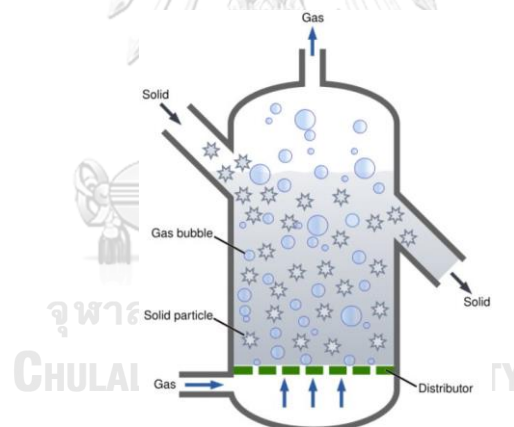


Figure 0.17 Fluidized bed reactor (FBR)

A fluidized bed reactor has several advantages, such as the ability to operating the reactor in a continuous flow, excellent particle mixing, and uniform temperature gradients. Nevertheless, there are some drawbacks, such as pressure drop and erosion. This reactor is suitable for high conversion and exothermic reactions [74].

2.7.2.2 Slurry reactor

A slurry reactor has been widely used in biochemical, petrochemical, and environmental processes. This reactor is the multiphase (solid, liquid, or gas) reactor, as displayed in Fig. 2.18. The catalyst can be powder or granular form. The reactant gases are fed and dissolved in liquid, followed by spread to the surface of the catalyst. The advantages of the slurry reactor are (1) easy to set on a large scale, (2) excellent in temperature control, and (4) high catalytic activity. Moreover, this reactor can operate in both semi-batch and continuous mode. However, this reactor is needed to separated catalyst from the liquid, which is a complicated process.

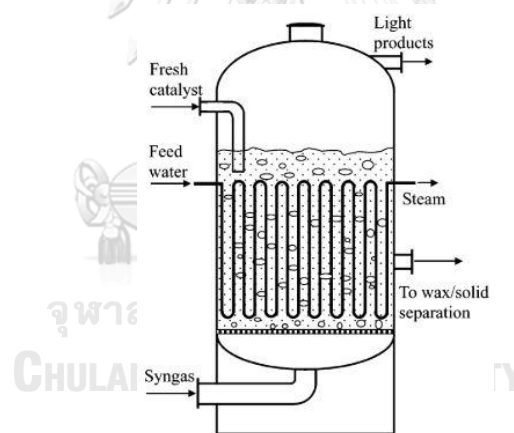
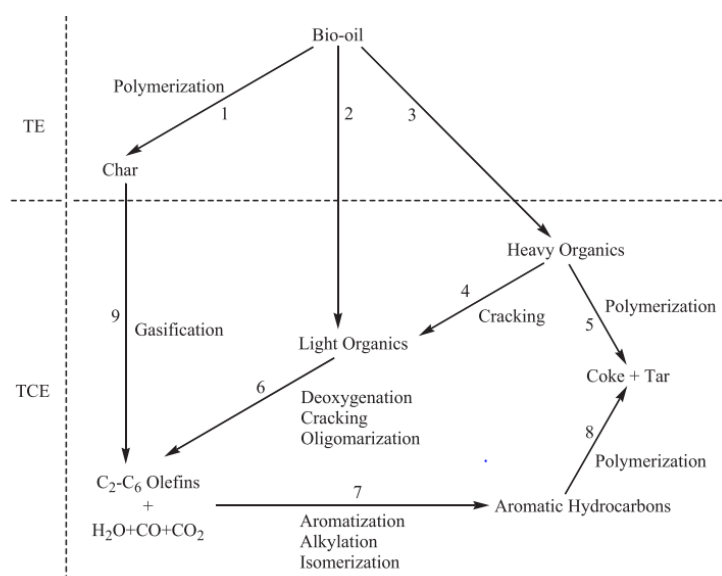


Figure 0.18 Slurry reactors [75]

2.8 literature reviews

2.8.1 Catalytic conversion of oxygenated compounds over zeolites



Scheme 1. Overall reaction pathway proposed for conversion of bio-oil over zeolite catalysts (TE: thermal effect; TCE: thermo-catalytic effect).
Adopted from Ref. [31].

Figure 0.19 Overall reaction pathway for conversion of bio-oil over zeolite catalyst
(TE: Thermal effect, TCE: Thermo-catalytic effect)

Rezaei et al. [15] reviewed the catalytic cracking of bio-oils over zeolites catalysts. The overall reaction pathway for conversion of bio-oil is shown in Fig. 2.19. Typically, the reactions are performed at a medium temperature range between 350-650°C at atmospheric pressure under the presence of a catalyst. As revealed, the thermal effect plays a vital role in the converting of bio-oil to chars, light organics, and heavy organics. Under the catalytic condition, the heavy feedstocks can be transformed into the desired products, such as light olefins and aromatic hydrocarbons, via various catalytic reactions. Once the heavy hydrocarbons are cracked into the

lighter ones, the light oxygenated hydrocarbons are deoxygenated with depleting the oxygen as H_2O , CO , and CO_2 . Moreover, various reactions such as cracking and oligomerization occur with converting into C2-C6 light olefins over acidic zeolites. These light olefins are further converted to aromatic hydrocarbons via aromatization, alkylation, and isomerization. The coke formation is the polymerization of aromatic hydrocarbons. Therefore, the catalyst and reaction conditions play critical roles to control the desired products and suppress coke deposition.

Zhang [26] et al. developed co-fast pyrolysis of fusel alcohol and biomass to enhance aromatic hydrocarbon products. The reaction was carried out in a fluidized bed reactor over a ZSM-5 catalyst. The influent of co-CFP temperature, catalyst loading, and the mass ratio of fusel alcohol to biomass were also evaluated. The high catalyst loading amount favored aromatics because of the associability of acid sites and the optimal temperature was up to $500^\circ C$. The maximum carbon and hydrogen yield of total aromatic hydrocarbons (94.0% and 52.7%, respectively) were obtained at a temperature of $550^\circ C$, and the fusel alcohol/biomass mass ratio of 1:1 with a catalyst to feedstock ratio of 1:5. Fig. 2.20 reveal the pathway of the co-conversion of fusel oil and biomass to aromatic hydrocarbons. Under optimal conditions, fusel oil is deoxygenated to the hydrocarbon pool as intermediated to aromatic hydrocarbons. In addition, the depolymerization of hemicellulose fragments and bio-derived anhydro-oligosaccharides produce furans. These reactants can be combined with the olefins

from fusel oil dehydration via diel alder reaction. Then, their further deoxygenated to the desired aromatic rings (benzene, toluene, xylene).

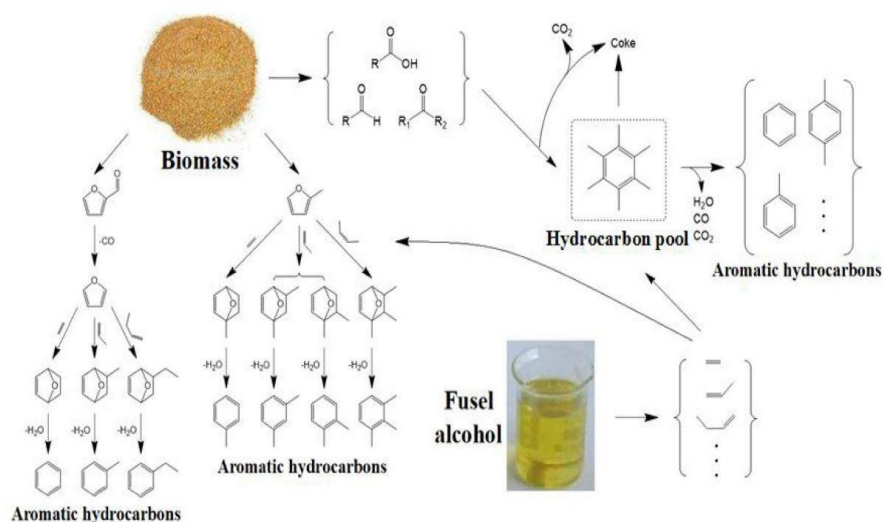


Figure 0.20 overall reaction pathway for co-pyrolysis of biomass and fusel oil over a zeolite catalyst.

Babu *et al.* [76] modified the alumina, zeolite, silica-alumina, and zeolite by doped with Alkali and Phosphoric acid and investigated their performance dehydration of isoamyl alcohol. Product composition obtained from dehydration isoamyl alcohol reactions is 3 methyl-1-butene, 2-methyl-1-butene, 2-methyl-2-butene, C1-C4, and others. They found that the catalytic performance and product distribution was depended on the nature of the active center. On less acidic supports such as silica, progressively doping with phosphoric acid enhances the alcohol conversion selectively to dehydrated/isomerized products.

Nash *et al.* [77] investigated the dehydration of mixed alcohol over Brønsted and Lewis acidic catalysts. In this study, they focus on the catalytic activity and selectivity of 4 Brønsted and Lewis acidic catalysts for this reaction. A Lewis acidic Zr-incorporated mesoporous silicate (Zr-KIT-6), a commercial Al-containing mesoporous silicate (Al-MCM-41), a commercial microporous aluminosilicate (HZSM-5), and a commercial microporous silicoaluminophosphate (SAPO-34) were used in various range of temperature. Among them, the zeolite materials displayed a 98% of ethanol conversion at all temperatures while the mesoporous materials only revealed a significant activity at above 300 °C. They explained that is because Brønsted acidic sites are more active than Lewis acidic sites for alcohol dehydration.

2.8.2 Role of feedstocks

Chen *et al.* [25] studied the catalytic cracking of bio-oil over HZSM-5 in a fluid catalytic cracking. The different bio-oil compounds such as n-heptane, acetic acid, ethyl acetate, acetol, acetic acid, and guaiacol were employed as feedstocks. Under the same reaction condition, the different catalytic activity and product distribution were obtained by different feedstocks. At 500°C with a feed flowrate of 0.5ml/min, the highest olefins yield was obtained from Acetic acid at 68.3%, followed by ethyl acetate (51.3%), cyclohexane (30.7%), n-heptane (27.5%), and Guaiacol (16.5%). The tendency of carbon olefins selectivity decreases in the following order;

ethylene>propylene>butylene. Thus, the reactant of catalytic cracking reaction plays an important role in the reaction pathway to product distribution.

Zhang et al. [78] employed HZSM-5 catalyst over the catalytic fast pyrolysis of pinewood, and the mixture of alcohols. The reaction was carried out in a bubbling fluidized bed reactor. The effect of feedstocks was investigated by the addition of alcohol in a different ratio. They found that the catalytic performance and product selectively depend on the hydrogen to carbon effective (H/C_{eff}) ratio of feedstock. With H/C_{eff} ratio increasing, the C2-C4 olefins yield and aromatic yield both rose. This might be due to the alter of the hydrocarbon pool in the reaction pathways after additional alcohol.

A similar trend was observed by Zhang et al. [18], they studied the catalytic conversion of different biomass feedstocks over modified HZSM-5 catalysts. Corn stalks, cellulose, hemicellulose, and lignin were selected as feedstocks. At 600°C and a gas rate of 100ml/min, cellulose gave a maximum weight yield of olefins (4.36%wt); while lignin gave a minimum amount of 1.26%. They reported that the high C/H ratio could easily convert to light olefins. Besides, the smaller oxygenated molecules are more easily to be transferred and adsorbed on the catalyst sites, leading to higher light olefins production.

2.8.3 Role of zeolite topology

Luo et al [24]. studied the influence of zeolite topology on n-Hexane cracking using four well-known zeolites (HZSM-5, H-BEA, HMOR, and USY). The reaction was performed at a temperature range between 300°C to 450°C with a pressure of 1-137 bar. Table 2.4 compares the catalytic cracking of n-hexane over HZSM-5, H-BEA, HMOR, and USY. Under reaction temperatures of 350°C and 137 bar, the H-BEA showed the highest n-hexane cracking conversion at 15.4%, followed by USY (12.1%), HZSM-5 (11.7%), and H-MOR (6.8%). The high catalytic performance of H-HBA and USY is because of their larger open pore, which allows the reactant molecules to flow through inside of zeolite. However, HZSM-5 gave a greater propylene selectivity (10.3%) compared to other zeolites. This result is due to the moderate pore size and unique framework of HZSM-5, which suitable to produce light olefins and suppress isomerization in the reaction pathways.

Table 0.4 Molar selectivity (%) for n-hexane cracking over HZSM-5, HBEA, and HMOR

	H-ZSM-5	H-BEA	USY	H-MOR
<C ₂	<0.5	<0.5	<0.5	<0.5
C ₃	10.3	4.7	2.2	8.2
Iso-C ₄ H ₁₀	14.1	16.4	6.7	13.3
n-C ₄ H ₈	1.8	-	-	-
n-C ₄ H ₁₀	17.6	3.7	1.5	6.4
Iso-C ₅ H ₁₂	11.0	12.3	6.4	11.7
n-C ₅ H ₁₂	20.7	4.1	1.4	3.8
n-C ₆ H ₁₂	3.3	-	-	-
Iso-C ₆ H ₁₄	14.6	55.8	79.8	56.6
>C ₇	6.2	2.8	1.7	<1
Conversion (%)	11.7	15.4	12.1	6.8

S.B Sousa et al. [79] examined the role of the pore structure of HMCM-22 and HZSM-5 on the bioethanol conversion into hydrocarbons over the coke deposition and product distribution. According to their results, HMCM-22 zeolites showed a higher coke formation than HZSM-5. The authors reported that HMCM-22 has a large porous structure (7.1 × 18.2 Å, and 4.0 × 5.5 Å) that favored accommodating the bulky intermediate precursors of coke formed. Even though HZSM-5 exhibited a high acidity which favored the formation of coke, it gave less amount of coke and aromatic hydrocarbons due to its suitable framework structure.

2.8.4 Effect of co-feeding water

Gilbert et al. [80] studied the influence of co-feeding water on converting lignocellulose (Furan) into aromatic and light olefins via a catalytic fast pyrolysis process. The reaction was carried out over HZSM-5 in a continuous flow fixed bed reactor. The partial water pressure was various between 0 and 28 kPa. At 600°C, the furan conversion rose from 48.4% at 0 kPa to 84.8% at 28 kPa with increasing water pressure. Besides, there was an increase in light olefins, while the aromatic yield declined by increasing water addition. These results show that water addition can enhance the catalytic performance because water promotes the hydrolysis reaction in furan conversion. However, water can cause zeolite deactivation by dealumination, leading to the loss of the acid site of the catalyst.

Dong et al. [81] explored the catalytic pyrolysis of microalga *chlorella pyrenoidosa* over a modified HZSM-5 catalyst in a two-step reaction system. The light olefins (ethylene, propylene, and butanes) were the target products. The effect of water flow rate was studied by various water flow rates from 10 ml/hr to 60 ml/hr. Under the reaction temperature of 550°C, the results showed that the total carbon olefins yield increased from 21% at the water flow rate of 10 ml/hr to the highest point (30%) at 30ml/hr. Then, it dropped to 18% at 60 ml/hr. They reported that the effect of water is related to the contact time between reactants and the catalyst sites. In other words, a high water flow rate leads to short contact time for cracking to light olefins. Conversely, a low flow rate can cause an undesired reaction, contributing to the long-chain hydrocarbons or aromatic hydrocarbons.

Blay et al.[30] reported that the effect of water is dependent upon reaction variables. At low temperatures (400°C), water is adsorbed on the bridging hydroxyl groups of zeolites, leading to the reduction in the active sites. At high temperatures (500°C), the water behaves as a heat carrier and as a diluent in the fluidized catalytic cracking process.

Lehmann et al. [82] studied the thermodynamic appraisal of gas-phase conversion of ethylene to propylene. The impact of co-feeding water on the conversion of ethanol to propylene was examined. The addition of water in the system acts solely as a quasi-inert diluent from the thermodynamic perspective. Fig. 2.21

displays the effect of co-feeding water and temperature on the yield of propylene at 1 bar. As revealed, the trend of propylene yield on the function of water/ethanol ratio changes with adjusting the temperature from 250°C to 750°C. Thus, the effect of co-feeding water also depends on temperature. However, they reported that equilibrium calculations of co-feeding water on the conversion of ethylene to propylene is needed to study and improve in future work.

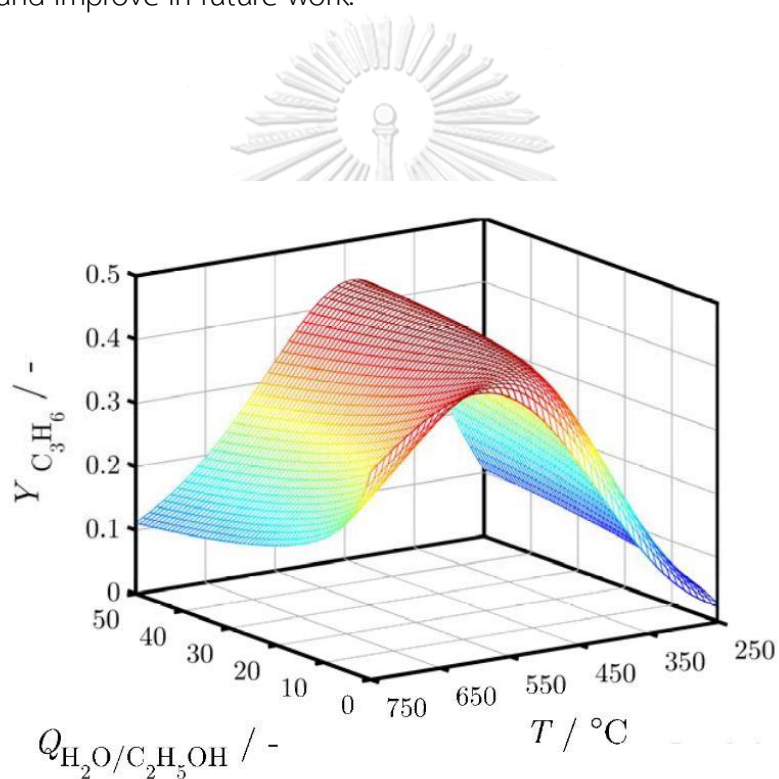


Figure 0.21 The effect of co-feeding water on the conversion of ethanol to propylene on the function of reaction temperature.

2.8.5 Role of operating parameters

2.8.5.1 Effect of reaction Temperature

Zhang et al. [18] investigated biomass conversion (cellulose) to light olefins over Fe-modified ZSM-5. The effect of reaction temperature was studied by various temperatures from 400°C to 700°C under in-situ experiment conditions. Based on olefins carbon selectivity, the ethylene yield increased from 55% at 400°C to 67% at 700°C. Meanwhile, the propylene and butylene yield fell with increasing temperature. They reported that high temperature could promote cracking reaction to form small olefins (C₂H₄, C₃H₆). However, the temperature up to 700°C can cause thermal cracking and secondary cracking reaction, leading to the smaller undesired products such as CO₂ and CH₄. Thus, the reaction temperature plays a vital role in product selectivity on the catalysis conversion of biomass to light olefins.

Gong et al. [19] examined the catalytic cracking of bio-oil to light olefins over 6wt% La/HZSM-5. The catalytic reactions were performed in a continuous flowing fixed-bed reactor. The effect of reaction temperature was studied by varying the temperature from 500°C to 750°C at WHSV= 0.4 h⁻¹. The total carbon conversion of bio-oil was over 70% at 500°C and almost reached 100% at the reaction temperature of 750°C, indicating the favorable of oxygenated cracking at high temperature. Nevertheless, the light olefins yield was most elevated at 600°C, then fell slightly at 750°C. Conversely, the selectivity of CO₂ and CH₄ increased with increasing

temperature. These results agree with Zhang et al. The secondary cracking at too high temperature leads to undesired product and coke deposition.

2.8.5.2 Effect of space velocity

Sousa et al. [79] studied the influence of reaction space velocity (WHSV) on ethanol conversion into olefins and aromatics over HZSM-5 zeolite by various space velocities ($165-0.65 \text{ g}_{\text{ethanol}}\text{g}_{\text{cat}}^{-1}\text{h}^{-1}$). The highest aromatic hydrocarbons (BTX) were found at the lowest space velocity (0.65) due to long-chain hydrocarbons forming at long contact times. Moreover, the long contact time leads to coke formation via undesired reactions such as oligomerization, isomerization, H-transfer, aromatization, Diel alder reaction. In contrast, the light olefins (ethene, propene, butenes, and pentenes) were favorable by moderate contact time ($6.5 \text{ g}_{\text{ethanol}}\text{g}_{\text{cat}}^{-1}\text{h}^{-1}$).

2.8.6 Stability of zeolite on catalytic cracking

Nabavi et al. [83] studied the stability of ZSM-5. They reported that HZSM-5 is one of the important in the petrochemical industry due to its acidity and high thermal stability. Besides, Brønsted acid site of HZSM- 5 is the catalytically active site in various reactions such as cracking, isomerization, and dehydration reaction. Typically, the HZSM-5 has high thermal stability up to 900°C. Nevertheless, the zeolite can be deactivated by dealumination with the stream treatment around 500°C. Under the stream condition and high temperature, the hydrolysis of the Si-O-Al bond causes the loss of aluminum oxide, leading to acidity reduction and destructure.

Rahat Javaid et al. [84] investigated the coke formation on HZSM-5 during the catalytic cracking of naphtha to benzene, toluene, and xylene (BTX). Fig. 2.22 shows the possible routed catalytic cracking of naphtha. The reactants are cracked to light olefins via intermediates. BTX can be formed by light olefins or intermediate and diffuse out as products. However, BTX can convert to a coke precursor inside the micropore of ZSM-5 and then transform to coke deposits at the outer surface of HZSM-5. This coke blockage leads to reduce the accessibility of reactant to the active site inside the pore of ZSM-5. Therefore, the shorter residence time of the reaction can suppress coke formation. For example, the smaller crystalline size and shorter channel of zeolite reduce the contact time inside the pore of zeolite.

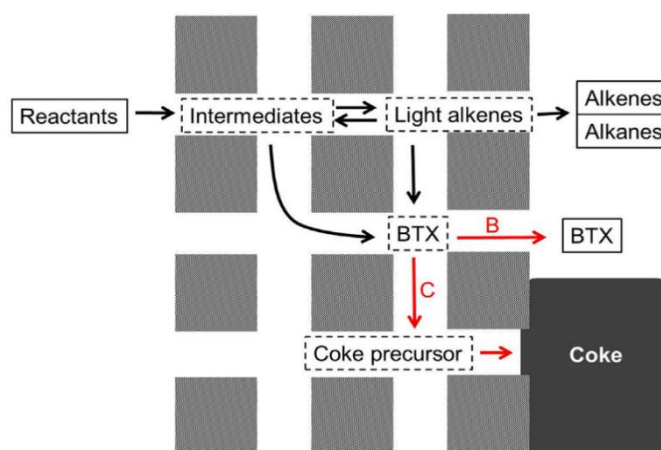
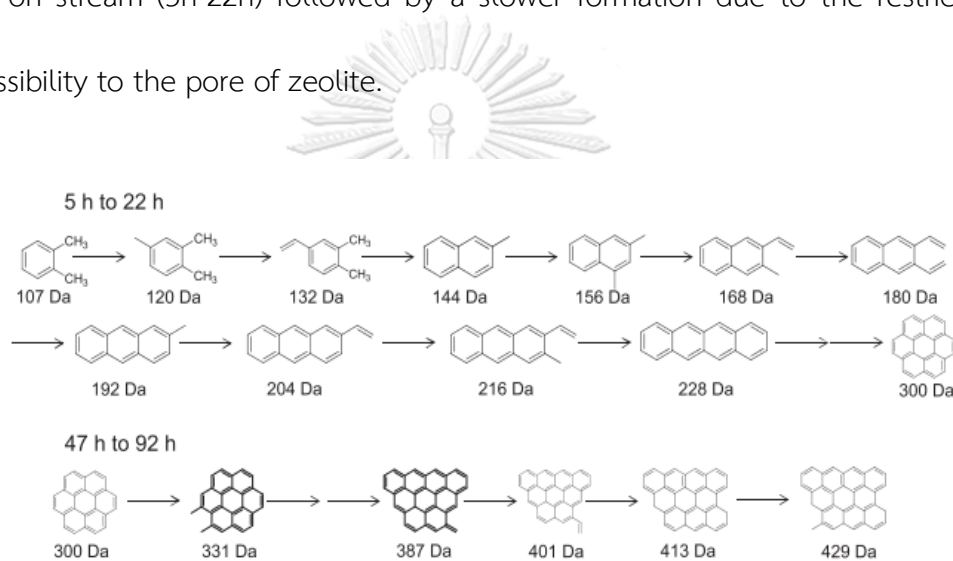


Fig. 9. Reaction routes of catalytic naphtha cracking on H-ZSM-5 catalysts.

Figure 0.22 Reaction route of catalytic cracking of naphtha on ZSM-5 catalyst

Similar to

Müller et al. [85], the coke formation on methanol to olefin (MTO) is formed outer surface of zeolite, leading to Brønsted acid site inaccessibility. The possible route of coke formation versus time on stream is displayed in Fig. 2.23. The aromatic coke is mostly formed via the hydrogen transfer of olefin. Then, multiple methylation reactions or polymerization occur to grow the carbon. Coke is formed rapidly at a short time on stream (5h-22h) followed by a slower formation due to the restriction of accessibility to the pore of zeolite.



Scheme 2. Possible route of coke formation on the outer surface.

Figure 0.23 Possible route of coke formation on the outer surface

CHAPTER 3

METHODOLOGY

3.1 Chemicals

All materials and sources are listed in table 3.1. All chemical was used without further purification.

Table 0.1 The list of chemicals and sources.

Chemical	Source
Fusel oil, the composition as follows; <ul style="list-style-type: none"> - Isoamyl alcohol (66.7wt%) - isobutanol (12.3wt%) - butanol (0.7wt%) - n-propanol (4.3wt%) - ethanol (3.4wt%) - water (12.6 wt%) 	KTIS bioethanol Co., Ltd, Thailand
Methanol (CH ₃ OH, 99.9%, AR)	QRèC, New Zealand
Ethanol (C ₂ H ₅ OH, 99.9%, AR)	QRèC, New Zealand
1-propanol (C ₂ H ₅ OH, 99.5%, AR)	QRèC, New Zealand
1-Butanol (C ₂ H ₅ OH, 99.5%, AR)	QRèC, New Zealand
Isobutyl alcohol (C ₂ H ₅ OH, 99.0%, AR)	QRèC, New Zealand
Isoamyl alcohol (C ₂ H ₅ OH, 98.5%, AR)	QRèC, New Zealand
DI water	-
Zeolite beta (NH ₃ form, SiO ₂ /Al ₂ O ₃ = 40),	TosohCorporation, Japan
Zeolite Y (NH ₃ form, SiO ₂ /Al ₂ O ₃ = 12),	Tosoh Corporation, Japan

Chemical	Source
Zeolites ZSM-5 (NH ₃ form, SiO ₂ /Al ₂ O ₃ = 40),	Tosoh Corporation, Japan
Silica gel	
Wij's solution	Panreac Quimica, Spain
Potassium iodide (KI)	Ajax Finechem, Australia,
Nitrogen gas (N ₂ , 9.999% purity)	Praxair, America
Standard synthesis gas (1% of H ₂ /CO/CH ₄ /C ₂ H ₂ /C ₂ H ₆ bal N ₂)	BOC scientific
Quartz Wool	

3.2 Instruments

1. Fixed bed reactor
2. Furnace
3. HPLC pump
4. Mass flow controller
5. Thermocouple
6. Temperature controller
7. Vaporizer
8. Water trap
9. Cooling trap
10. Heating tape
11. Pressure gauge



12. Flow bubble checking

13. Gas chromatography (Shimadzu GC-2014) connected with FID detector and TCD detector

3.3 Physicochemical properties of fusel oil

3.3.1 The higher heating value (HHV)

The higher heating value (HHV) was determined by the standard ASTM D240 test method using a 6200 Parr bomb calorimeter.

3.3.2 Density

Density was measured at 20°C using a hydrometer, according to the ASTM D1298 method

3.3.3 water content

The water content was measured by the ASTM D6344 method using Karl Fisher titration.

3.3.4 Chemical composition of fusel oil

The chemical composition of the fusel oil was calculated by the standard sample test using gas chromatography (GC) with a flame ionization detector (FID). The injection and the detector temperature were set at 200°C, and 180°C, respectively. The column temperature program was set as in table 3.2. The selectivity of each component in fusel oil was calculated as the following

$$selectivity (\%) = \frac{A_Y \times 100\%}{A_{total}}$$

Where; A_Y represents the peak area of substance Y and A_{total} is the peak area of total substance in a liquid.

Table 0.2 Temperature program for fusel oil components analysis

Temperature (°C)	Rate (°C/min)	Hold (min)
50	10	3
100	5	0
150	3	0
180	-	32

3.4 The textural properties and acidity of zeolites

The textural properties of all three zeolite catalysts were measured by nitrogen (N_2) adsorption-desorption isotherms at 77 K using a Quantachrome (AUTOSORB 1) instrument. Before measurement, each sample was pretreated at 400 °C for 3 h under low pressure (vacuum) to eliminate adsorbents from the surface. The specific surface area was determined by the Brunauer-Emmet-Teller (BET) equation. The total pore volume was calculated from the adsorbed amount at $p/p_0 > 0.99$, while the average pore size was determined from the BJH desorption branch.

The acidity of zeolites was evaluated using ammonia-temperature programmed desorption (NH_3 -TPD). Each sample was first degassed at 300 °C under a helium atmosphere for 1 h. After NH_3 adsorption to saturation, the temperature program was increased from room temperature to 600 °C at a constant ramp rate of 10 °C/min to desorption.

3.5 Catalytic cracking performance

The catalytic cracking reactions were performed in a fixed bed reactor. Fig. 3.1 displays the diagram of the catalytic cracking of fusel oil in a fixed bed reactor. The reactor is stainless steel with 6.6 mm of internal diameter and 40 cm of total effective length. In catalyst packing, 0.2 g of zeolites catalyst catalytic were loaded in the reactor. The quartz wool (0.05 g) was inserted into the top and bottom of the catalyst inside the reactor. Nitrogen gas was fixed at 20 ml/min and fed into the system during the

reaction. The vaporizer and the furnace were heated to 300°C and desired reaction temperature (350, 450, 550, and 650°C), receptivity. In a typical cracking process, the fusel oil was fed to vaporized by HPLC pump at the desired feed flow rate (0.02, 0.04, 0.08, and 1.6 mL/min). Then, the liquid fusel oil turned to volatilized fusel oil and flowed to the reactor. After reaction completion, the heavy mixture product was trapped in the cooling trap. The light mixture gases products were checked the flowrate by a bubble flow meter and further investigated by gas chromatography.

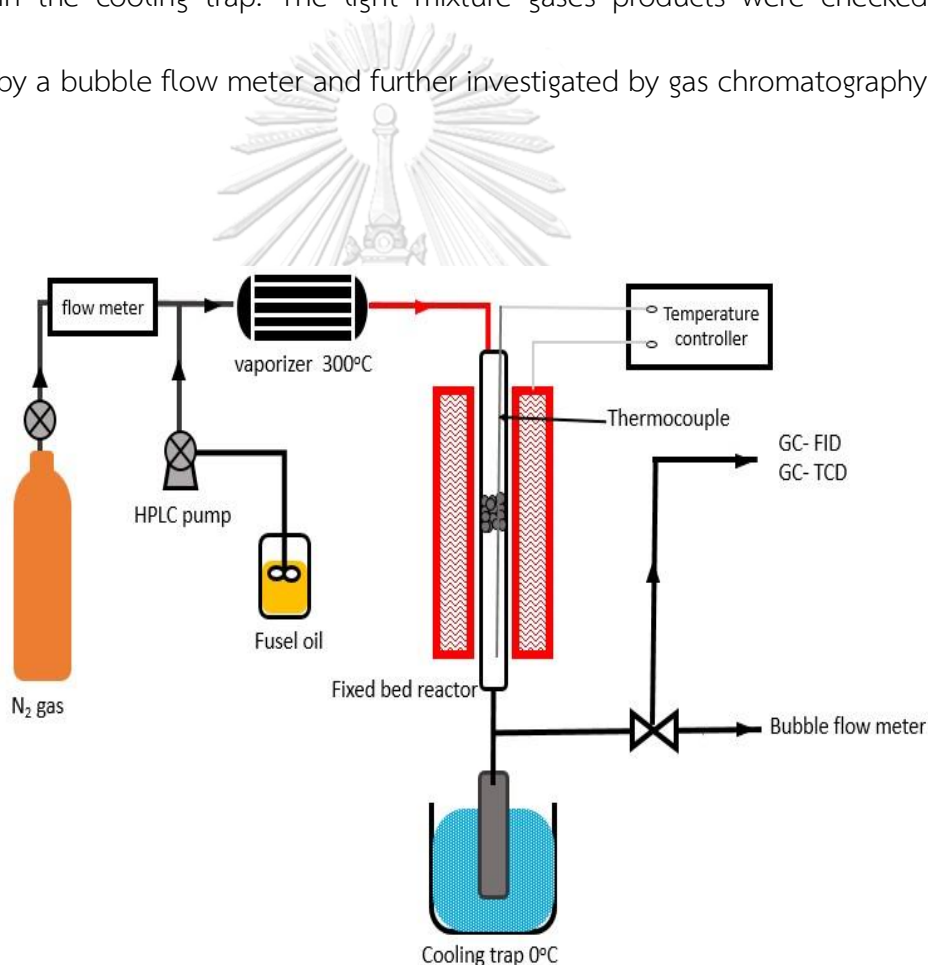


Figure 0.1 Schematic diagram of the fixed bed reactor process for catalytic cracking of fusel oil

3.5.1 Effect of zeolite topology

Three well-known zeolites, H-beta, HZSM-5, and HY are selected to study the effect of zeolite topology. The reactions were performed at 550°C and fusel oil feed flowrate of 0.04 mL/min with a catalyst loading of 0.2 g.

3.5.2 Effect of reaction temperature

The effect of reaction temperature was investigated over HZSM-5 by four different temperatures (350, 450, 550, and 650°C). The fusel oil feed flowrate at 0.04 mL/min was fixed at 0.04 mL/min with a catalyst loading of 0.2 g.

3.5.3 Effect of feed flowrate

The feed flowrate of fusel oil was varied from 0.02 to 1.6 mL/min to study the effect of space velocity. The weight hourly space velocity (WHSV) was represented in Appendix A-2. The other parameters were fixed at the temperature of 550°C and the HZSM-5 catalyst loading of 0.2 g.

3.5.4 Effect of feedstock

Five pure chemical components in fusel oil (e.g. ethanol, propanol, isobutyl alcohol, and n-butanol, isoamyl alcohol), were employed as feedstock to study the effect of feedstock on the catalytic cracking activity. The model fusel oil, the manual mixture of the fusel oil components in the same ratio of fusel oil, was also tested to compare the catalytic cracking of fusel oil. The reactions were performed at 550°C

over HZSM-5 catalyst with the fusel oil feed flow rate of 0.04 ml/min and catalyst loading of 0.2g.

3.5.5 Effect of co-feeding water

The effect of co-feeding water on the catalytic cracking of fusel oil was investigated by varied water content (0wt%, 6.25 wt%, 12.5 wt%, and 25 wt%). The various content of water was mixed manually with each alcohol components in fusel oil. The chemical composition of feedstocks for the study effect of co-feeding of fusel oil is shown in Appendix A-3. The mixture was stirred vigorously before feeding to the reactor. The reactions were carried out over HZSM-5 at 550°C, fusel oil feed flowrate of 0.04 ml/min, and 0.2 g of catalyst.

3.5.6 The stability of zeolite on catalytic cracking of fusel oil

The stability of ZSM-5 on catalytic cracking of fusel oil was performed over 20 h of time on stream. The reaction was conducted at 550°C with a fusel oil feed flow rate of 0.04 ml/min with 0.2 g catalyst.

3.6 Product analysis

3.6.1 Gas products analysis

The gas mixture products from the catalytic cracking of fusel oil were analyzed by online GC. The TCD detector was used to determined carbon dioxide (CO₂), carbon monoxide (CO). While hydrocarbons gas products (CH₄, C2-C5 alkanes, and C2-C5 alkenes) were analyzed by FID detector. hydrogen gas (H₂) was employed as a carrier

gas. The temperature of the injector, TCD detector, and FID detector was set at 70°C, 70°C, and 180°C, respectively. The column temperature program was set as expressed in Table 3.3

Table 0.3 Temperature program for gas product analysis

Temperature (°C)	Rate (°C/min)	Hold (min)
50	5	3
100	40	0
150	3	0
165	3	0
180	-	6

The percentage of carbon yield and carbon selectivity in gaseous products are calculated as follows. Where A represents gas products. The calculated procedure is described scrupulously as in Appendix A-4.

$$\text{Carbon yiled (A) (\%)} = \frac{\text{Carbon in A}}{\text{Total carbon in feed}} \times 100 \quad \dots\dots\dots(1)$$

$$\text{Carbon selecity (A) (\%)} = \frac{\text{Carbon in A}}{\text{Total carbon in gas products}} \times 100 \quad \dots\dots\dots (2)$$

The total carbon and The total carbon for hydrocarbons in gaseous products were calculated in equation (3), and equation (4), respectively.

Total carbon yield in gas product (%) (3)

$$= \%C_{CH_4} + \%C_{C_2H_4} + \%C_{C_2H_6} + \%C_{C_3H_6} + \%C_{C_3H_8} + \%C_{C_4H_8} + \%C_{C_4H_{10}} \\ + \%C_{C_5H_{10}} + \%C_{C_5H_{12}} + \%C_{CO} + \%C_{CO_2}$$

Total carbon yield for hydrocarbons in gas product (%) (4)

$$= \%C_{CH_4} + \%C_{C_2H_4} + \%C_{C_2H_6} + \%C_{C_3H_6} + \%C_{C_3H_8} + \%C_{C_4H_8} + \%C_{C_4H_{10}} \\ + \%C_{C_5H_{10}} + \%C_{C_5H_{12}}$$

3.6.1 Liquid products analysis

The liquid products derived from catalytic cracking of fusel oil at optimum conditions were selected to investigate in order to study the side reaction of catalytic cracking of fusel oil. The liquid fraction was collected from the cooling trap after completing the reaction. The water phase in the liquid product was separated by a separating funnel. The chemical compositions in organic phases were determined by GC-MS (Shimadzu, QP2020-NX) equipped with a DB-5 capillary column. The chemical quantitative was reported as the area percentage on GC-FID.

The liquid yield under optimal conditions was calculated based on the weight of feedstock (eq. 4).

$$\text{liquid yiled (wt\%)} = \frac{\text{liquid product (g)}}{\text{Feedstock (g)}} \times 100 \text{(4)}$$

Fusel oil conversion is assumed by isoamyl alcohol conversion, as expressed in equation 5.

$$\text{isoamyl alcohol conversion (wt\%)} = \frac{\text{isoamyl alcohol feed out (g)}}{\text{isoamyl alcohol conversion feed in (g)}} \times 100 \quad \dots(5)$$

3.7 Catalyst deactivation analysis

The catalytic cracking reaction was performed at 550°C with fusel oil feed flowrate 0.04ml/min for 20 h to study the stability of zeolite with the function of time. The spent catalyst at a different TOS was recovery after cooling down under N₂ atmosphere. To better understand catalyst deactivation, the spent catalyst was investigated by TGA analysis, N₂ adsorption-desorption, elemental analysis, and acidity.

3.7.1 Thermogravimetric Analysis (TGA)

The coke deposition was determined by the TGA instrument (Perkin Elmer, TGA8000). Approximately 0.02 g of samples were loaded on the Pt pan. The temperature program was heated from room temperature to 800°C at a ramp rate of 10 °C/min under airflow.

3.7.2 Elemental analysis

The percentage of carbon and hydrogen composition on the coking sample was calculated by a CHN analyzer (Perkin Elmer, Series II-EA2400).

3.7.3 The textual properties and acidity of zeolites

The spent catalyst was calcined at 500°C for 2h to remove the adsorbed molecules prior to N₂ adsorption/desorption and NH₃- adsorption. The measurement conditions of each instrument were described in section 3.4.



CHAPTER 4

RESULTS AND DISCUSSION

4.1 Physicochemical of fusel oil

Fusel oil is a yellowish liquid with odor piquant. Fig 4.1 illustrates the physical appearance of fusel oil. The physicochemical properties are shown in Table 4.1. As can be seen, the fusel oil, which was obtained by KTIS bioethanol co. ltd has a density of 836.8 kg/m^3 , and a higher heating value of 32.58 (MJ/kg) with a moisture content of 12.68 (wt.\%) . However, the physicochemical of fusel oil depends on various factors of the bioethanol production process.



Figure 0.1 Fusel oil

Table 0.1 Physicochemical of fusel oil

Properties	Test method	Fusel oil
Density (kg/m^3)	ASTM D1298	836.8
Higher heating value (MJ/kg)	ASTM D240	32.58
Moisture content (wt.%)	ASTM D6344	12.68

*Obtained by KTIS bioethanol co. ltd

The chemical composition of fusel oil is shown in Table 4.2. As revealed, the fusel oil is a mixture of various alcohols with mainly isoamyl alcohol of 66.7%wt. Additionally, the water content is a significant component in fusel oil as 12.6%wt. However, the water removal process is difficult to operate and high cost. Therefore, fusel oil was used as feedstock without further purification.

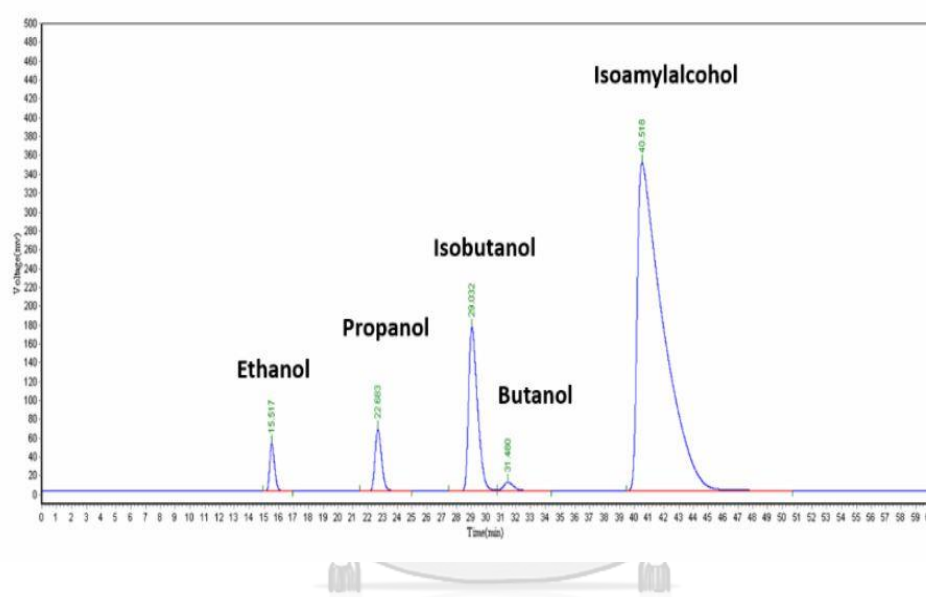


Figure 0.2 The GC chromatogram of fusel oil

Table 0.2 Chemical Composition of fusel oil

Components	Molecular weight (g/mol)	Fusel oil	
		%wt.	%mol
Isoamyl alcohol	88.1	66.7	42.6
Isobutanol	74.1	12.3	9.3
n-Butanol	74.1	0.7	0.5
n-Propanol	60.1	4.3	4.0
Ethanol	46.1	3.4	4.2
H ₂ O ^a	18.0	12.6	39.4

^a determined by Karl Fisher Titration.

4.2 Effect of zeolite topology

The effect of zeolite topology on the catalytic cracking of fusel oil was studied over three well known zeolites (HZSM-5, HY, and H-beta). Fig 4.3 displays the carbon yield and carbon selectivity in gas products of the cracking of fusel oil over three different zeolites. As shown, the reactions were performed at 550°C with the fusel oil feed flow rate of 0.4 mL/min and 0.2 g of catalyst. The blank reaction was tested prior to study the influence of topology zeolite. Not surprisingly, the low carbon yield and selectivity in light olefins (< 5%) was observed under without catalyst condition. It is worth to noted that the catalyst plays an important role in the performance of cracking

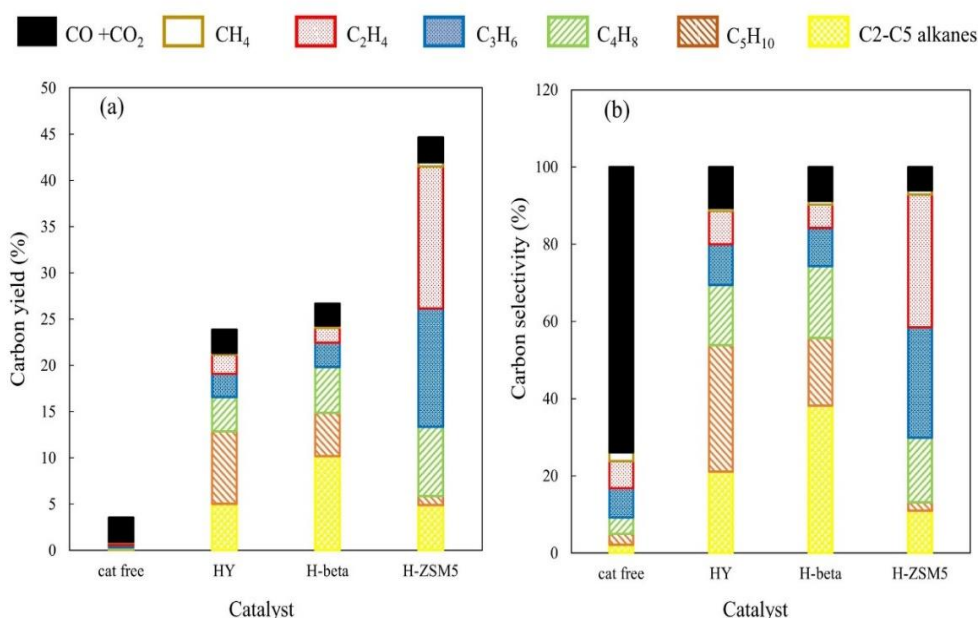


Figure 0.3 Catalytic activity of three zeolites in the catalytic cracking of fusel oil, in terms of the (a) carbon yield and (b) carbon selectivity of the gas mixture products.

Reaction condition: 550°C, feed flow rate of 0.04 mL/min, time on stream of 4 h.

of fusel oil to light olefins. Under catalyst reaction, the HZSM-5 zeolites gave the highest carbon yield (44.6%) in gas products (CO+CO₂, CH₄, C₂H₄, C₃H₆, C₄H₈, C₅H₁₀, and C₂-C₅ alkanes), followed by H-beta (26.67%) and HY (23.88%). In addition, HZSM-5 also produced the maximum carbon yield of ethylene, propylene, butylene as 15.35%, 12.78%, and 7.50%, respectively. The total performance of the zeolites in the catalytic cracking of fusel oil to light olefins decreased in the order: HZSM-5 > H-beta > HY, which is in accord with previous work for hexane cracking [24]. Thus, the textural and the topology of zeolites are significant influence on the and yield and product distribution in catalytic cracking reaction.

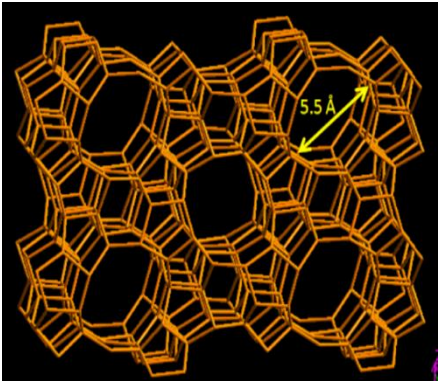
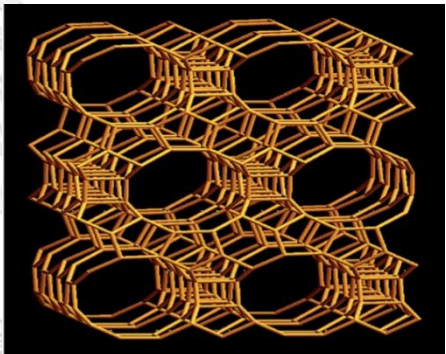
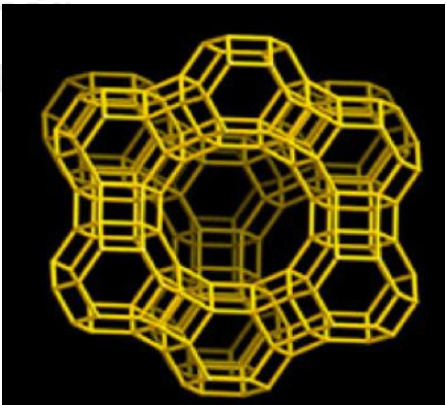
Table 4.3 shows the textural properties and acidity of three different Zeolites (HZSM-5, H-beta, and HY). The framework structure of zeolite (HZSM-5, H-beta and HY) are summarized in Table. 4.4. As revealed, the HZSM-5 exhibited the lowest BET surface area at 291.80 m² / g with moderate acidity (0.58 mmol H⁺/ g). While the H-beta exhibited a higher surface area and higher acidity. Even though H-beta shows good properties for cracking reaction, HZSM-5 gave a higher catalytic performance than H-Beta and HY, as can be seen in Fig 4.3. This is due to the large open-pore structure and long channel of the H-beta and HY catalyst lead to the side reactions (i.e., diels-alder reaction, oligomerization, aromatization, cyclization, and H-transfer), resulting in the formation of higher HC compounds in liquid fractions and rapid coke deposition [86], [87]. In contrast, HZSM-5 has structured a suitable pore structure to produce light

olefins and suppress coke formation [88], [89]. Thus, ZSM-5 was selected to study the parametric parameters front hr further experiments.

Table 0.3 The textural properties and acidity of three zeolite

Catalyst	BET surface	Pore volume (cm ³ /g)	Pore size (nm)	Total acidity (mmol H ⁺ /g)
	area (m ² /g)			
HZSM-5 (SiO ₂ /Al ₂ O ₃ = 40)	291.80	0.16	2.25	0.58
H-beta (SiO ₂ /Al ₂ O ₃ = 40)	511.83	0.47	3.68	0.54
HY (SiO ₂ /Al ₂ O ₃ = 12)	425.22	0.29	2.77	0.91

Table 0.4 The topology of three zeolites [90], [91]

Zeolite	Framework	Pore structure/pre system	Framework structure
HZSM-5	MFI	<ul style="list-style-type: none"> - 3D - 10 Membered ring - Pore size/channel [100] 5.2 x 5.7 nm, 10MR [101] 5.3 X5.6 nm, 10MR 	
H-beta	HBEA	<ul style="list-style-type: none"> -3D - 12 Membered ring - Pore size/channel [100] 7.7 x 6.6 nm, 12MR [001] 5.6 x 5.5 nm, 12MR 	
Zeolite Y	USY	<ul style="list-style-type: none"> --3D - 12 Membered ring - Pore size/channel [111] 7.4 x 7.7 nm, 12MR 	

4.3 Parametric study

4.3.1 Effect of reaction temperature

The influence of reaction temperature on the catalytic cracking of fusel oil was performed at 350, 440, 550, and 650°C. The reaction was conducted with the fusel oil feed rate of 0.04 mL/min over the HZSM-5 catalyst. Fig 4.4 display the catalytic cracking of fusel oil in term of carbon yield and carbon selectivity in gas products. With increasing temperature, the total carbon yield in gas products rose from 16.23% at 350°C to the high point (44.67%) at 550°C followed by a slightly dropped to 43.63% at

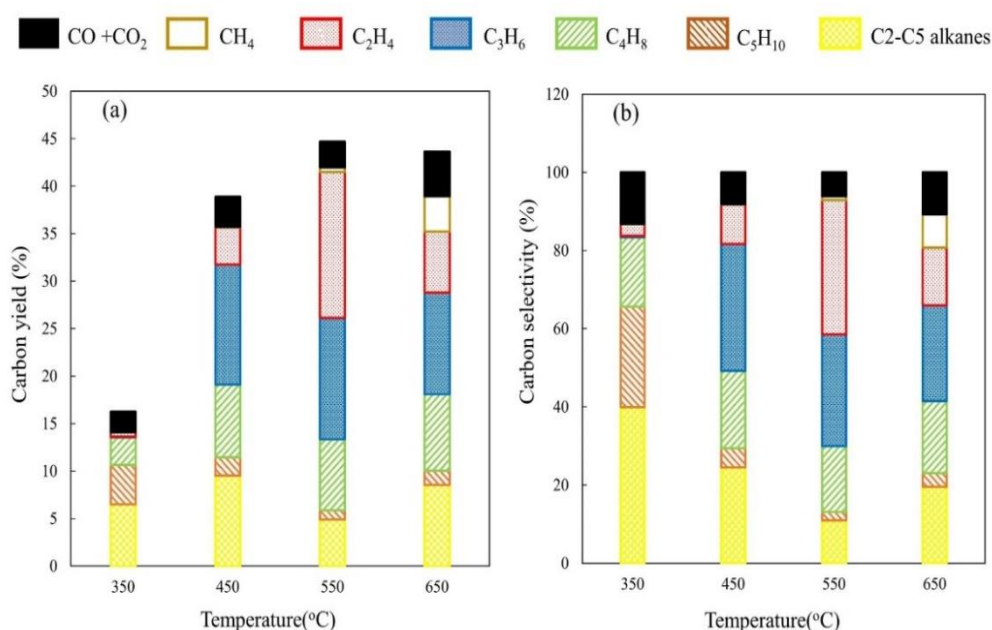


Figure 0.4 Effect of the reaction temperature on the (a) carbon yield and (b) carbon selectivity of the gaseous products in the catalytic cracking of fusel oil. Reaction condition: catalyst HZSM-5, feed flowrate of 0.04 mL/min, for 4 h.

650°C. These results agree with Dong et al. [81] in the case of the cracking of the microalga *Chlorella pyrenoidosa* over modified ZSM-5. The increasing gas product is because the cracking reaction is endothermic and it favors high temperature. Nevertheless, too high a reaction temperature can also promote coke deposition on the catalyst surface [87],[92].

Based on carbon selectivity results (Fig.4.4b), the carbon selectivity of ethylene and propylene was found as a small amount at 350°C (3.0% and 0.4%, respectively). While pentenes (C₅H₁₀) showed a higher carbon selectivity at 25.65%, resulting from the dehydration of isoamyl alcohol, which is the main component of fusel oil. These results indicated the dehydration reactions predominate at a low temperature under an acidic condition [14], [79], [93]. Meanwhile, at 550°C, the maximum selectivity of ethylene and propylene was obtained, indicating that the cracking is favored at high temperatures [32]. Moreover, methane (CH₄) was not detected at 350–450°C, but it was found at reaction temperatures above 550°C. As revealed, the carbon selectivity of CH₄ was 1.0% and 8.5% at 550°C and 650°C, respectively. These results could confirm thermal cleavage, which directly converts alcohol to olefins via deoxygenation, depleting the oxygen as H₂O, CO₂, and CO. The olefins are then further thermally cracked into small-molecule gases, like CH₄, at high temperature [18]. Thus, the product distribution in the catalytic cracking can be controlled by the reaction temperature.

Therefore, the reaction temperature at 550°C are the optimal temperature in the catalytic cracking of fusel oil to light olefins

4.3.2 Effect of feed flowrate

The influence of feed flow rate on catalytic cracking of fusel oil over HZSM-5 catalyst at 550°C is shown in Fig. 4.5. The fusel oil feed flow rate was varied from 0.02 to 0.16 mL/min. As depicted, the feed flow rate of the reactants had a significant effect on the product yields and product distribution in catalytic cracking of fusel oil. with increasing fusel oil feed flow rate, the gas production increasing from 27.7% at 0.02 mL/min to the highest point (44.67%) at 0.04 mL/min. Then, it dropped to 27.87%

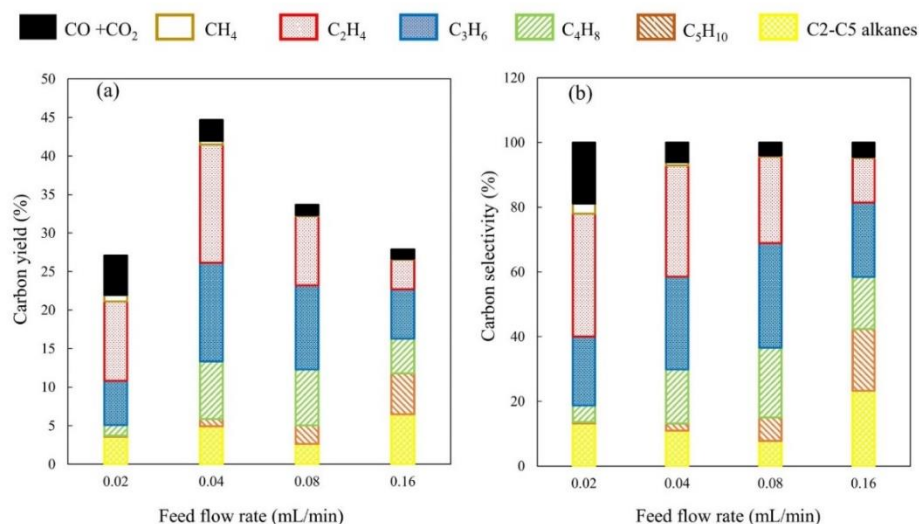


Figure 0.5 Effect of the feed flow rate on the (a) carbon yield and (b) carbon selectivity of the gaseous products in the catalytic cracking of fusel oil. Reaction condition: catalyst HZSM-5, 550°C, for 4 h.

at 0.16 ml/min. These results are related to the contact time between catalyst and fusel oil in the reactor. This decrease can be attributed to the short contact time to complete the reaction, resulting from the rapid feed flow rate of fusel oil. Nevertheless, at a long contact time (feed flow rate of 0.02 mL/min), a low carbon gas fraction (27.1%) was observed because the partial gaseous products converted to the higher HC compounds [94].

The carbon selectivity of the gas products is shown in Fig.4.5b. The ethylene and propylene yields were maximum at a feed flow rate of 0.04 mL/min, giving a carbon selectivity of 34.4% and 28.6% for ethylene and propylene, respectively. The ethylene and propylene yield decreased when increasing the feed flow rate. A similar trend was observed previously in converting cellulose to light olefins at 600°C [18]. Conversely, the pentenes fraction rose with increasing the feed flowrate. These findings confirm the rapid dehydration reaction at a short contact time. Although a long contact time gives a good selectivity of ethylene and propylene, too long a contact time also promotes side reactions [5]. .

4.4 Effect of feedstocks

To investigate the effect of the feedstock over HZSM-5 in the catalytic cracking of fusel oil, each component in fusel oil (ethanol, n-propanol, isobutanol, n-butanol, and isoamyl alcohol) was used on its own as the feedstock. Fig.4.6a and Fig.4.6b show the carbon yield and carbon selectivity in the gaseous mixture products. All reactions were performed for 4 h at 550°C with a feed flow rate of 0.04 mL/min and catalyst loading of 0.2 g. The total carbon gaseous yield from ethanol conversion was highest at 70%, followed by propanol (63.5%), isoamyl alcohol (51.1%), isobutanol (46.7%), and n-butanol (45.1%). As can be seen in Fig.4.6b, the ethanol and propanol conversion

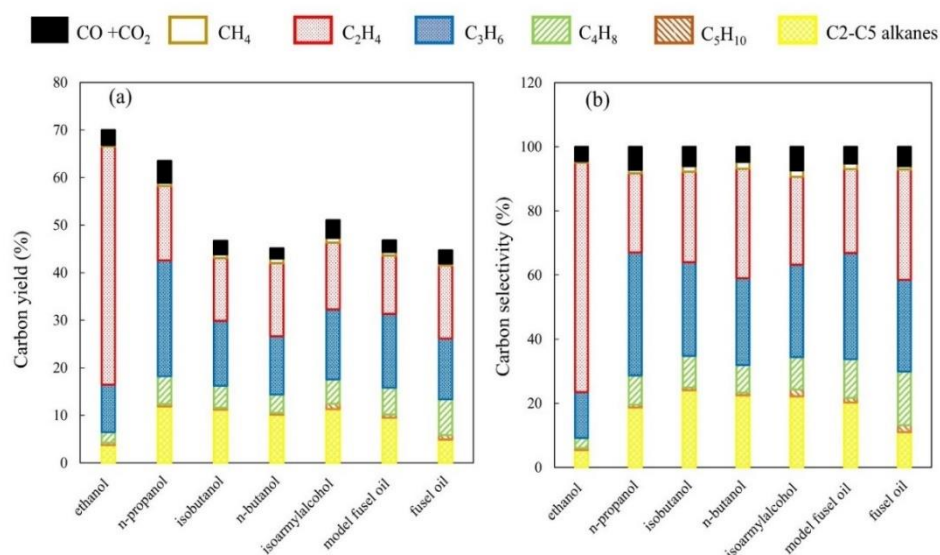


Figure 0.6 Effect of the reactant on the (a) carbon yield and (b) carbon selectivity on the gaseous products in the catalytic cracking of fusel oil. Reaction condition: catalyst HZSM-5, 550°C, feed flowrate of 0.04 mL/min, for 4 h.

exhibited the predominant carbon selectivity of ethylene (71.5%) and propylene (38.3%), respectively. In contrast, the conversion of isobutanol, n-butanol, and isoamyl alcohol showed an insignificant difference in product distribution. These results could be the fact that the small oxygenated molecules can easily access and adsorb on the active sites, leading to high catalytic conversion to light olefins. Meanwhile, the larger molecules are trending to form aromatics [18]. Rezaei et al. [15]. reported that the carbon to hydrogen ratio (C/H) of feedstock is the factor on yield and product distribution in the catalytic cracking process. The higher C/H ratio of feedstocks produces more light olefins and attenuates coke formation. Additionally, the reactant shape selectivity of HZSM-5 does not affect the catalytic cracking of fusel oil because all reactants can be diffused in the pore of HZSM-5 [95].

The model fusel oil, mixed to the same composition as many fusel oils, and fusel oil was compared and investigated in this process. There were no significant differences in both the carbon yield and selectivity under the same conditions from the comparison

4.5 Effect of co-feeding water

Typically, fusel oil has a water content of approximately 2.5–20.0 wt.%, which could influence the catalytic conversion. However, the water separating process has a high operating cost and is difficult to operate, especially in a larger scale plant. In addition, the dehydration of various alcohols in fusel oil under acidic conditions also produces water as a by-product. Therefore, the effect of co-feeding water in catalytic cracking of fusel oil over HZSM-5 was studied in this work, with results shown in Fig.4.7. The reactions were performed using model fusel oil as a reactant with water contents from 0–25.5 wt.%. As the water content in the fusel oil increased, the total carbon

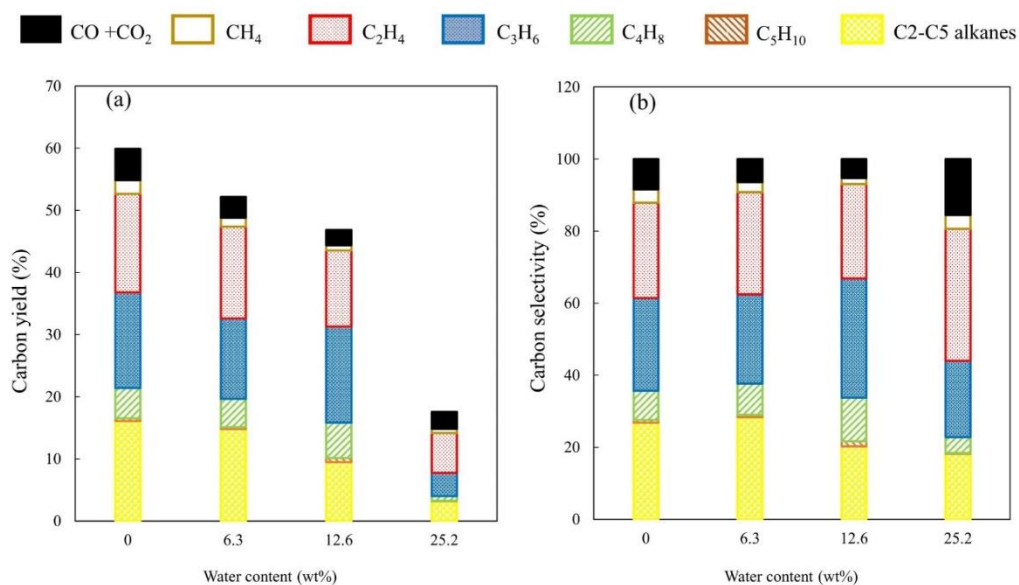


Figure 0.7 Effect of co-feeding water on the (a) carbon yield and (b) carbon selectivity of the gaseous products in the catalytic cracking of fusel oil. Reaction condition: catalyst HZSM-5, 550°C, feed flowrate of 0.04 mL/min, for 4 h.

yield in the gaseous mixture dropped significantly from 59.9% to 17.5%. This decreasing trend was found in the yield of the light olefins. There was no considerable change in product distribution. These observations are in contrast to a previous report on the effect of water on the pyrolysis of furan, where the additional water content enhanced the yield of light olefins and reduced the coke formation because it increased the furan hydrolysis rate into propylene and CO₂ [80]. Corma et. al [96] found that the co-feeding of water can suppress bimolecular reactions and the coking rate of catalysts. Oudejans et al. [97] reported that the influence of water on the catalytic efficiency also depended on various parameters (i.e. reaction temperature, contact time). In this case, the introduction of water exhibited the negative effect by decreasing in light olefins. This could be attributed to the dilution effect, where the increased water level decreased the accessibility of the reactant into the active sites of the catalyst [30]. Additionally, water can cause the dealumination, leading to loss of acid site and destructors in zeolite under high steam pressure and temperature condition (>550°C) [83].

4.6 Liquid fraction derived from catalytic cracking of fusel oil

To achieve a better understanding of the reaction pathways of catalytic cracking of fusel oil, the chemical composition of liquid fraction derived from catalytic cracking of fusel oil over HZSM-5 was analyzed by GC-MS. The chemical structure is shown in appendix A-5. Based on isoamyl alcohol calculation, the conversion of fusel oil was greater than 99.0% under optimum conditions (550°C, fusel oil feed flow rate of 0.04 ml/min). The liquid yield accounted for 31.9% based on the mass of feedstocks. As displayed in Table 4.5, it can be seen that water was observed in a large percentage weight of 86.77, owing to the release of water mostly from the intermolecular dehydration of various alcohols in fusel oil at high temperature [93]. The organics phase was 13.23 %wt. Based on the percentage of the area determined by GC analysis, the aromatic HCs accounted for 86.74% and the oxygenated compounds accounted for 12.83%. Benzene was found as the major HCs product at 74.22%, followed by toluene (10.85%), xylene (0.75%). These results confirm the transformation of olefins from cracking reaction to aromatic products through aromatization reaction, which is further polymerized to coke formation [98]. In oxygenated compounds, isoamyl alcohol, isobutanol, propanol are the remaining raw materials of fusel oil of incomplete reaction. The aldehyde products arose through alcohol dehydrogenation via Lewis acid sites of the HZSM-5 catalyst [99]. The acetal compounds can be generated by the

acetalization of aldehydes with alcohols under acidic conditions [100]. The overall reaction pathways for observed products were further summarized in section 4.6.

For unoptimized conditions, the lower in the desired gas product can be implied by the promotion of side reactions to form the organic liquid or coke deposition.



Table 0.5 Chemical composition of liquid fraction derived from catalytic cracking of fusel oil.

Liquid components	Percentage (%)
Water (wt%)	86.77
Hydrocarbons (wt%)	13.23
Aromatic hydrocarbon compounds (% Area)	86.74
Benzene	74.22
Toluene	10.85
Xylene	0.75
1-ethyl, 4-methyl benzene	0.70
Naphthalene	0.03
1,3-dimethyl naphthalene	0.19
Oxygenated compounds (% Area)	12.83
Propanol	0.23
Isobutanol	0.54
Isoamyl alcohol	0.66
Isobutaldehyde	1.34
Isovaleraldehyde	8.97
Isovaleraldehyde isopentyl propyl acetal (C13)	0.13
Isobutylaldehyde isobutyl isopentyl acetal (C13)	0.10
Isobutylaldehyde diisopentyl acetal (C14)	0.23
Isovaleraldehyde diisopentyl acetal (C15)	0.63
Others	0.43

Reaction condition; 550°C, fusel oil feed flow rate 0.04ml/min, time 20 h

4.7 Catalyst stability and deactivation

The stability of HZSM-5 in the catalytic cracking of fusel oil was evaluated at 550 °C with a feed flow rate of 0.04 mL/min over 20 h of TOS. As revealed in Fig. 4.8, the total carbon yield of HCs in the gaseous products rose sharply and reached the highest level at 44.8% at around 5 h on stream and then fell to 28.2% after 20 h. There was a similar trend in the level of ethylene and propylene, while butylene and pentene increased gradually. The reduction in the cracking performance indicates the catalyst deactivation with time.

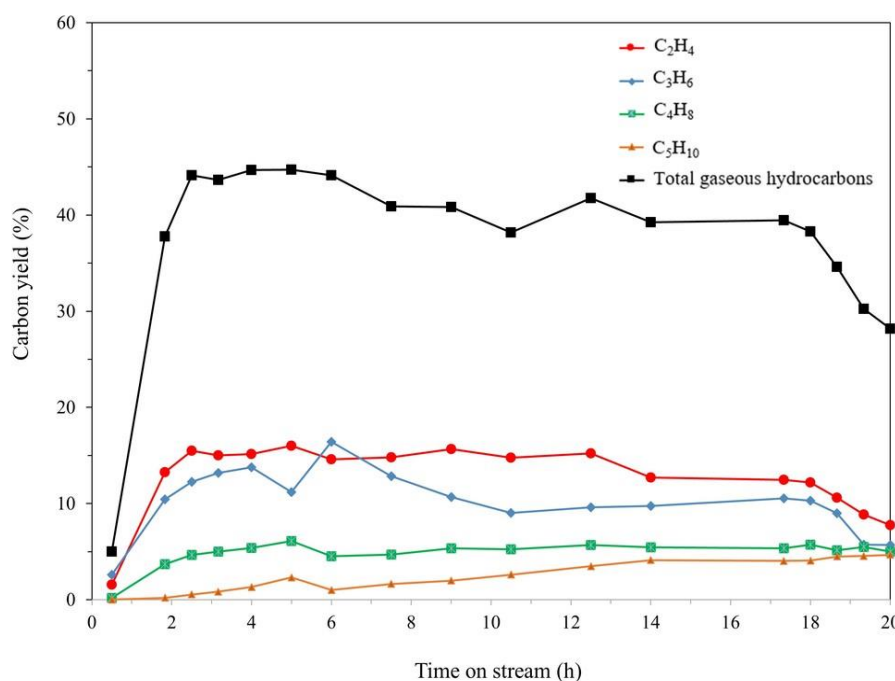


Figure 0.8 Stability of HZSM-5 in the catalytic cracking of fusel oil. Reaction condition: catalyst HZSM-5, 550°C, feed flowrate of 0.04 mL/min, for 4 h.

The thermogravimetric analysis (TGA) technique is a proper technique to determine coke deposition on the used catalyst, which is one of the main causes of catalytic deactivation [101]. The TGA and DTA thermograms of the used HZSM-5 at a different TOS are depicted in Fig. 4.9 and Fig. 4.10. As revealed, the TGA/DTA curves of spent HZSM5 exhibited three main regions of weight loss. The first weight loss at a temperature below 100°C is due to the evaporation of moisture and volatile species. The second weight loss (200-500°C), is attributed to “soft coke” (high H/C ratio), which is the adsorbed hydrocarbon molecules inside the catalyst pore system formed by coke precursor [102]. The third weight loss at above 500°C is related to “hard coke” associated with the polymerization of soft coke to more bulky carbonaceous compounds with a low H/C ratio [12].

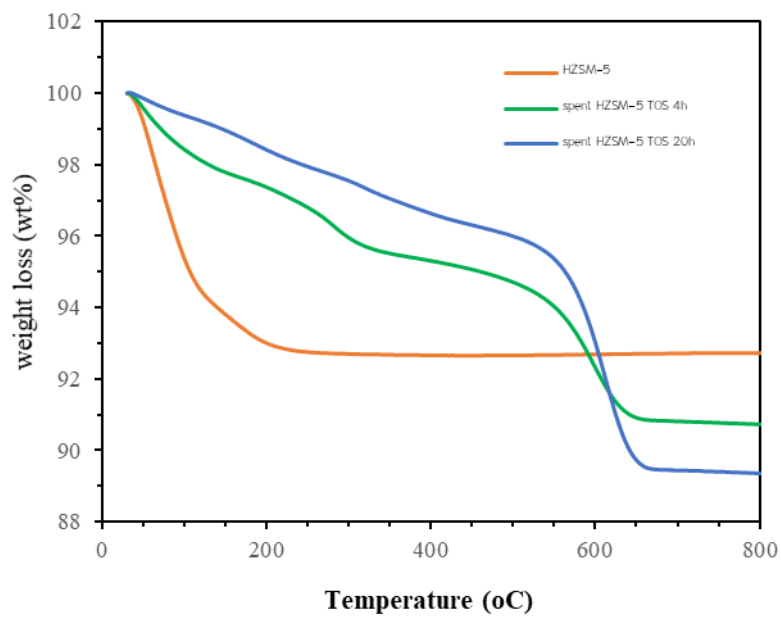


Figure 0.9 The TGA thermogram of fresh and spent HZSM-5 at different TOS

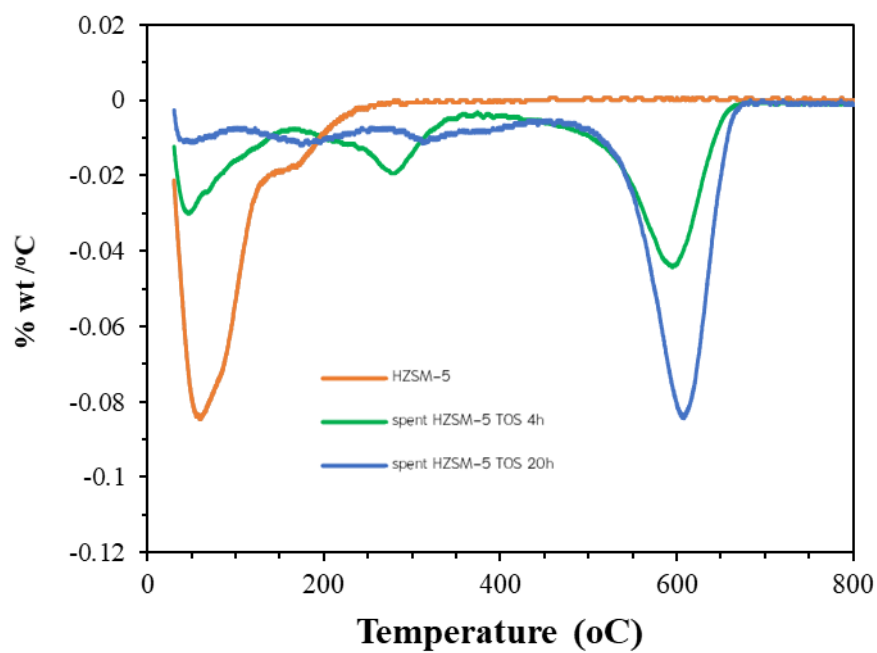


Figure 0.10 The TGA thermogram of fresh and spent HZSM-5 at different TOS

Table 4.6 summarised the coke content (wt%) and elemental analysis of spent HZSM-5. As shown, the coke deposition of spent catalyst increased by the function of TOS. The total coke content was up to 9.8% after 20 h of reaction. With longer TOS, the amount of hard coke increased considerably to 73% of total coke content; while soft coke decreased marginally. Both coking catalysts showed the predominant of hard coke up to 60%, indicating the major role of hard coke in catalyst deactivation after 4h of TOS. The elemental analysis results exhibited that the spent HZSM5-5 at a longer TOS have a higher %C content with the lower H/C ratio. These results confirm that the accumulation of hard coke at a long TOS.

Table 0.6 The coke content and the elemental analysis at different TOS for the used HZSM-5 sample

TOS (h)	Coke content (wt%)			Elemental analysis		
	Soft coke (200-500°C)	Hard coke (>500°C)	Total	%C	% H	H/C ratio
4	2.67	4.08	6.75	5.87	0.65	0.11
20	2.41	6.76	9.18	8.00	0.5	0.06

To emphasize hard coke deposition on HZSM-5, the used catalysts were calcined at 500°C to eliminate physisorbed products (soft coke) before investigating textural properties and acidity. After using the catalyst, the BET surface area and pore volume dropped, while the average pore size increased after employing the catalyst (see Table 4.7). This implies the coke deposition and the collapse of the micropore structure during the process [103]. Additionally, the losing of acidity in catalysts during the reaction also leads to a lower catalytic cracking performance [95].

Table 0.7 Textural properties and total acidity of three types of zeolite and the used HZSM-5 at different TOS

Catalyst	BET surface area (m ² /g)	Pore volume (cm ³ /g)	Pore size (nm)	Total acidity (mmol /g)
HZSM-5	291.80	0.16	2.25	0.58
HZSM-5 (used) 4 TOS	147.71	0.12	3.30	0.23
HZSM-5 (used) 20 TOS	100.60	0.14	5.78	0.20

The NH₃-TPD profiles of spent HZSM-5 at different TOS are illustrated in Fig. 4.11. The acidity determined by NH₃-TPD is shown in Table 4.8. As revealed, there were two distinct NH₃ desorption peaks. The first desorption peak around 200°C is assigned to weak acid sites and the second broad peak around 443°C is related to the strong acid sites. The NH₃-TPD profiles of spent HZSM-5 illustrated the reduction in both NH₃ desorption peaks with the decrease in total acidity up to 66% after 20 of TOS, attributing to both the dealumination effect (see Fig 4.12) and coke deposition [104].

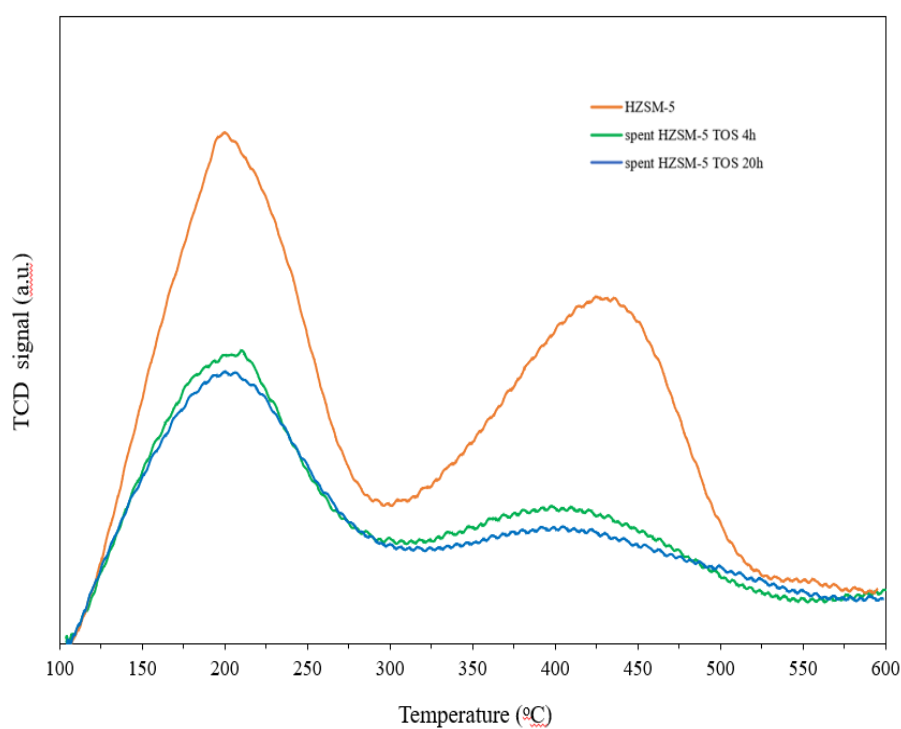


Figure 0.11 the NH₃-TPD profiles of the fresh and spent HZSM-5 at different TOS

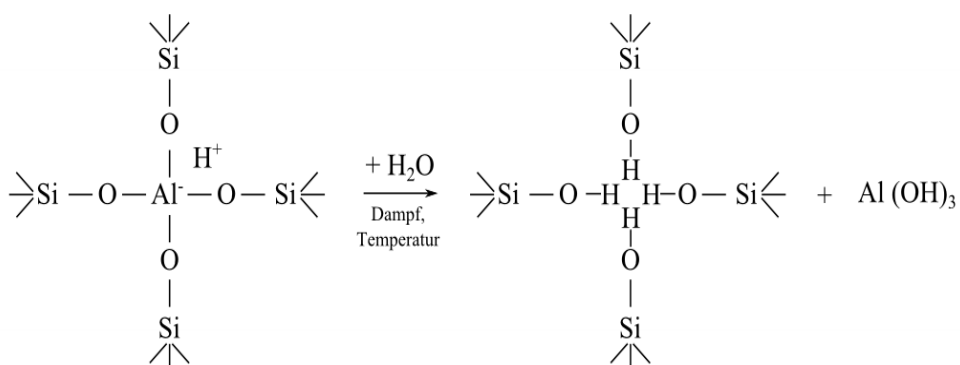


Figure 0.12 Dealumination hydrothermal of zeolite

Table 0.8 The acidity of fresh and spent HZSM-5 at different TOS

Sample	Weak acidity	Strong acidity	Total acidity (mmol/g)
	(mmol/g)	(mmol/g)	
HZSM-5	0.339	0.241	0.580
Spent HZSM-5 TOS 4h	0.180	0.054	0.234
Spent HZSM-5 TOS 20h	0.159	0.038	0.197

As compared to weak acid sites, the strong acid sites of the spent HZSM-5 exhibited a vast reduction and the shifting to lower desorption peak, which is mainly due to the presence of hard coke (> 500°C) on the strong acid sites [105, 106]. It can conclude that coke deposition is the significant cause of downgrading catalytic cracking of fuel oil performance by pore blocking and covering active sites [107]. Thus, the development of HZSM-5 to improve its stability and suppress coke deposition in the fusel oil cracking reaction is necessary for future work.

4.8 Purpose mechanisms

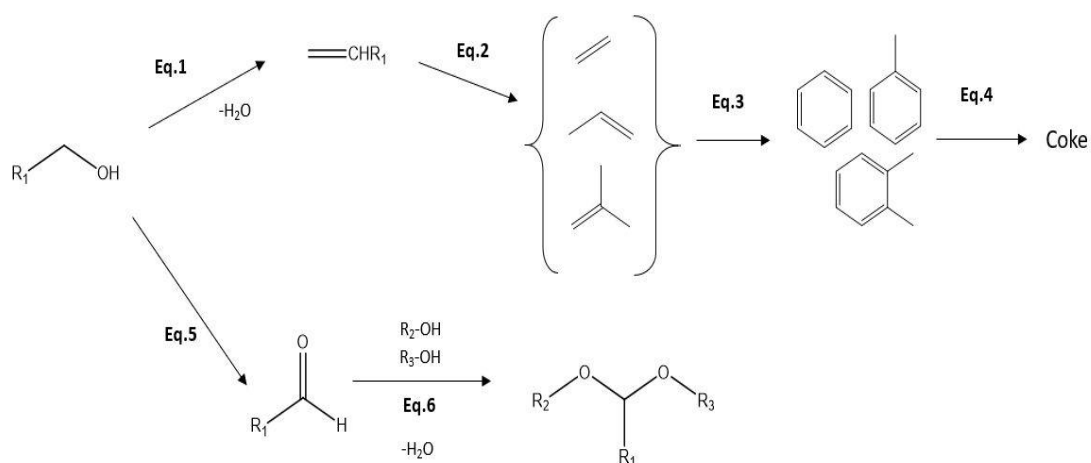


Figure 0.13 overall reaction pathway for observed products on catalytic cracking of fusel oil over HZSM-5 catalyst

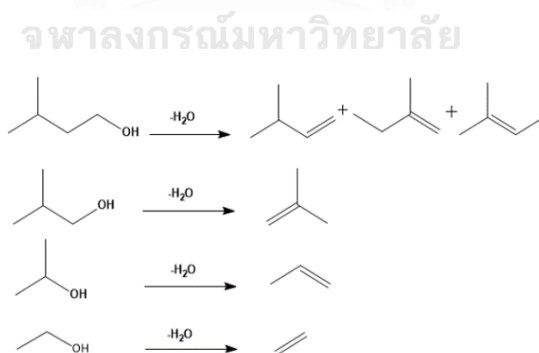
Figure 4.13 summarizes the overall reaction pathways for observed products on catalytic cracking of fusel oil over HZSM-5 under optimum conditions (Temperature $550^{\circ}C$, fusel oil feed flowrate $0.04ml/min$). The various alcohols in fusel oil are converted to olefins via intramolecular dehydration with releasing water (Eq. 1). Then, the olefins are further cracked to light olefins (ethylene, propylene, butylene) (Eq. 2), which was found in the gaseous fraction. The side reactions are identified as the reactions leading to the production of undesired products. The various olefins can be transformed into aromatic hydrocarbon through the hydrocarbon pool by aromatization reactions (Eq.3). More accumulation of carbon species can generate coke

deposition by the polymerization reaction (Eq. 4.). For the other pathways, the alcohol fusel oil can be also converted to aldehyde via dehydrogenation reaction (Eq. 5.). Then, the acetals compound cloud formed by the acetalization of the aldehyde with Alcon under acidic conditions (Eq. 6.). Thus, to achieve the highest light olefins, the various factors have to be controlled to suppress side reactions.

The purpose mechanisms of each reaction are described as follows:

(1) Dehydration reaction in catalytic cracking of fusel oil

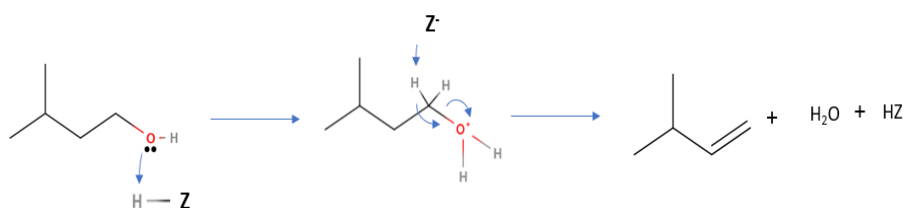
Scheme 1 shows the dehydration of various alcohol in fusel oil to alkenes. Under low reaction temperature and short contact time, the dehydration of various alcohol in fusel oil to alkenes is dominant under zeolite catalyst. Therefore, pentenes, from then intramolecular dehydration of isoamyl alcohol, were found to be the vast proportion.



Scheme 1 The dehydration of various alcohols in fusel oil to alkenes

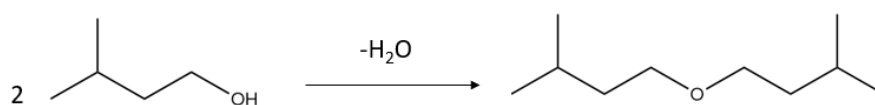
The dehydration of isoamyl alcohol to pentenes mechanism over

HZSM-5 catalysts is shown in Scheme 2. Under the acidic condition, hydroxy groups are protonated by the Brønsted acid site of HZSM-5. Then, the conjugate base reacts hydrogen atom with depleting alkyloxonium ion as water, forming pentenes.



Scheme 2 Mechanism of dehydration of isoamyl alcohol to pentenes.

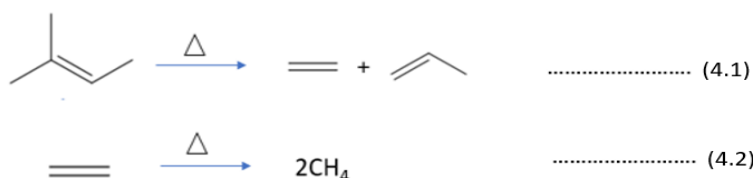
In addition, the diisoamyl ether was not observed in this case, suggesting that the intermolecular dehydration did not occur due to the high reaction temperature (550°C). Scheme 3 illustrates the intermolecular dehydration of isoamyl alcohol.



Scheme 3 The intermolecular dehydration of isoamyl alcohol.

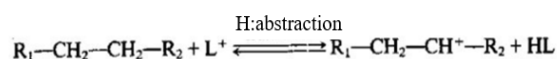
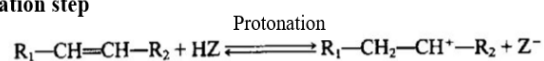
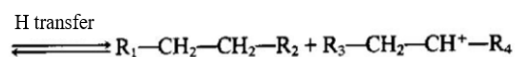
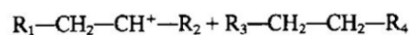
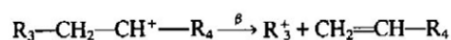
(2) Cracking reaction.

Cracking reaction is dominant at high temperatures and long contact time. In cases of fusel oil, the C-C bond of olefins is broken and formed to ethylene or as a smaller molecule (Scheme 4.1). However, too high a temperature can promote secondary cracking to smaller molecules such as CH_4 (Scheme 4.2).



Scheme 4 Cracking reaction of alkenes to smaller molecules

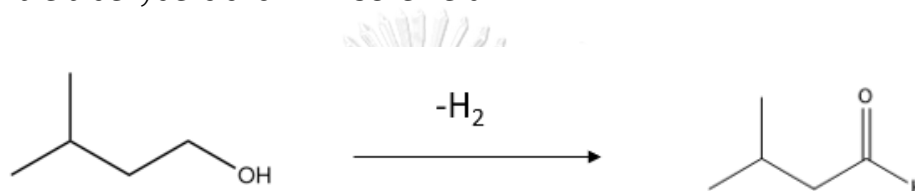
The mechanism of the catalytic cracking of fusel oil to light olefins over the HSM-5 catalyst is shown in Scheme 5.

Initiation step**Propagation step****Cracking step (β -scission)**

Scheme 5 Mechanism for catalytic cracking over a zeolite catalyst

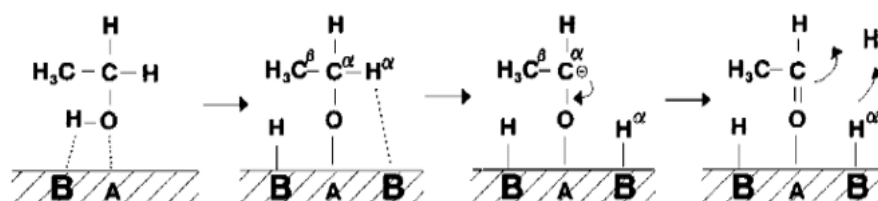
(3) Dehydrogenation cracking reaction

The dehydrogenation of alcohols to aldehyde during the cracking reaction can occur during the cracking reaction depending on the ratio of Brønsted sites and Lewis sites [88]. The Lewis acid is the catalytically active site for dehydrogenation reaction. The dehydrogenation of isoamyl alcohol to Isovaleraldehyde is shown in Scheme 6.



Scheme 6 The dehydrogenation cracking of isoamyl alcohol to Isovaleraldehyde

The example mechanism of dehydrogenation of ethanol to acetaldehyde is shown in scheme 7, where A and B are Lewis acid sites and Brønsted basic sites, respectively [99].

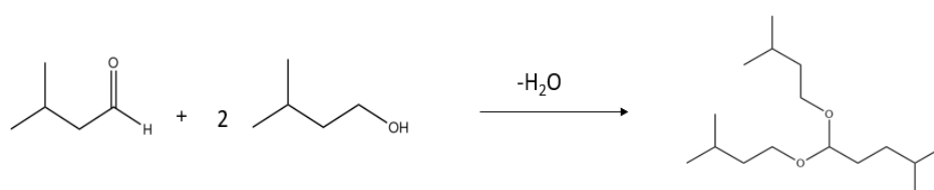


Scheme 7 Mechanism of dehydrogenation cracking over a zeolite catalyst.

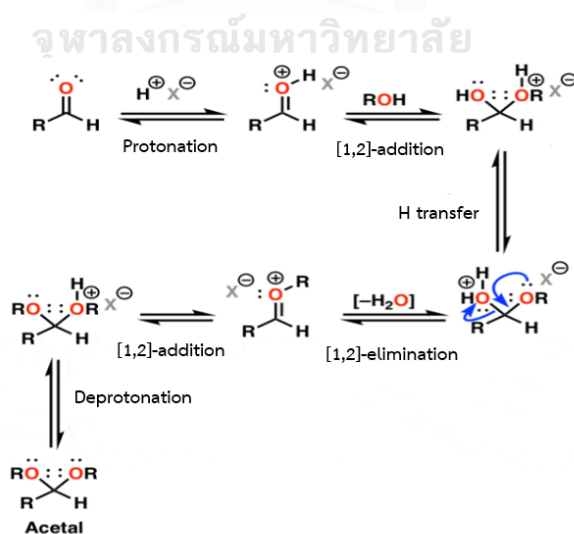
(4) Acetalization reaction.

The acetal compounds were found as a minor amount in the liquid fraction over catalytic cracking of fusel oil. The isopentyl group was observed in acetal compounds, indicating that the acetal compounds could be regenerated from the acetalization between aldehyde and isoamyl alcohol under acidic conditions.

Scheme 8 displays the formation of Isovaleraldehyde diisopentyl acetal from isoamyl alcohols and Isovaleraldehyde. The mechanism of the acetalization is illustrated in Scheme 9.



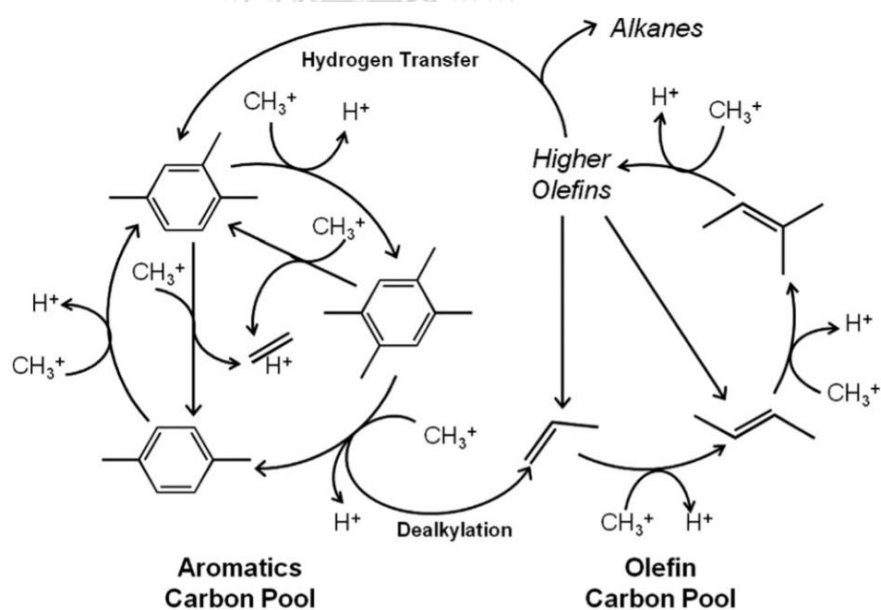
Scheme 8 The acetalization of Isovaleraldehyde with isoamyl alcohols.



Scheme 9 Mechanism of acetalization of aldehyde to acetal [108]

(5) Side reaction via Hydrocarbon pool.

Scheme 10 shows a detailed proposed mechanism, indicating the role that both hydrocarbon and hydrogen transfer processes play in the production of olefins. As revealed, olefins are a precursor for hydrocarbon via various side reactions. The aromatic hydrocarbons are further formed to coke deposition in the longer time on stream. This is a reaction in favor of the high temperature, and long contact time. In addition, the pore structure of zeolite can control the reaction pathway inside porous as well.



Scheme 10 The hydrocarbon pool mechanism over HZSM-5 catalyst [109]

CHAPTER 5

CONCLUSIONS

Fusel oil is a mixture of various alcohol with has amyl alcohol as the main component up to 63% wt. The catalytic cracking of fusel oil was studied in a fixed bed reactor under an N₂ atmosphere to produce light olefins. HZSM-5 zeolite was selected in the parametric study because it revealed better catalytic performance than HY and H-beta. The maximum total carbon yield in the gaseous product with excellent carbon selectivity of ethylene and propylene was 44.7%, 34.4 %, and 28.6%, respectively, under the optimal condition (Temperature= 550°C, feed flow rate of fusel oil = 0.04 mL/min, catalyst =0.02 g). High temperature can promote cracking reaction but it is also favored to side reaction and secondary cracking to the undesired product as well. The feed flowrate of fusel oil has a significant effect on gaseous yield and product distribution in order to control contact time between reactant and the active site of catalyst (Brønsted acid site). The short contact time leads to incomplete reaction but too high contact time can promote side reaction effects. Based on the effect of feedstocks, the smaller feedstock exhibited a higher light olefins yield due to it easier to diffuse and adsorb to the active site. Moreover, the co-feeding water of fusel oil can cause a reduction in catalytic cracking performance by 16.67% as compared to the dehydrated model fusel oil. Under a long time on stream (20h), there was a slight reduction in catalytic performance due to the deactivation of HZSM-5. In the reaction

pathways study, the fusel oil can be converted to light olefins via dehydration and cracking reaction under acidic and thermal conditions. However, this process needs to suppress side reactions by controlling the operating parameters and employing suitable catalysts. It can be concluded that the catalytic cracking of fusel oil is one of the promising approaches for light olefins production. Nevertheless, the decrease of HZSM-5 stability was found after a long time on stream. Thus, the enhancement of catalyst efficiency in the cracking of fusel oil reaction is also required for future work.

Recommendations for future work.

Since Fusel oil is considered a novel renewable resource, there is a few research that studies this material. It is a valuable opportunity to enhance the knowledge and technologies to add the value of fusel oil. In order to achieve the highest benefit and complete this research, the suggestions for future work are expressed as follows.

- (1) Modify zeolite to improve the catalyst lifetime and the catalytic cracking performance in the catalytic cracking of fusel oil.
- (2) Study the liquid composition and yield under unoptimized conditions to better understand the reaction mechanism and to enhance the evident results in this research.

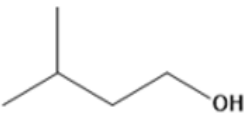
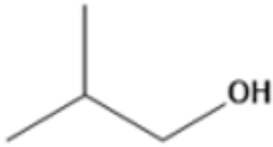



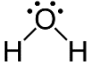
- (3) Study the insight characteristic of the spent catalyst under various conditions.
- (4) Study the catalytic cracking of fusel oil to other value products (e.g., BTX)
- (5) Investigate the other factors (e.g. acidic strength of zeolite) that influence the catalytic cracking of fusel oil.
- (6) Develop the novel strategy and reactor to enhance the cracking performance and to improve the efficiency of use in terms of collecting experimental data and convenience to use.



APPENDIX

A-1 The chemical and physical properties of various alcohol in fusel oil are listed in Table A.1

Table A. 1 The chemical and physical properties of various alcohol in fusel oil

Chemical	Chemical structure	Molecular weight (mol/g)	Boiling point (°C)	Density (kg/m)
Isoamyl alcohol		88.1	131	810
Isobutanol		74.1	108	802
n-Butanol		74.1	117	810
n-Propanol		60.1	97	803
Ethanol		46.1	78	789
H ₂ O		18.0	100	1000

A-2 Weight hourly space velocity calculation

The effect of fusel oil feed flowrate on the catalytic cracking if fuel oil was studied by varied the fusel oil feed flowrate from 0.02 mL/min to 0.16 mL/min. The weight hourly space velocity (WHSV) was calculated eq as follows;

$$\text{WHSV } [h^{-1}] = \frac{\text{total mass feed flow rate to the reactor}}{\text{total catalyt weight}}$$

The weight hourly space velocity in this study are expressed in Table A.3

Table A. 2 The conversion of fusel oil feed flowrate to WHSV

Fuel oil feed flow rate (ml/min)	WHSV (h ⁻¹)
0.02	4.93
0.04	9.86
0.08	19.71
0.16	39.42

For example, the calculation of WHSV(h⁻¹) for fusel oil feed flowrate were described as follows;

$$\begin{aligned} \text{WHSV (h}^{-1}\text{)} &= \left(\frac{0.02 \text{ ml}}{\text{min}} \right) \left(\frac{0.8213 \text{ g}}{1 \text{ ml}} \right) \left(\frac{60 \text{ min}}{\text{h}} \right) \left(\frac{1}{0.2 \text{ g cat}} \right) \\ &= 4.93 \text{ h}^{-1} \end{aligned}$$

(The additional data for calculation; Density of fusel oil at RT =0.8213 g/ml, catalyst weight = 0.2 g)

A-3 Chemical composition of model fusel oil by varied the water content

Due to the limitation in the water removal in fusel oil, the model fusel oil with different water content was mixed manually with the pure component of each composition of fusel oil in the same ratio, as shown in Table A.2. The water content in the range of 0-25.5% was selected because of its similarity to the commercial fusel oil in the industry.

Table A. 3 Chemical composition of model fusel oil by varied the water content

Chemical composition	Water content (wt%)			
	0.00	6.30	12.60	25.20
Isoamyl alcohol	76.32	71.51	66.70	57.08
Isobutanol	14.07	13.19	12.30	10.53
n-Butanol	0.80	0.75	0.70	0.60
n-Propanol	4.92	4.61	4.30	3.68
Ethanol	3.89	3.65	3.40	2.91
H ₂ O ^a	0.00	6.30	12.60	25.20
Total	100.00	100.00	100.00	100.00

A-4 Product analysis

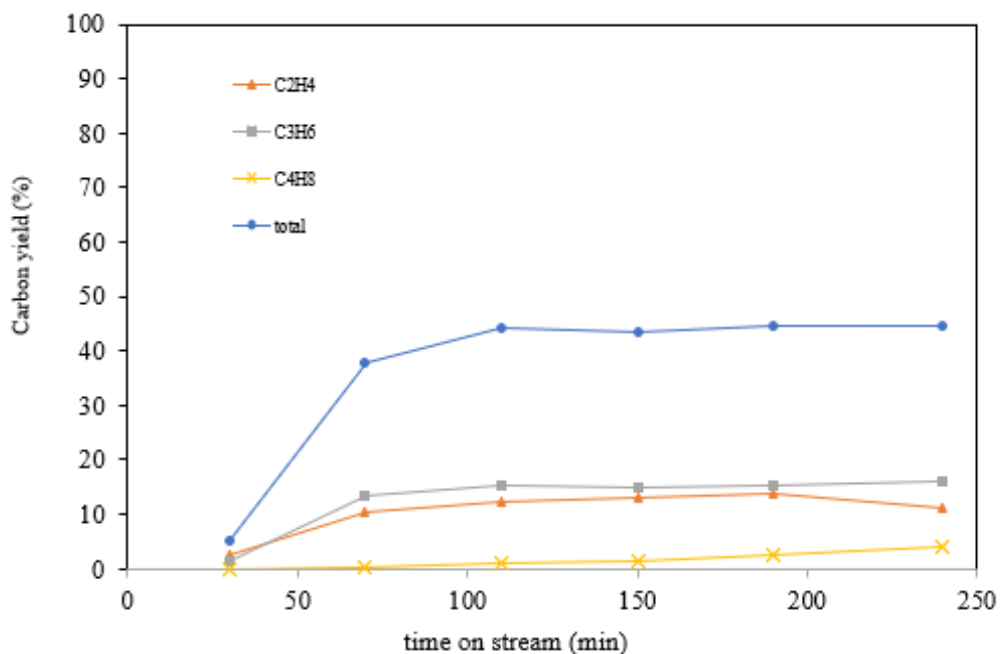
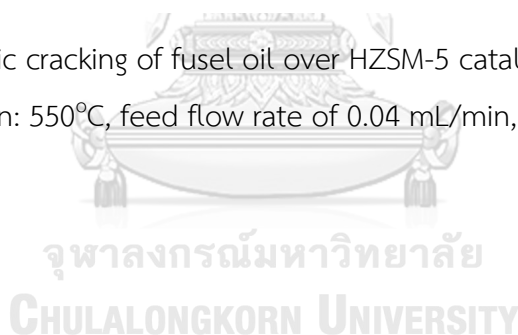


Figure A.1 Catalytic cracking of fusel oil over HZSM-5 catalyst for 4h

Reaction condition: 550°C, feed flow rate of 0.04 mL/min, time on stream of 4 h



For example, the carbon yield and carbon selectivity of C₂H₄ for catalytic cracking of fusel oil are calculated by equations (1) and (2).

$$\text{Carbon yield (A) (\%)} = \frac{\text{Carbon in A}}{\text{Total carbon in feed}} \times 100 \quad \dots\dots\dots (1)$$

$$\text{Carbon selectivity (A) (\%)} = \frac{\text{Carbon in A}}{\text{Total carbon in gas products}} \times 100 \quad \dots\dots\dots (2)$$

(1) Calculation for carbon yield in gas products

(1.1) Total carbon in feed.

- Mol Carbon in fusel oil

$$= \text{mol C}_{\text{isoamyl alcohol}} + \text{mol C}_{\text{isobutanol}} + \text{mol C}_{\text{n-butanol}} + \text{mol C}_{\text{propanol}}$$

$$+ \text{mol C}_{\text{ethanol}}$$

- Mol Carbon in 100 g of fusel oil

$$= \left(\frac{5 \times 66.77 \text{ gC5}}{88.17 \text{ g/mol}} \right) + \left(\frac{4 \times 12.25 \text{ gC4}}{74.122 \text{ g/mol}} \right) +$$

$$\left(\frac{4 \times 0.7 \text{ gC5}}{74.122 \text{ g/mol}} \right) + \left(\frac{3 \times 4.26 \text{ gC5}}{60.09 \text{ g/mol}} \right) + \left(\frac{2 \times 3.43 \text{ gC5}}{42.07 \text{ g/mol}} \right)$$

$$= 4.84 \text{ mol C/100g}$$

$$= 48.4 \text{ mmol C/g}$$

- Fusel oil feed flowrate = 0.04 mL/min

$$= 0.04 \times 0.8638$$

$$= 0.03347 \text{ g/min}$$

Mol Carbon in fusel oil feed flow

$$= 48.4 \text{ mmol C/g} \times 0.03347 \text{ g/min}$$

$$= 1.6226 \text{ mmol C/min}$$

(1.2) Total carbon in ethylene.

Peak STD of 1 % ethylene = 402502.3

Peak area of C₂H₄ in gas product = 4025068.5

Average Flowrate of Gas product = 27.90 ml/min

$$\text{Feed out of C}_2\text{H}_4 = \left(\frac{\text{Area of C}_2\text{H}_4}{\text{Area STD of C}_2\text{H}_4} \right) = \left(\frac{4025068.5}{402502.3} \right) = 10 \%$$

$$= \left(\frac{10.00 \times 27.90 \text{ ml/min} \times 1000}{100 \times 22400 \text{ ml/mol}} \right)$$

$$= 0.12455 \text{ mmol C}_2\text{H}_4 / \text{min}$$

$$= 0.2491 \text{ mmol C/min}$$

$$\text{Carbon yiled (\%)} = \frac{\text{carbon in C}_2\text{H}_4}{\text{Total carbon in feed}} \times 100 \dots\dots\dots (1)$$

$$= \left(\frac{0.2491 \text{ mmol C/min}}{1.62 \text{ mmol C/min}} \right) \times 100$$

$$= 15.36 \% \text{ C yield (in ethylene)}$$

(2) Calculation for carbon selectivity in gas products

$$\text{Carbon selectivity of } C_2H_4 \text{ (\%)} = \frac{\text{Carbon in } C_2H_4 \times 100}{\text{Total carbon in gas products}}$$

(2.1) Total carbon in gas products

$$\begin{aligned} &= CH_4 + C_2H_4 + C_2H_6 + C_3H_6 + C_3H_8 + C_4H_8 + C_4H_{10} + C_5H_{10} + C_5H_{12} \\ &+ CO_2 + CO \end{aligned}$$

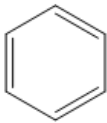
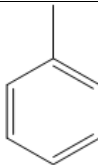
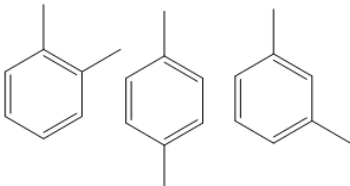
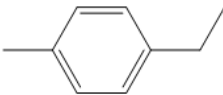
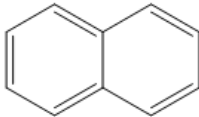
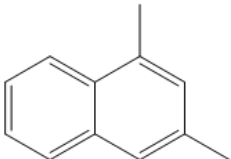
Total percentage of carbon in gas product for catalytic cracking of fusel oil at 550°C with fusel oil feed flowrate under 4 h of time on stream = 44.67 % C yield

(2.1) Carbon in C_2H_4 = 15.36 %

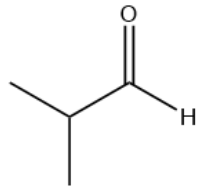
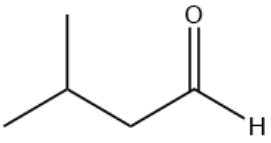
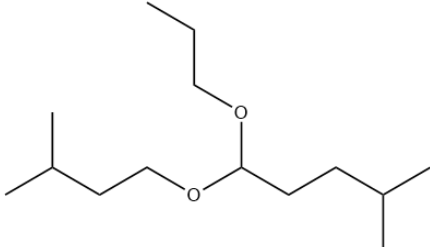
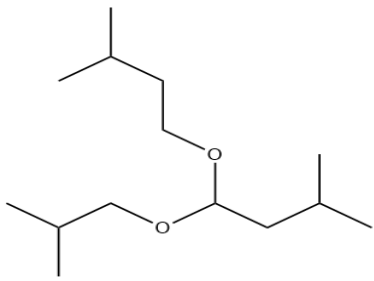
$$\begin{aligned} \text{Carbon selectivity of } C_2H_4 &= \frac{\text{Carbon in } C_2H_4}{\text{Total carbon in gas products}} \times 100 \\ &= \frac{15.36}{44.67} \times 100 \\ &= 34.36 \% \end{aligned}$$

A-5 The chemical structure of the observed products in the liquid fraction derived from catalytic cracking of fusel oil over HZSM-5 catalyst is shown in Table A.4

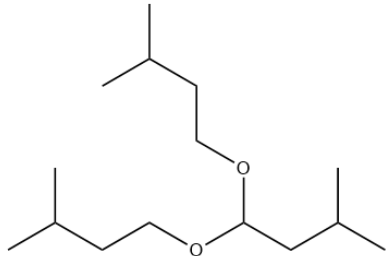
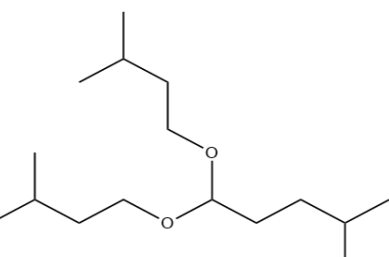
The chemical structure of the observed products in the liquid fraction

Chemical name	Chemical structure
Benzene	
Toluene	
Xylene	
1-ethyl, 4-methyl benzene	
Naphthalene	
1,3-dimethyl naphthalene	

A-5 The chemical structure of the observed products in the liquid fraction derived from catalytic cracking of fusel oil (cont.)

Chemical name	Chemical structure
Isobutaldehyde	
Isovaleraldehyde	
Isovaleraldehyde isopentyl propyl acetal (C13)	
Isobutyraldehyde isobutyl isopentyl acetal (C13)	

A-5 The chemical structure of the observed products in the liquid fraction derived from catalytic cracking of fusel oil

Chemical name	Chemical structure
Isobutylaldehyde diisopentyl acetal (C14)	
Isovaleraldehyde diisopentyl acetal (C15)	

REFERENCES

1. Stefanidis, S.D., et al., *In-situ upgrading of biomass pyrolysis vapors: catalyst screening on a fixed bed reactor*. *Bioresour Technol*, 2011. **102**(17): p. 8261-7.
2. Zhang, Q., et al., *Enhancing bioethanol production from water hyacinth by new combined pretreatment methods*. *Bioresour Technol*, 2018. **251**: p. 358-363.
3. Zaky, A.S., et al., *Improving the productivity of bioethanol production using marine yeast and seawater-based media*. *Biomass and Bioenergy*, 2020. **139**.
4. Morais, R.R., et al., *Bioethanol production from Solanum lycocarpum starch: A sustainable non-food energy source for biofuels*. *Renewable Energy*, 2019. **140**: p. 361-366.
5. Sun, J. and Y. Wang, *Recent Advances in Catalytic Conversion of Ethanol to Chemicals*. *ACS Catalysis*, 2014. **4**(4): p. 1078-1090.
6. Niphadkar, S., P. Bagade, and S. Ahmed, *Bioethanol production: insight into past, present and future perspectives*. *Biofuels*, 2017. **9**(2): p. 229-238.
7. Montoya, N., et al., *Colombian fusel oil*. *Ingeniería e Investigación*, 2016. **36**(2): p. 21-27.
8. Awad, O.I., et al., *Effects of fusel oil water content reduction on fuel properties, performance and emissions of SI engine fueled with gasoline-fusel oil blends*. *Renewable energy*, 2018. **118**: p. 858-869.
9. Mayer, F.D., et al., *Influence of fusel oil components on the distillation of hydrous ethanol fuel (HEF) in a bench column*. *Brazilian Journal of Chemical Engineering*, 2015. **32**(2): p. 585-593.
10. Güvenç, A., et al., *Enzymatic esterification of isoamyl alcohol obtained from fusel oil: Optimization by response surface methodology*. *Enzyme and microbial technology*, 2007. **40**(4): p. 778-785.
11. Wako, F.M., et al., *Catalytic cracking of waste cooking oil for biofuel production using zirconium oxide catalyst*. *Industrial Crops and Products*, 2018. **118**: p. 282-289.

12. Li, X., et al., *Catalytic cracking of n-hexane for producing light olefins on 3D-printed monoliths of MFI and FAU zeolites*. Chemical Engineering Journal, 2018. **333**: p. 545-553.
13. Ji, Y., H. Yang, and W. Yan, *Strategies to Enhance the Catalytic Performance of ZSM-5 Zeolite in Hydrocarbon Cracking: A Review*. Catalysts, 2017. **7**: p. 367.
14. Wang, Y. and J. Wang, *Multifaceted effects of HZSM-5 (Proton-exchanged Zeolite Socony Mobil-5) on catalytic cracking of pinewood pyrolysis vapor in a two-stage fixed bed reactor*. Bioresour Technol, 2016. **214**: p. 700-710.
15. Rezaei, P.S., H. Shafaghat, and W.M.A.W. Daud, *Production of green aromatics and olefins by catalytic cracking of oxygenate compounds derived from biomass pyrolysis: A review*. Applied Catalysis A: General, 2014. **469**: p. 490-511.
16. Campanella, A. and M.P. Harold, *Fast pyrolysis of microalgae in a falling solids reactor: Effects of process variables and zeolite catalysts*. Biomass and Bioenergy, 2012. **46**: p. 218-232.
17. Rahimi, N. and R. Karimzadeh, *Catalytic cracking of hydrocarbons over modified ZSM-5 zeolites to produce light olefins: A review*. Applied Catalysis A-general - APPL CATAL A-GEN, 2011. **398**: p. 1-17.
18. Zhang, S., et al., *The conversion of biomass to light olefins on Fe-modified ZSM-5 catalyst: effect of pyrolysis parameters*. Science of The Total Environment, 2018. **628**: p. 350-357.
19. Gong, F., et al., *Selective conversion of bio-oil to light olefins: controlling catalytic cracking for maximum olefins*. Bioresour Technol, 2011. **102**(19): p. 9247-54.
20. Yu, Y., et al., *The role of shape selectivity in catalytic fast pyrolysis of lignin with zeolite catalysts*. Applied Catalysis A: General, 2012. **447-448**: p. 115-123.
21. Wu, T., et al., *Enhanced catalytic performance in butylene cracking by hierarchical surface silicon-rich ZSM-5*. Fuel Processing Technology, 2017. **167**: p. 162-170.
22. Du, S., et al., *The effect of ZSM-5 catalyst support in catalytic pyrolysis of biomass and compounds abundant in pyrolysis bio-oils*. Journal of Analytical and Applied Pyrolysis, 2016. **122**: p. 7-12.

23. Liang, J., et al., *Enhancement of bio-oil yield and selectivity and kinetic study of catalytic pyrolysis of rice straw over transition metal modified ZSM-5 catalyst*. Journal of Analytical and Applied Pyrolysis, 2017. **128**: p. 324-334.
24. Luo, J., et al., *n-Hexane cracking at high pressures on H-ZSM-5, H-BEA, H-MOR, and USY for endothermic reforming*. Applied Catalysis A: General, 2014. **478**: p. 228-233.
25. Chen, G., et al., *Catalytic cracking of model compounds of bio-oil over HZSM-5 and the catalyst deactivation*. Science of the Total Environment, 2018. **631**: p. 1611-1622.
26. Zhang, B., et al., *Catalytic fast co-pyrolysis of biomass and fusel alcohol to enhance aromatic hydrocarbon production over ZSM-5 catalyst in a fluidized bed reactor*. Journal of Analytical and Applied Pyrolysis, 2018. **133**: p. 147-153.
27. Ferreira, M.C., A.J.A. Meirelles, and E.A.C. Batista, *Study of the Fusel Oil Distillation Process*. Industrial & Engineering Chemistry Research, 2013. **52**(6): p. 2336-2351.
28. Awad, O.I., et al., *The effect of adding fusel oil to diesel on the performance and the emissions characteristics in a single cylinder CI engine*. Journal of the energy Institute, 2017. **90**(3): p. 382-396.
29. KÜÇÜCÜK, Z. and K. CEYLAN, *Potential utilization of fusel oil: A kinetic approach for production of fusel oil esters through chemical reaction*. Turkish Journal of Chemistry, 1998. **22**(3): p. 289-300.
30. Blay, V., et al., *Engineering Zeolites for Catalytic Cracking to Light Olefins*. ACS Catalysis, 2017. **7**(10): p. 6542-6566.
31. Park, Y.-K., et al., *Catalytic cracking of lower-valued hydrocarbons for producing light olefins*. Catalysis surveys from Asia, 2010. **14**(2): p. 75-84.
32. Goyal, G., J.N. Kuhn, and G.P. Philippidis, *Light alkene production by cracking Picochlorum oculatum microalgae using aluminosilicate catalysts*. Biomass and Bioenergy, 2018. **108**: p. 252-257.
33. True, W.R., *Global ethylene capacity poised for major expansion*. Oil & gas journal, 2013. **111**(7): p. 90-95.

34. Fan, D., D.-J. Dai, and H.-S. Wu, *Ethylene formation by catalytic dehydration of ethanol with industrial considerations*. *Materials*, 2013. **6**(1): p. 101-115.
35. Wu, T., et al., *Butylene catalytic cracking to propylene over a hierarchical HZSM-5 zeolite: Location of acid sites controlling the reaction pathway*. *Molecular Catalysis*, 2018. **453**: p. 161-169.
36. Akah, A. and M. Al-Ghrami, *Maximizing propylene production via FCC technology*. *Applied Petrochemical Research*, 2015. **5**(4): p. 377-392.
37. Ren, T., M. Patel, and K. Blok, *Olefins from conventional and heavy feedstocks: Energy use in steam cracking and alternative processes*. *Energy*, 2006. **31**(4): p. 425-451.
38. Wu, T., et al., *Enhanced selectivity of propylene in butylene catalytic cracking over W-ZSM-5*. *Fuel Processing Technology*, 2018. **173**: p. 143-152.
39. Castrovinci, A., M. Lavaselli, and G. Camino, *9 - Recycling and disposal of flame retarded materials*, in *Advances in Fire Retardant Materials*, A.R. Horrocks and D. Price, Editors. 2008, Woodhead Publishing. p. 213-230.
40. Sadrameli, S., *Thermal/catalytic cracking of liquid hydrocarbons for the production of olefins: A state-of-the-art review II: Catalytic cracking review*. *Fuel*, 2016. **173**: p. 285-297.
41. Kissin, Y.V., *Chemical Mechanisms of Catalytic Cracking over Solid Acidic Catalysts: Alkanes and Alkenes*. *Catalysis Reviews*, 2001. **43**(1-2): p. 85-146.
42. Corma, A. and A. Orchillès, *Current views on the mechanism of catalytic cracking*. *Microporous and mesoporous materials*, 2000. **35**: p. 21-30.
43. Vogt, E.T. and B.M. Weckhuysen, *Fluid catalytic cracking: recent developments on the grand old lady of zeolite catalysis*. *Chem Soc Rev*, 2015. **44**(20): p. 7342-70.
44. Dewanto, M.A.R., et al. *Catalytic and thermal cracking processes of waste cooking oil for bio-gasoline synthesis*. in *AIP Conference Proceedings*. 2017. AIP Publishing LLC.
45. Phung, T.K. and G. Busca, *Diethyl ether cracking and ethanol dehydration: Acid catalysis and reaction paths*. *Chemical Engineering Journal*, 2015. **272**: p. 92-101.

46. Alaba, P.A., et al., *Insight into catalyst deactivation mechanism and suppression techniques in thermocatalytic deoxygenation of bio-oil over zeolites*. *Reviews in Chemical Engineering*, 2016. **32**(1).
47. Mores, D., et al., *Space- and time-resolved in-situ spectroscopy on the coke formation in molecular sieves: methanol-to-olefin conversion over H-ZSM-5 and H-SAPO-34*. *Chemistry*, 2008. **14**(36): p. 11320-7.
48. Daramola, M., E. Aransiola, and T. Ojumu, *Potential Applications of Zeolite Membranes in Reaction Coupling Separation Processes*. *Materials*, 2012. **5**(11): p. 2101-2136.
49. Li, C., M. Moliner, and A. Corma, *Building Zeolites from Precrystallized Units: Nanoscale Architecture*. *Angew Chem Int Ed Engl*, 2018. **57**(47): p. 15330-15353.
50. Moshoeshoe, M., M.S. Nadiye-Tabbiruka, and V. Obuseng, *A review of the chemistry, structure, properties and applications of zeolites*. *Am. J. Mater. Sci*, 2017. **7**(5): p. 196-221.
51. Mgbemere, H., I. Ekpe, and G. Lawal, *Zeolite synthesis, characterization and application areas: a review*. *International Research Journal of Environmental Sciences*, 2017. **6**(10): p. 45-59.
52. Weitkamp, J., *Zeolites and catalysis*. *Solid state ionics*, 2000. **131**(1-2): p. 175-188.
53. Xu, M., et al., *Elucidating Zeolite Deactivation Mechanisms During Biomass Catalytic Fast Pyrolysis from Model Reactions and Zeolite Syntheses*. *Topics in Catalysis*, 2015. **59**(1): p. 73-85.
54. Nuruzzaman, M., et al., *Chapter 4 - Nanobiopesticides: Composition and preparation methods*, in *Nano-Biopesticides Today and Future Perspectives*, O. Koul, Editor. 2019, Academic Press. p. 69-131.
55. Busca, G., *Acidity and basicity of zeolites: A fundamental approach*. *Microporous and Mesoporous Materials*, 2017. **254**: p. 3-16.
56. Deka, R.C., *Acidity in zeolites and their characterization by different spectroscopic methods*. 1998.

57. Juzsakova, T., et al., *Study on the alkylaton mechanism of isobutane with 1-butene using environmental friendly catalysts*. Environmental Engineering and Management Journal, 2014. **13**(9): p. 2343-2347.
58. Degnan, T.F., *The implications of the fundamentals of shape selectivity for the development of catalysts for the petroleum and petrochemical industries*. Journal of Catalysis, 2003. **216**(1): p. 32-46.
59. Miller, J., "Shape Selective Catalysis: Chemicals Synthesis and Hydrocarbon Processing" C. Song, J. M. Garcés and Y. Sugj, Eds., ACS Symp. Ser. 738, Amer. Chem. Soc., Washington, DC, 2000, 410 pp. Energy & Fuels, 2002. **16**(1): p. 219-219.
60. Cirujano, F.G. and F.X. Llabrés i Xamena, *Metal Organic Frameworks as Nanoreactors and Host Matrices for Encapsulation*, in *Organic Nanoreactors*. 2016. p. 305-340.
61. Degnan, T., G. Chitnis, and P.H. Schipper, *History of ZSM-5 fluid catalytic cracking additive development at Mobil*. Microporous and Mesoporous materials, 2000. **35**: p. 245-252.
62. Barbera, K., et al., *Structure–deactivation relationship for ZSM-5 catalysts governed by framework defects*. Journal of Catalysis, 2011. **280**(2): p. 196-205.
63. Yang, X., et al., *Effect of hydrothermal aging treatment on decomposition of NO by Cu-ZSM-5 and modified mechanism of doping Ce against this influence*. Materials, 2020. **13**(4): p. 888.
64. Yu, K., et al., *Synthesis and characterization of polypyrrole/H-Beta zeolite nanocomposites*. RSC advances, 2014. **4**(62): p. 33120-33126.
65. Lutz, W., *Zeolite Y: Synthesis, Modification, and Properties—A Case Revisited*. Advances in Materials Science and Engineering, 2014. **2014**: p. 1-20.
66. Hinchiranan, N., *Catalyst Technology*. Vol. 1. 2013, Chemical Technology, Chulalongkorn University. 364.
67. Rase, H.F., *Fixed-bed reactor design and diagnostics: gas-phase reactions*. 2013: Butterworth-Heinemann.

68. Hafeez, S., et al., *Catalytic Conversion and Chemical Recovery*, in *Plastics to Energy*. 2019. p. 147-172.
69. Herskowitz, M. and J. Smith, *Trickle-bed reactors: A review*. *AIChE Journal*, 1983. **29**(1): p. 1-18.
70. Mederos, F.S., J. Ancheyta, and J. Chen, *Review on criteria to ensure ideal behaviors in trickle-bed reactors*. *Applied Catalysis A: General*, 2009. **355**(1-2): p. 1-19.
71. Shirzad, M., et al., *Moving Bed Reactors: Challenges and Progress of Experimental and Theoretical Studies in a Century of Research*. *Industrial & Engineering Chemistry Research*, 2019. **58**(22): p. 9179-9198.
72. Visscher, F., et al., *Rotating reactors—a review*. *Chemical Engineering Research and Design*, 2013. **91**(10): p. 1923-1940.
73. Liu, Y.-z., et al., *Liquid-solid mass transfer in a rotating packed bed reactor with structured foam packing*. *Chinese Journal of Chemical Engineering*, 2020. **28**(10): p. 2507-2512.
74. Foutch, G.L. and A.H. Johannes, *Reactors in Process Engineering*, in *Encyclopedia of Physical Science and Technology*. 2003. p. 23-43.
75. Wang, T., J. Wang, and Y. Jin, *Slurry reactors for gas-to-liquid processes: a review*. *Industrial & Engineering chemistry research*, 2007. **46**(18): p. 5824-5847.
76. Babu, G., R. Murthy, and V. Krishnan, *Conversion of isoamyl alcohol over acid catalysts: Reaction dependence on nature of active centers*. *Journal of Catalysis*, 1997. **166**(1).
77. Nash, C.P., et al., *Mixed alcohol dehydration over Brønsted and Lewis acidic catalysts*. *Applied Catalysis A: General*, 2016. **510**: p. 110-124.
78. Zhang, H., et al., *Catalytic fast pyrolysis of wood and alcohol mixtures in a fluidized bed reactor*. *Green Chem.*, 2012. **14**(1): p. 98-110.
79. Sousa, Z.S., et al., *Bioethanol conversion into hydrocarbons on HZSM-5 and HMCM-22 zeolites: use of in situ DRIFTS to elucidate the role of the acidity and of the pore structure over the coke formation and product distribution*. *Catalysis Today*, 2014. **234**: p. 182-191.

80. Gilbert, C.J., et al., *The effect of water on furan conversion over ZSM-5*. ChemCatChem, 2014. **6**(9): p. 2497-2500.
81. Dong, X., et al., *Catalytic pyrolysis of microalga *Chlorella pyrenoidosa* for production of ethylene, propylene and butene*. RSC advances, 2013. **3**(48): p. 25780-25787.
82. Lehmann, T. and A. Seidel-Morgenstern, *Thermodynamic appraisal of the gas phase conversion of ethylene or ethanol to propylene*. Chemical Engineering Journal, 2014. **242**: p. 422-432.
83. Nabavi, M.S., et al., *Stability of colloidal ZSM-5 catalysts synthesized in fluoride and hydroxide media*. Microporous and Mesoporous Materials, 2019. **278**: p. 167-174.
84. Javid, R., et al., *Factors affecting coke formation on H-ZSM-5 in naphtha cracking*. Applied Catalysis A: General, 2015. **491**: p. 100-105.
85. Müller, S., et al., *Coke formation and deactivation pathways on H-ZSM-5 in the conversion of methanol to olefins*. Journal of Catalysis, 2015. **325**: p. 48-59.
86. Hou, X., et al., *Promotion on light olefins production through modulating the reaction pathways for n-pentane catalytic cracking over ZSM-5 based catalysts*. Applied Catalysis A: General, 2017. **543**: p. 51-60.
87. Galadima, A. and O. Muraza, *Zeolite catalysts in upgrading of bioethanol to fuels range hydrocarbons: A review*. Journal of Industrial and Engineering Chemistry, 2015. **31**: p. 1-14.
88. Li, X., et al., *Light olefins from renewable resources: Selective catalytic dehydration of bioethanol to propylene over zeolite and transition metal oxide catalysts*. Catalysis Today, 2016. **276**: p. 62-77.
89. Ramasamy, K.K. and Y. Wang, *Ethanol conversion to hydrocarbons on HZSM-5: Effect of reaction conditions and Si/Al ratio on the product distributions*. Catalysis Today, 2014. **237**: p. 89-99.
90. Baxter, N., et al., *Kraft Lignin Ethanolysis over Zeolites with Different Acidity and Pore Structures for Aromatics Production*. Catalysts, 2021. **11**: p. 270.

91. *Appendix E - Channel System Dimensions, in Atlas of Zeolite Framework Types (Sixth Edition)*, C. Baerlocher, L.B. McCusker, and D.H. Olson, Editors. 2007, Elsevier Science B.V.: Amsterdam. p. 381-386.
92. Liu, S., et al., *Bio-oil production from sequential two-step catalytic fast microwave-assisted biomass pyrolysis*. Fuel, 2017. **196**: p. 261-268.
93. Sousa, Z.S.B., et al., *Ethanol conversion into olefins and aromatics over HZSM-5 zeolite: Influence of reaction conditions and surface reaction studies*. Journal of Molecular Catalysis A: Chemical, 2016. **422**: p. 266-274.
94. Hu, C., R. Xiao, and H. Zhang, *Ex-situ catalytic fast pyrolysis of biomass over HZSM-5 in a two-stage fluidized-bed/fixed-bed combination reactor*. Bioresour Technol, 2017. **243**: p. 1133-1140.
95. Nishu, et al., *A review on the catalytic pyrolysis of biomass for the bio-oil production with ZSM-5: Focus on structure*. Fuel Processing Technology, 2020. **199**: p. 106301.
96. Corma, A., J. Mengual, and P.J. Miguel, *Stabilization of ZSM-5 zeolite catalysts for steam catalytic cracking of naphtha for production of propene and ethene*. Applied Catalysis A: General, 2012. **421**: p. 121-134.
97. Oudejans, J.C., P.F. Van Den Oosterkamp, and H. Van Bekkum, *Conversion of ethanol over zeolite h-zsm-5 in the presence of water*. Applied Catalysis, 1982. **3**(2): p. 109-115.
98. Uslamin, E.A., et al., *Aromatization of ethylene over zeolite-based catalysts*. Catalysis Science & Technology, 2020. **10**(9): p. 2774-2785.
99. Di Cosimo, J., et al., *Structure and surface and catalytic properties of Mg-Al basic oxides*. Journal of Catalysis, 1998. **178**(2): p. 499-510.
100. Grabowski, J., J.M. Granda, and J. Jurczak, *Preparation of acetals from aldehydes and alcohols under basic conditions*. Organic & biomolecular chemistry, 2018. **16**(17): p. 3114-3120.
101. Muhammad, I., N. Makwashi, and G. Manos, *Catalytic degradation of linear low-density polyethylene over HY-zeolite via pre-degradation method*. Journal of Analytical and Applied Pyrolysis, 2019. **138**: p. 10-21.

102. Ruelas-Leyva, J., et al., *A Comprehensive Study of Coke Deposits on a Pt-Sn/SBA-16 Catalyst during the Dehydrogenation of Propane*. *Catalysts*, 2021. **11**: p. 128.
103. Wang, L., et al., *Catalytic fast pyrolysis of corn stalk for phenols production with solid catalysts*. *Frontiers in Energy Research*, 2019. **7**: p. 86.
104. Hoff, T.C., et al., *Thermal stability of aluminum-rich ZSM-5 zeolites and consequences on aromatization reactions*. *The Journal of Physical Chemistry C*, 2016. **120**(36): p. 20103-20113.
105. lisa, K., et al., *Catalytic pyrolysis of pine over HZSM-5 with different binders*. *Topics in Catalysis*, 2016. **59**(1): p. 94-108.
106. Zhou, F., et al., *Improved catalytic performance and decreased coke formation in post-treated ZSM-5 zeolites for methanol aromatization*. *Microporous and Mesoporous Materials*, 2017. **240**: p. 96-107.
107. Ye, G., et al., *Pore network modeling of catalyst deactivation by coking, from single site to particle, during propane dehydrogenation*. *AIChE Journal*, 2019. **65**(1): p. 140-150.
108. Cordes, E. and H. Bull, *Mechanism and catalysis for hydrolysis of acetals, ketals, and ortho esters*. *Chemical Reviews*, 1974. **74**(5): p. 581-603.
109. Collett, C.H. and J. McGregor, *Things go better with coke: the beneficial role of carbonaceous deposits in heterogeneous catalysis*. *Catalysis Science & Technology*, 2016. **6**(2): p. 363-378.

VITA

NAME Rachatawan Yaisamlee

DATE OF BIRTH 27 November 1991

INSTITUTIONS ATTENDED Program for Petrochemical and Polymer Science, Faculty of Science, Chulalongkorn University

PUBLICATION (1) R.Yaisamlee, P. Reubroycharorn, Light olefin production from the catalytic cracking of fusel oil in a fixed bed reactor, Biomass & Bioenergy journal. (Submitted)

(2) R. Yaisamlee, M. Mohamedali, H. Ibrahim, Evaluation of Piperazine/MIL-101 sorbents for enhanced low-temperature CO₂ capture, Microporous and Mesoporous Materials journal. (Submitted)